

Femtosecond Time-Resolved Photoelectron Spectroscopy

Albert Stolow*

Steele Institute for Molecular Sciences, National Research Council of Canada, 100 Sussex Drive, Ottawa, Ontario, K1A 0R6 Canada

Arthur E. Bragg and Daniel M. Neumark*

Department of Chemistry, University of California, Berkeley, California 94720

Received August 6, 2003

Contents

1. Introduction	1719
2. General Aspects of Femtosecond TRPES	1721
2.1. Neutral and Anionic Systems	1722
2.2. Photoelectron Angular Distributions	1724
2.3. Intensity Effects	1725
3. Development of Time-Resolved Photoelectron Spectroscopy: 1985–1998	1726
3.1. Time-Resolved Photoelectron Spectroscopy Experiments	1726
3.2. Time-Resolved Photoelectron Angular Distributions	1727
3.3. Theoretical Developments	1727
4. Experimental Methods	1728
4.1. Photoelectron Spectroscopy of Neutrals and Anions	1728
4.2. Photoelectron–Photoion Coincidence Methods	1729
4.3. Femtosecond Laser Technology	1730
5. Applications	1730
5.1. Non-adiabatic Intramolecular Dynamics	1730
5.2. Excited-State Intramolecular Proton Transfer	1736
5.3. Photophysics of Model Molecular Switches	1737
5.4. Superexcited States	1738
5.5. Time-Resolved VUV/XUV/X-ray Photoelectron Spectroscopy	1739
5.6. Neutral Photodissociation Dynamics	1740
5.7. Neutral Reaction Dynamics	1742
5.8. Anion TRPES: I_2^- Nuclear Wave Packet Dynamics	1743
5.9. Dissociation Dynamics of Polyatomic Anions	1744
5.10. Photodissociation, Recombination, and Reaction Dynamics in Anionic Clusters	1744
5.11. Anion Vibrational Wave Packet and Relaxation Dynamics	1746
5.12. Charge-Transfer-to-Solvent and Solvated Electron Dynamics	1746
5.13. Anion Intramolecular Electronic Relaxation Dynamics	1747
5.14. Photoelectron Angular Distributions	1749
6. Conclusions and Future Directions	1753
7. Acknowledgments	1753

8. References

1754

1. Introduction

The development of femtosecond time-resolved methods for the study of gas-phase molecular dynamics is founded upon the seminal studies of Zewail and co-workers, as recognized in 1999 by the Nobel Prize in Chemistry.¹ This methodology has been applied to chemical reactions ranging in complexity from bond-breaking in diatomic molecules to dynamics in larger organic and biological molecules, and has led to breakthroughs in our understanding of fundamental chemical processes. Photoexcited polyatomic molecules and anions often exhibit quite complex dynamics involving the redistribution of both charge and energy.^{2–6} These processes are the primary steps in the photochemistry of many polyatomic systems,⁷ are important in photobiological processes such as vision and photosynthesis,⁸ and underlie many concepts in molecular electronics.⁹

Femtosecond time-resolved methods involve a pump–probe configuration in which an ultrafast pump pulse initiates a reaction or, more generally, creates a nonstationary state or wave packet, the evolution of which is monitored as a function of time by means of a suitable probe pulse. Time-resolved or wave packet methods offer a view complementary to the usual spectroscopic approach and often yield a physically intuitive picture. Wave packets can behave as zeroth-order or even classical-like states and are therefore very helpful in discerning underlying dynamics. The information obtained from these experiments is very much dependent on the nature of the final state chosen in a given probe scheme. Transient absorption and nonlinear wave mixing are often the methods of choice in condensed-phase experiments because of their generality. In studies of molecules and clusters in the gas phase, the most popular methods, laser-induced fluorescence and resonant multiphoton ionization, usually require the probe laser to be resonant with an electronic transition in the species being monitored. However, as a chemical reaction initiated by the pump pulse evolves toward products, one expects that both the electronic and vibrational structures of the species under observation will change. Hence, these probe methods can be

* To whom correspondence should be addressed. A.S.: telephone (613) 993-7388, fax (613) 991-3437, E-mail albert.stolow@nrc.ca. D.M.N.: telephone (510) 642-3505, fax (510) 642-3635, E-mail dan@radon.cchem.berkeley.edu.



Albert Stolow was born in Ottawa. He began studies in biochemistry at Queen's University, Kingston, but turned to chemistry and physics after his second year. He did his Ph.D. studies in physical chemistry with John C. Polanyi at the University of Toronto. Albert was an NSERC postdoctoral fellow with Yuan T. Lee at the University of California, Berkeley, where he became interested in the dynamics of polyatomic molecules. In 1992, he joined the Femtosecond Science Program of the Steacie Institute for Molecular Sciences (National Research Council of Canada) to begin a research program in femtosecond dynamics based upon time-resolved photoelectron spectroscopy. He is currently a Senior Research Officer at the NRC. His research interests include the development and applications of femtosecond time-resolved spectroscopies for the study of non-adiabatic molecular dynamics in both gas and condensed phases, the coherent quantum control of molecular processes using nonperturbative laser fields, and the behavior of polyatomic molecules and clusters in strong nonresonant laser fields.



Arthur Bragg was born in 1977 in Rochester, Michigan. He studied chemistry and physics at Albion College, Albion, Michigan, as a Dow Chemical and Barry M. Goldwater Scholar, graduating with a B.A. and honors in 1999. Art subsequently received a National Science Foundation predoctoral fellowship and began graduate studies at the University of California, Berkeley. He currently studies the dynamics of anions using time-resolved photoelectron imaging in the group of Professor Daniel M. Neumark, with particular interest in the intramolecular electronic relaxation and alignment dynamics of photoexcited molecular and cluster anions.

restricted to observation of the dynamics within a small region of the reaction coordinate.

The present review article focuses upon gas-phase time-resolved photoelectron spectroscopy, a probe methodology that has been demonstrated to be able to follow dynamics along the entire reaction coordinate. In these experiments, the probe laser generates free electrons through photoionization or photodetachment, and the electron kinetic energy (and/or angular) distribution is measured as a function of time. Time-resolved photoelectron spectroscopy (TRP-



Daniel Neumark received his B.A. in chemistry and physics and his M.A. in chemistry from Harvard University in 1977, where he did undergraduate research with Dudley Herschbach. He spent a year at Cambridge University working with David Buckingham, and then attended graduate school at Berkeley, where he joined the research group of Yuan Lee. He received his Ph.D. in physical chemistry in 1984, and then worked as a postdoctoral researcher with Carl Lineberger at the University of Colorado, Boulder, from 1984 to 1986. In 1986, he returned to Berkeley as a faculty member in the Chemistry Department. His research interests focus on several areas in chemical dynamics and spectroscopy, including (i) studies of reaction dynamics using transition-state spectroscopy, time-resolved photoelectron spectroscopy, and state-resolved photodissociation experiments on stable molecules and reactive free radicals, (ii) size-dependent spectroscopy and dynamics of clusters ranging from semiconductor clusters to He nanodroplets, and (iii) the effects of clustering and solvation on fundamental chemical processes. These issues are addressed through a combination of negative ion photodetachment and neutral beam experiments.

ES) was first developed in the early 1980s and applied to electronic dynamics on semiconductor surfaces.¹⁰ In this review of the literature from 1999 until the present, we focus only on applications of femtosecond TRPES to isolated molecules and clusters, both neutral and negatively charged, in the gas phase. The first reviews of TRPES were published in 2000–2001,^{11,12} followed soon after by others.^{13–17}

TRPES experiments have been performed on neutral molecules for several years using nanosecond (ns), picosecond (ps), and femtosecond (fs) lasers to generate the pump and probe pulses. The type of dynamics one can follow depends on the temporal resolution of the laser system. TRPES experiments with ns or ps resolution have been used to probe lifetimes and radiationless decay pathways of excited electronic states. With fs resolution, experiments of this type can be done on very short-lived electronic states. In addition, one can follow a host of vibrational dynamics including dissociation, vibrational relaxation, and coherent wave packet motion. The results of ns or ps TRPES experiments are often complementary to information obtained with other techniques such as laser-induced fluorescence and dispersed emission. Femtosecond TRPES experiments are differential versions of experiments in which mass-selected ion yields are measured as a function of pump–probe delay. For example, in photodissociation problems, ion-yield experiments are very useful for identifying any transient species and monitoring the production of products,¹⁸ whereas TRPES provides an additional level of detail concerning the energy content of and charge redistribution in these species as a function of time.

TRPES experiments have also been performed on mass-selected negative ions. While the more complex sources and lower number densities in negative ion experiments present challenges that are absent in the neutral experiments, detachment energies are generally significantly lower than ionization energies in neutral species and are typically overcome with easily generated probe laser wavelengths. Whereas in studies of radiationless transitions most neutral TRPES experiments “lose track” of dynamics once internal conversion to the ground state occurs, this limitation does not hinder negative ion experiments. In addition, studies of clusters are straightforward in negative ion experiments because the ions can be mass-selected prior to their interaction with the laser pulses; analogous neutral studies require collecting photoions in coincidence with photoelectrons so that the identity of the ionized species can be ascertained.

In a typical instrument for a gas-phase experiment, a skimmed neutral molecular beam or mass-selected negative ion beam interacts with pump and probe laser pulses in the interaction region of a photoelectron (PE) analyzer. Since these experiments involve pulsed lasers, time-of-flight electron energy analyzers have been used in most time-resolved PE experiments to date, although both 2D and 3D imaging methods are beginning to contribute. It is particularly useful to use high collection efficiency analyzers to increase the data acquisition rate; hence, parabolic reflectors¹⁹ or, more commonly, “magnetic bottle” analyzers^{20–22} with a collection efficiency of 50% or better have been incorporated into many of the instruments currently in use. The recent development of high-power femtosecond lasers with repetition rates of 1 kHz or higher has also greatly facilitated time-resolved PE experiments with femtosecond temporal resolution. The combination of photoelectron spectroscopy and femtosecond lasers is particularly appealing because the energy resolution of typical electron energy analyzers (10–50 meV) is comparable to the energy resolution of a typical femtosecond pump–probe experiment (~25 meV for 100 fs pulses).

TRPES is particularly well-suited to the study of ultrafast non-adiabatic processes because photoelectron spectroscopy is sensitive to both electronic configurations (molecular orbitals) and vibrational dynamics. An elementary but useful picture is that emission of an independent outer electron occurs without simultaneous electronic reorganization of the “core” (be it cation or neutral)—this is called the “molecular orbital” or Koopmans’ picture.²³ These simple correlation rules indicate the continuum state expected to be formed upon single photon, single active electron ionization or detachment of a given molecular orbital. The probabilities of partial ionization into specific continuum electronic states can differ drastically with respect to the molecular orbital nature of the probed electronic state. If a given probed electronic configuration correlates—upon removal of a single active outer electron—to the ground electronic configuration of the continuum, then the photoionization probability is generally higher than if it does not. This suggests the possibility of using

the electronic structure of the continuum as a probe of non-adiabatically evolving electronic configurations in the neutral excited state, as was first proposed theoretically by W. Domcke in 1991.^{24,25}

2. General Aspects of Femtosecond TRPES

From a physical point of view, time-resolved experiments involve the creation and detection of wave packets, defined to be coherent superpositions of molecular eigenstates. Due to the differing energy phase factors of the eigenstates, this superposition is nonstationary. Extensive theoretical treatment of the propagation and probing of nonstationary states in a TRPES experiment may be found elsewhere;^{26–32} only a descriptive summary of the theory follows.

The three aspects of a femtosecond pump–probe wave packet experiment are (i) the preparation or pump, (ii) the dynamical evolution, and (iii) the probing of the nonstationary superposition state. The amplitudes and initial phases of the set of prepared excited eigenstates are determined by the amplitude (i.e., the “spectrum”) and phase (i.e., the “temporal shape”) of the pump laser field and the transition probabilities between the ground state $|\tilde{g}\rangle$ and the excited state of interest. Once the pump laser pulse is over, the wave packet $\chi(\Delta t)$, given by eq 1, evolves freely according to relative energy phase factors in the superposition. The \tilde{a}_n complex coefficients contain

$$|\chi(\Delta t)\rangle = \sum_n \tilde{a}_n |\Psi_n\rangle e^{-i2\pi c E_n \Delta t} \quad (1)$$

both the amplitudes and initial phases of the exact (non-Born–Oppenheimer) molecular eigenstates $|\Psi_n\rangle$, which are prepared by the pump laser. The E_n are the excited-state eigenenergies, given here in wave-numbers. The probe laser field interacts with the wave packet typically after the pump pulse is over, projecting it onto a specific final state $|\Psi_f\rangle$ at some time delay Δt . This final state acts like a “movie screen” onto which the wave packet dynamics is projected. Knowing something about this “movie screen” and whether the projection is “faithful” will obviously be important. The time dependence of the differential signal, $S_f(\Delta t)$, for projection onto a *single* final state $|\Psi_f\rangle$ can thus be written:

$$S_f(\Delta t) = |\langle \Psi_f | \vec{\mu}(\vec{r}) \cdot \vec{E}_{\text{PROBE}} | \chi(\Delta t) \rangle|^2 = \left| \sum_n \tilde{b}_n e^{-i2\pi c E_n \Delta t} \right|^2 \quad (2)$$

where

$$\tilde{b}_n = \tilde{a}_n \langle \Psi_f | \vec{\mu}(\vec{r}) \cdot \vec{E}_{\text{PROBE}}(\Delta t) | \Psi_n \rangle$$

$$S_f(\Delta t) = \sum_n \sum_{m \leq n} |\tilde{b}_n| |\tilde{b}_m| \cos\{(E_n - E_m)2\pi c \Delta t + \Phi_{nm}\}$$

The complex coefficients \tilde{b}_n contain the \tilde{a}_n from eq 1 as well as the probe transition dipole moment and generalized vibronic overlap factors to the final state $|\Psi_f\rangle$. The most detailed information in this final state is the resolved differential signal $S_f(\Delta t)$. It arises from a coherent sum over all two-photon transition am-

plitudes consistent with the pump and probe laser bandwidths and therefore implicitly contains interferences between degenerate two-photon transitions. It can be seen that the signal as a function of Δt contains modulations at frequencies ($E_n - E_m$), the set of level spacings in the superposition. This is the relationship between the wave packet dynamics and the observed pump–probe signal. It is the interference between individual two-photon transitions arising from an initial state, through different excited eigenstates, and terminating in the same single final state, which leads to these modulations. It is, in essence, a multilevel quantum beat. The power spectrum of this time domain signal is comprised of frequencies and amplitudes (i.e., modulation depths) which give information about the set of level spacings in the problem and their respective overlaps with a specific, chosen final state $|\Psi_f\rangle$. Different final states $|\Psi_f\rangle$ will generally have differing overlaps with the wave packet leading to differing amplitudes in the power spectrum (due to differing modulation depths in the time domain signal). By carefully choosing different final states, it is possible for the experimentalist to emphasize particular aspects of the dynamics. In general, there is often a set of final states $|\Psi_f\rangle$ which may fall within the probe laser bandwidth. We must differentiate, therefore, between integral and differential detection techniques. With integral detection techniques (e.g., total fluorescence, total ion yield), the experimentally measured total signal, $S(\Delta t)$, is proportional to the total population in the set of all energetically allowed final states, $\sum S_f(\Delta t)$, created at the end of the two-pulse sequence. Information is lost in carrying out the sum $\sum S_f(\Delta t)$ since the individual final states $|\Psi_f\rangle$ may each have different overlaps with the wave packet. Therefore, differential techniques such as dispersed fluorescence, translational energy spectroscopy, or photoelectron spectroscopy, which can disperse the observed signal with respect to final state $|\Psi_f\rangle$, will be important. Clearly, the choice of the final state is of great importance, as it determines the experimental technique and significantly determines the information content of an experiment. In many studies of non-adiabatic processes in polyatomic molecules, the initially prepared “bright” state is often coupled to a lower-lying “dark” state. The fact that this latter state is “dark” means that observation of its dynamics is potentially obscured, depending greatly upon the nature of the final state.

The molecular ionization (or detachment) continuum as the final state in polyatomic wave packet experiments has both practical and conceptual advantages.^{24,25,33,34} (a) Charged particle detection is extremely sensitive. (b) Detection of the ion or preselection of the anion provides mass information on the carrier of the spectrum. (c) Ionization/detachment is always an “allowed” process, with relaxed selection rules due to the range of symmetries of the outgoing electron. Any molecular state can be ionized/detached—there are no “dark” states. (d) The final state in an ionization/detachment process is often a stable cation/neutral species providing a well-characterized template on which to project the evolving wave packet.

(e) Highly detailed, multiplexed information can be obtained by differentially analyzing the outgoing photoelectron as to its kinetic energy and angular distribution. (f) Higher order (multiphoton) processes, which can be difficult to avoid in femtosecond experiments, are readily revealed. (g) Photoelectron–photon coincidence and anion photodetachment measurements allow for studies of cluster solvation effects as a function of cluster size and for studies of vector correlations in photodissociation dynamics.

2.1. Neutral and Anionic Systems

As discussed in the Introduction and illustrated by the work of Baumert³⁵ and Neumark,^{36,37} TRPES has the multiplexed ability to follow detailed vibrational wave packet dynamics in excited molecular states, in some cases all the way to the products. In the work by Baumert and co-workers on Na_2 , two-photon excitation was used to create a wave packet on the excited $2^1\Pi_g$ state of Na_2 , and the PE spectrum was measured after delayed ionization with a probe pulse, as schematically depicted in Figure 1a. The photoelectron spectrum changes with the phase of the wave packet because of the difference between the potentials for the $2^1\Pi_g$ state and the $X^2\Sigma_g^+$ state of Na_2^+ , with higher (lower) electron kinetic energy at the inner (outer) turning point. As a result, a plot of the photoelectron spectra vs time (Figure 1b) shows the complete excited-state wave packet dynamics. The negative ion TRPES experiments on I_2^- by Neumark and co-workers probed the time scale for direct dissociation to $\text{I}(^2P_{3/2}) + \text{I}^-$ on the repulsive $A'^2\Sigma_{g,1/2}^+$ state, schematically drawn in Figure 15a; the PE spectrum evolves from a broad transient feature associated with dissociating I_2^- to very sharp features associated with the atomic I^- product in about 300 fs, as shown in Figure 2.

Hayden³⁸ first demonstrated that dynamics due to non-adiabatic processes can also be monitored by TRPES, using internal conversion in hexatriene as an example. Non-adiabatic processes lead to changes in electronic symmetry, and, as proposed by Domcke,²⁴ the simple Koopmans' picture suggests that one might be able to directly monitor the evolving excited-state electronic configurations during non-adiabatic processes while simultaneously following the coupled nuclear dynamics via the vibrational structure within each photoelectron band. In Figure 3, we show a picture of excited-state polyatomic wave packet dynamics probed via TRPES, shown here for the case of neutral molecule dynamics. (A similar picture can be envisaged for the case of anion excited-state dynamics.) A zeroth-order bright state, α , is coherently prepared with a femtosecond pump pulse. According to the Koopmans' picture, it should ionize into the α^+ continuum, the electronic state of the cation obtained upon removal of the outermost valence electron (here chosen to be the ground electronic state of the ion). This process produces a photoelectron band ϵ_1 .

We now consider any non-adiabatic coupling process which transforms the zeroth-order bright state α into a lower lying zeroth-order “dark” state, β , as induced by promoting vibrational modes of appropri-

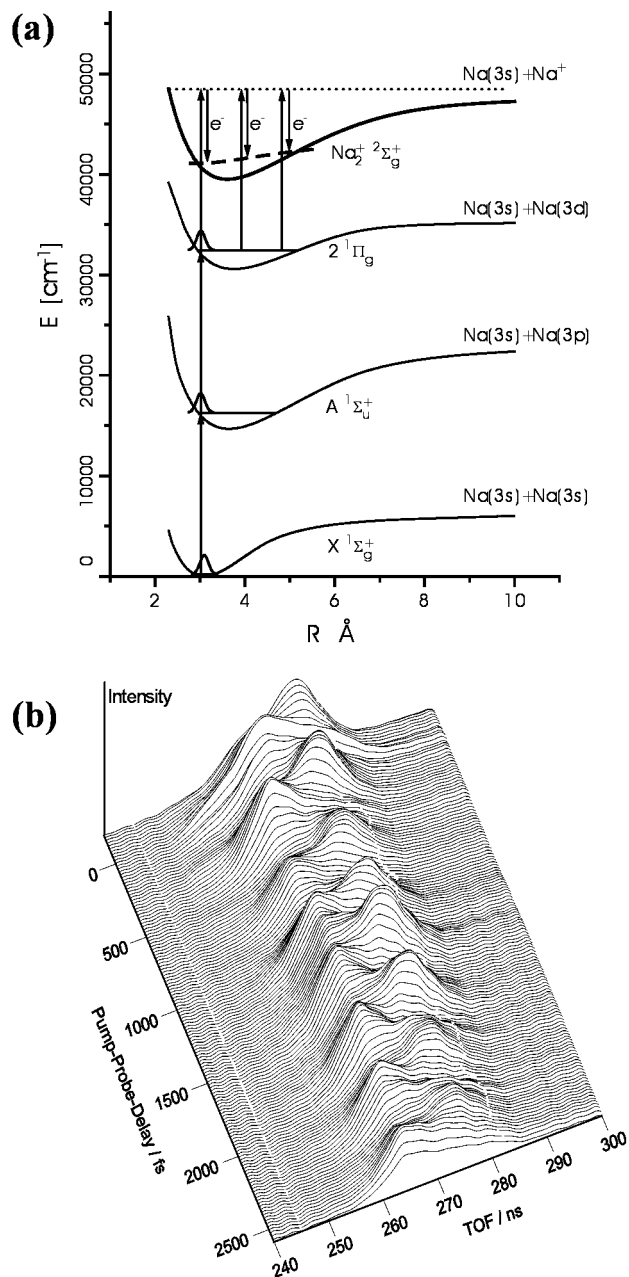


Figure 1. Femtosecond PE spectroscopy of Na_2 . (a) Potential energy curves of $\text{Na}_2/\text{Na}_2^+$ and experimental excitation schema: one- and two-photon excitation at 618 nm creates vibrational wave packets at the inner turning point of the $A^1\Sigma_u^+$ and $2^1\Pi_g$ states, respectively, with dynamics probed via nuclear-induced changes in the ionization potential. (b) Time-resolved photoelectron spectra showing coherent wave packet motion on the excited Na_2 states. Reprinted with permission from ref 35. Copyright 1996 American Physical Society.

ate symmetry. Again, according to the Koopmans' picture, the β state should ionize into the β^+ ionization continuum (here assumed to be an electronically excited state of the ion), producing a photoelectron band ϵ_2 . Therefore, for a sufficiently energetic probe photon (i.e., with both ionization channels open), we expect a switching of the electronic photoionization channel from ϵ_1 to ϵ_2 during the non-adiabatic process. This simple picture suggests that one can directly monitor the evolving excited-state electronic configurations (i.e., the electronic population dynam-

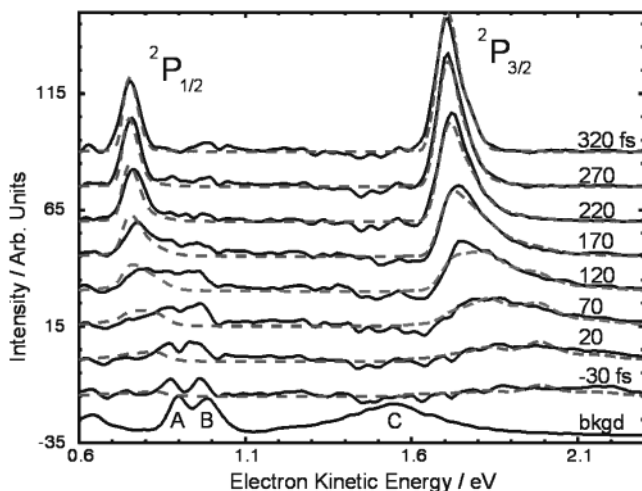


Figure 2. Experimental fs photoelectron spectra of I_2^- . Spectra at various delays (-30 to 320 fs); A, B, and C correspond to the $X^1\Sigma_g^+$, $A^3\Pi_{2u}$, and $A^3\Pi_{1u}$ states of I_2 measured in a one-photon UV background spectrum, while dashed lines indicate the results of time-resolved wave packet simulations. Reprinted with permission from ref 37. Copyright 1999 American Institute of Physics.

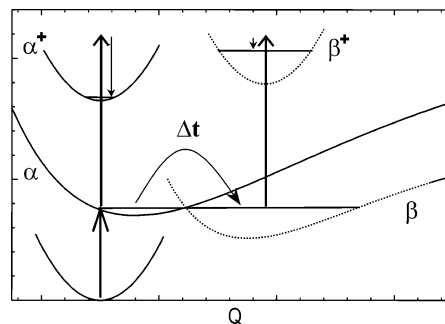


Figure 3. A TRPES scheme for disentangling electronic from vibrational dynamics in excited polyatomic molecules. A zeroth-order electronic state α is prepared by a fs pump pulse. Via a non-adiabatic process it converts to a vibrationally hot lower-lying electronic state, β . The Koopmans'-type ionization correlations suggest that these two states will ionize into different electronic continua: $\alpha \rightarrow \alpha^+ + e^-(\epsilon_1)$ and $\beta \rightarrow \beta^+ + e^-(\epsilon_2)$. When the wave packet has zeroth-order α character, any vibrational dynamics in the α state will be reflected in the structure of the ϵ_1 photoelectron band. After the non-adiabatic process, the wave packet has β zeroth-order electronic character; any vibrational dynamics in the β state will be reflected in the ϵ_2 band. This allows for the simultaneous monitoring of both electronic and vibrational excited-state dynamics. Reprinted with permission from ref 91. Copyright 2000 Elsevier.

ics) during non-adiabatic processes while simultaneously following the coupled nuclear dynamics via the vibrational structure within each photoelectron band. In other words, the electronic structure of the molecular ionization (or detachment) continuum acts as a "template" for the disentangling of electronic from vibrational dynamics in the excited state, as was first experimentally demonstrated for fs non-adiabatic processes in 1998–1999.^{39,40}

The two limiting cases for Koopmans'-type correlations in such experiments, as initially proposed by Domcke,^{24,25} have been demonstrated experimentally.^{41,42} The first case, Type I, is when the neutral excited states α and β clearly correlate to different

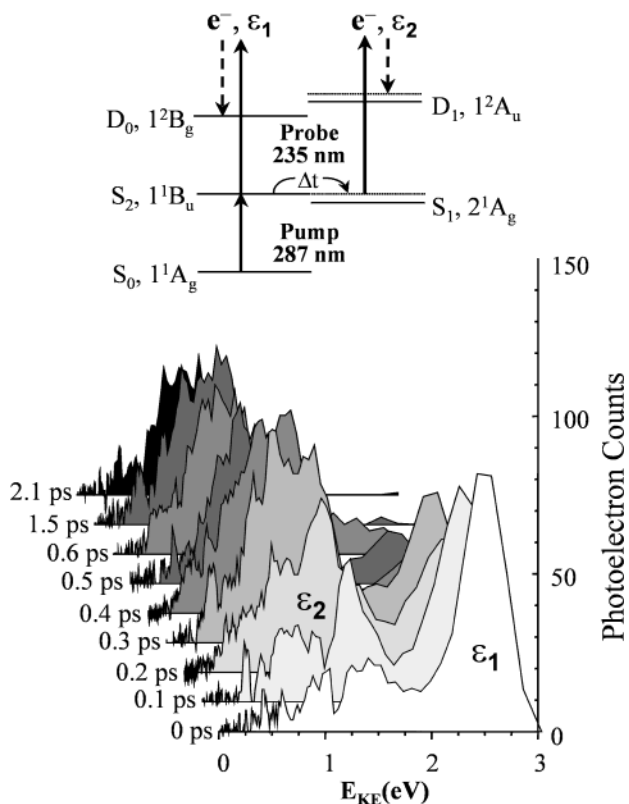


Figure 4. (Top) Energy level scheme for TRPES of *all-trans*-decatetraene (DT), a molecule exhibiting Type I Koopmans' correlations. The pump laser prepares the optically bright state S_2 . Due to ultrafast internal conversion, this state converts to the lower-lying state S_1 with ~ 0.7 eV of vibrational energy. The expected complementary Type I Koopmans' correlations are shown: $S_2 \rightarrow D_0 + e^-(\epsilon_1)$ and $S_1 \rightarrow D_1 + e^-(\epsilon_2)$. (Bottom) TRPES spectra of DT pumped at 287 nm and probed at 235 nm. There is a rapid shift (~ 400 fs) from ϵ_1 , an energetic band at 2.5 eV due to photoionization of S_2 into the D_0 cation ground electronic state, to ϵ_2 , a broad, structured band at lower energies due to photoionization of vibrationally hot S_1 into D_1 , the first excited electronic state of the cation. The structure in the low-energy band reflects the vibrational dynamics in S_1 . These results illustrate the disentangling of the vibrational from the electronic population dynamics. Reprinted with permission from *Nature* (<http://www.nature.com>), ref 40. Copyright 1999 Nature Publishing Group.

ion electronic continua, as suggested by Figure 3. Even if there are large geometry changes upon internal conversion and/or ionization, producing vibrational progressions, the electronic correlations should favor a disentangling of the vibrational dynamics from the electronic population dynamics. As an example, Stolow and co-workers studied ultrafast internal conversion in a linear polyene (decatetraene, DT). The DT optically bright S_2 state internally converts to S_1 on ultrafast time scales. As discussed in more detail in a following section, the S_2 state electronically correlates with the D_0 cation ground state, and S_1 correlates with the D_1 cation first excited state. In Figure 4 (top), we show the energy level scheme relevant to this experiment. A femto-second pump pulse at 287 nm prepared the excited S_2 state at its origin. This then evolved into a vibrationally hot S_1 state via internal conversion. The coupled states were probed using single-photon 235 nm ionization. As suggested by Figure 3, the evolving

electronic and vibrational character of the wave packet alters the photoionization electronic channel, leading to large shifts in the time-resolved photoelectron spectrum. The experimental photoelectron kinetic energy spectra, shown in Figure 4 (bottom), indeed show a dramatic shift as a function of time. This shift is the direct (as opposed to inferred) signature of the changing electronic-state character induced by non-adiabatic coupling. This example demonstrates the selectivity of the molecular ionization (or detachment) continuum for specific excited-state configurations and shows that electronic population dynamics can be disentangled from vibrational dynamics during ultrafast non-adiabatic processes.^{40,42} The other limiting case, Type II, is when the neutral excited states α and β correlate equally strongly to the same ion electronic continua. This is expected to hinder the disentangling of electronic from vibrational dynamics⁴² and is discussed in more detail in a following section.

2.2. Photoelectron Angular Distributions

The other component of the molecular ionization or detachment continuum is that of the free electron. Within the molecular frame, the symmetries of the outgoing electron partial waves are likewise related to the symmetry of the electronic state undergoing ionization. This can be viewed most simply (eq 3) as being due to the requirement that the product of the symmetry species of the prepared excited state Γ_{ex} , the dipole operator Γ_{μ} , the ion state Γ_{+} , and the free electron wave function Γ_{e} must equal or contain the totally symmetric irreducible representation Γ_{TS} of the molecular symmetry group, in order that the transition be allowed.

$$\Gamma_{\text{ex}} \otimes \Gamma_{\mu} \otimes \Gamma_{+} \otimes \Gamma_{\text{e}} \supseteq \Gamma_{\text{TS}} \quad (3)$$

If, owing to a non-adiabatic process, the symmetry species of the initial zeroth-order state Γ_{ex} changes, then the symmetry species of the outgoing electron Γ_{e} must also change in order that the product remain (or contain) the totally symmetric species Γ_{TS} . It is the symmetry species of the outgoing electron Γ_{e} that relates to the photoelectron angular distribution. Hence, measurement of time-resolved photoelectron angular distributions (PADs) also provides a probe of electronically non-adiabatic processes. We note, however, that a change in symmetry is not always required to produce a change in the PAD. Two excited-state wave functions of identical electronic symmetry may have quite different ionization matrix elements, leading to differences in the PADs. The photoemission is, in general, sensitive to orientation of the molecular frame with respect to the photoelectron recoil vector (however, unfavorable ionization dynamics may obscure this effect). In favorable cases, a laboratory-frame alignment of the molecular frame will lead to anisotropies in the PAD. A coherent superposition of rotational states leads to a time-evolving molecular axis distribution in the laboratory frame. In this situation, the PAD may evolve due to the evolution of the rotational superposition state and can directly reflect the axis distribution. The use of

time-resolved PADs in excited-state molecular dynamics has been recently reviewed, and we refer the reader to these reviews for detailed discussions.^{13,14,17} The measurement of time-resolved PADs is expected to be particularly valuable when dynamical processes are not discernible from a photoelectron kinetic energy analysis alone. In general, PAD measurements are more involved and their calculation more challenging in polyatomic systems than for the case of photoelectron energy distributions. A consideration of practical issues such as the nature of the laboratory-frame alignment (i.e., how the pump pulse creates an anisotropic distribution of excited-state molecular axes in the laboratory frame) and the sensitivity of the ionization dynamics to the orientation of the molecular frame is important. Unfavorable laboratory-frame alignment can potentially obscure the underlying photoionization dynamics and reduce the efficacy of the PAD as an experimental probe.

2.3. Intensity Effects

Amplified femtosecond laser pulses are inherently intense. The neglect of intensity effects can lead to misinterpretation of results. For example, even moderate ($f/40$) focusing of a 100 fs pulse (at $\lambda = 300$ nm) yields an intensity of 10^{12} W/cm² with a pulse energy of only 1 μ J! It can be seen that amplified femtosecond pulse experiments will be very difficult to carry out in the perturbation theory (Golden Rule) limit. As the strong laser field physics of molecules is amply discussed elsewhere,⁴³ we summarize here only briefly some potential manifestations of nonperturbative electric fields that can appear in almost any femtosecond experiment using amplified pulses. A characteristic phenomenon observed in photoelectron spectroscopy via strong field ionization is above-threshold ionization (ATI), the absorption of additional photons by an electron already above the ionization potential (IP) that leads to a series of peaks in the photoelectron spectrum spaced by the photon energy.⁴⁴

Other strong field phenomena may also directly affect femtosecond photoelectron spectra. As discussed below, strong Rabi oscillations can lead to aligned states and to ground-state wave packets. Another important related consequence is the dynamic (or AC) Stark effect—the shifting and modification of potential energy surfaces during the strong electric field of the laser pulse. As discussed below, this leads to an alteration of the molecular dynamical evolution and to sweeping field-induced resonances that may introduce phase shifts in the probe laser signal. From a very practical point of view, it is often difficult to use one-photon preparation of an excited-state wave packet unless the absorption cross section for this step is large, as high-intensity femtosecond pulses generally favor nonlinear over linear processes. Since the ratio of one- to two-photon cross sections is fixed (for a given molecule) and the ratio of the one- to two-photon transition probabilities scales inversely with intensity, the only possibility is to reduce the laser intensity (W/cm²) until the one-photon process dominates. The signal levels at this point, however, may be very small, and very sensitive

detection techniques such as single particle counting are usually required.

In the electronic continuum, the dynamic Stark effect manifests itself in terms of the ponderomotive potential U_p , well-known in strong-field atomic physics.⁴⁴ Classically, the ponderomotive potential of an electron in a laser field of strength E and frequency ω is given by the time-averaged “wiggling” energy:

$$U_p = \frac{e^2 E^2}{4m\omega^2} \quad (4)$$

A convenient rule of thumb is that the ponderomotive shift is ~ 60 meV TW⁻¹ cm⁻² at 800 nm (N.B.: 1 TW = 1×10^{12} W): U_p scales linearly with laser intensity and quadratically with wavelength. Due to the spatio-temporal averaging of intensities in the pulse, the ponderomotive effect is observed as a red shift in electron kinetic energy and broadening of the photoelectron spectrum.⁴⁵

It is well-known in atomic physics that the dynamic Stark effect causes field-induced changes in the energies of the atomic levels and, hence, leads to field-induced multiphoton resonances known as “sweeping” or “Freeman” resonances and to fine structure in atomic ATI photoelectron spectra.⁴⁶ As the dynamic Stark effect is general, similar arguments apply to molecular systems. Beginning in 1996, Baumert and Gerber and their co-workers made extensive studies on the effect of laser intensity on TRPES.^{47–51} In particular, using the Na₂ system as a model, they made the first studies of ATI photoelectron spectra as a function of time, using intense 40 fs pulses at 618 nm. This study (and following studies⁵²) showed in detail how TRPES maps the alteration of nuclear dynamics in intense laser fields, using sweeping resonances as a new tool for controlling molecular dynamics. Y. Chen and co-workers also reported the observation of intensity effects on time-resolved PE spectra, using 2 + 1 ionization of NO through its C²Π Rydberg state.⁵³ They observed field-induced Freeman resonances attributed to the $v = 3$ level of the NO A²Σ⁺ state being shifted about 200 meV into near-resonance with the NO C ($v = 0$) level. A 2003 paper by S. L. Cong and co-workers showed how the dynamic Stark effect could be used constructively to tune or select specific ionization pathways in TRPES of the NO molecule, with resonances chosen between the F²Δ and E²Σ⁺ states.⁵⁴

Nonperturbative intensities can have a particularly pronounced effect on the measurement of photoelectron angular distributions (PADs). The anisotropic nature of the photoexcitation pump process results in an alignment of both the angular momentum and molecular axis distributions of the excited state in the laboratory frame (defined by the polarization direction of the pump laser field). In the Golden Rule limit, for a single photon pump excitation, a $\cos^2 \theta$ distribution of excited-state molecular axes in the laboratory-frame results from a parallel transition ($\sin^2 \theta$ from a perpendicular transition). Nonperturbative intensities will, due to rotational Rabi cycling between the initial and intermediate states, give rise

to higher than expected alignment and can be used to align the molecular states in the laboratory frame.^{55–57} Seideman has shown that, although the pump laser intensity can have significant effects on PADs, the intensity effects of the probe laser are minimal.⁵⁸ This is due to the fact that the “lifetime” of a free electron “near” the molecular core is usually much less than the Rabi period. The pump laser alignment of the molecular axis distribution in the laboratory frame directly affects the observed PADs since the relative contributions of parallel and perpendicular ionization channels and the interferences between them depend on the degree of alignment. In cases of favorable ionization dynamics, this can be exploited to follow the evolution of molecular axis alignment as a probe of rotation–vibration coupling in both diatomic⁵⁹ and polyatomic⁶⁰ molecules.

3. Development of Time-Resolved Photoelectron Spectroscopy: 1985–1998

3.1. Time-Resolved Photoelectron Spectroscopy Experiments

TRPES experiments performed between 1985 and 1998 have been reviewed previously¹² and are therefore considered only briefly in the following discussion. The first gas-phase TRPES experiments using ns and ps lasers were demonstrated in the mid-1980s, by Pallix and Colson⁶¹ on sym-triazine and by Sekreta and Reilly⁶² on benzene. In both cases, PES was used to follow excited-state relaxation via intersystem crossing to a triplet state in real time.

In the early 1990s, experiments by Reilly,⁶³ Knee,⁶⁴ and their co-workers showed that TRPES with ps resolution could be used to follow intramolecular vibrational relaxation (IVR) in excited electronic states. In IVR, the vibrational character of the initially excited zeroth-order vibrational state evolves (i.e., dephases) with time, but the molecule remains in the same electronic state. Reilly's experiments were performed on *p,n*-alkylanilines, while Knee investigated IVR in fluorene, benzene, and aniline-CH₄ clusters.

Syage^{65,66} demonstrated that picosecond TRPES could be used to follow reaction and solvation dynamics within clusters, the first example of a particularly powerful application of the technique. This experiment was applied to excited-state proton transfer in phenol·(NH₃)_{*n*} clusters. In a seminal study, Weber and co-workers used picosecond TRPES to follow spin–orbit coupling (intersystem crossing) from the S₁ state in aniline and 2- and 3-aminopyridine, making use—for the first time—of the very important role of electronic symmetry correlations upon ionization.⁶⁷ This work presaged the fs studies of non-adiabatic processes that were to follow. C. A. de Lange and co-workers used picosecond TRPES to follow dissociation in the repulsive *A* band of CH₃I,⁶⁸ and to measure lifetimes of the predissociative \tilde{B}^1E' and \tilde{C}^1A_1' Rydberg states of NH₃.⁶⁹ Fischer, Schultz, and co-workers used picosecond TRPES to measure lifetimes of vibrational levels of the *B*, *C*, and *D* excited electronic states of the allyl radical, all of which lie about 5 eV above the ground state.^{70–72}

The first experiments at femtosecond time resolution incorporating electron detection were reported in the mid-1990s. In 1993, Baumert, Gerber and co-workers,⁷³ followed by Stolow and co-workers in 1995,^{33,34} applied femtosecond time-resolved ZEKE spectroscopy to vibrational wave packet dynamics in Na₃ and I₂, respectively. Gerber used a femtosecond pump pulse to create a vibrational wave packet in the *B* state of Na₃ and measured both total ion and ZEKE electron yield as a function of pump–probe delay. Stolow's experiments, applied to the I₂ *B* state, were similar in principle but more extensive and presented an outline of the experimental prospects for fs TRPES as applied to excited-state dynamics in polyatomic molecules, emphasizing the role of the molecular ionization continuum as the final state.

In 1996, Cyr and Hayden³⁸ used femtosecond TRPES in its first application to non-adiabatic dynamics in polyatomic molecules, investigating the dynamics of internal conversion in 1,3,5-hexatriene. In this work, the S₂ state of 1,3,5-hexatriene was excited, and a combination of time-resolved ion yield and PE spectroscopy measurements was used to unravel the ensuing dynamics. The PE spectra for the *cis* isomer showed very rapid (~20 fs) internal conversion from the S₂ to the S₁ state, followed by IVR within the S₁ state on a time scale of 300 fs. This experiment was the first example of how TRPES can be used to follow ultrafast non-adiabatic dynamics in polyatomic molecules.

The Stolow and Hayden experiments were soon followed by a flurry of activity in other laboratories, including the first negative ion experiments by Neumark³⁶ on the photodissociation of I₂[−] and wave packet dynamics experiments by Baumert³⁵ on Na₂. Baumert also studied intensity effects on the coherent control of wave packet dynamics of threshold⁵² and above-threshold ionization (ATI)⁴⁸ photoelectrons, as well as the chirp- and pulse-length dependence of molecular photoionization dynamics.⁷⁴

The first TRPES experiments on metal cluster anions were performed by Ganteför et al.⁷⁵ in 1998 on Au₃[−]. These negative ion experiments are discussed further in the context of more recent work in the following sections. Femtosecond TRPES was also applied to studies of dynamics in neutral clusters. In 1997, Soep and Syage studied the dynamics of the double proton-transfer reaction in the 7-azaindole dimer.⁷⁶ By comparing PE spectra obtained by (1 + 1) ionization with 0.8 and 5.0 ps laser pulses, they found significantly higher PE yield with shorter pulse ionization, indicating a subpicosecond excited-state lifetime.

Stolow and Blanchet⁷⁷ applied fs TRPES to the photodissociation dynamics of polyatomic molecules, using the nitric oxide dimer (NO)₂ as an example. Nanosecond studies of (NO)₂ photodissociation dynamics at 193 nm revealed that two product channels are open:⁷⁸ (NO)₂^{*} → NO(A²Σ⁺ v, J) + NO(X²Π v', J') and (NO)₂^{*} → NO(B²Π v, J) + NO(X²Π v'', J''). Femtosecond pump–probe measurement of the decaying (NO)₂⁺ parent ion signal as a function of delay time yielded a time constant of 322 ± 12 fs, while fs

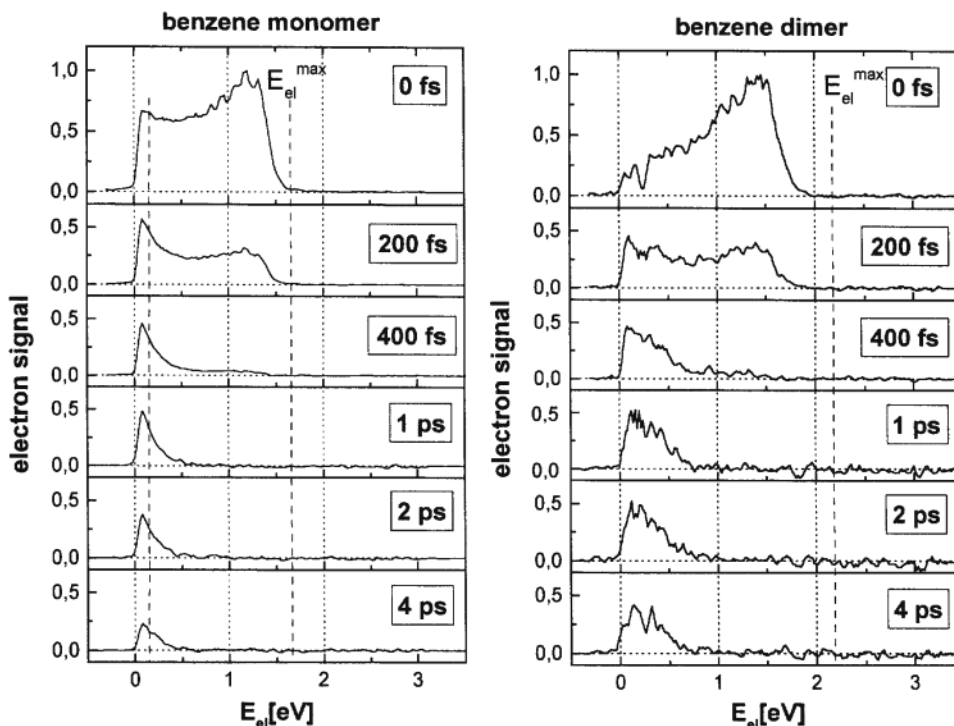


Figure 5. Time-resolved PEPICO spectra of benzene monomer (left) and dimer (right) with $\lambda_{\text{pump}} = 200$ nm and $\lambda_{\text{probe}} = 267$ nm. The ultrafast internal conversion process can be seen to be very different in the dimer than in the monomer. The PEPICO technique allows complete separation of these channels. Reprinted with permission from ref 80. Copyright 1997 Elsevier.

TRPES spectra showed a prominent sharp peak at 0.52 eV due to the appearance of the $\text{NO}(A^2\Sigma^+,v)$ photodissociation product with a considerably slower appearance time of 0.7 ps. This difference in time scales between excited parent signal disappearance and product signal appearance was attributed to a two-step, likely non-adiabatic mechanism, rather than a direct photodissociation mechanism. This work showed that relying on parent ion yield measurements as a function of time in order to determine dissociation mechanisms and time scales may be potentially misleading, especially if non-adiabatic processes are involved.

In 1997 Radloff, Hertel, Jouvot, and co-workers introduced an important extension of TRPES. They applied the photoelectron–photoion coincidence (PEPICO) detection technique to fs pump–probe spectroscopy,^{79,80} allowing the dynamics of size-selected neutral clusters to be studied via TRPES. As an illustrative example, shown in Figure 5, these authors studied internal conversion dynamics in benzene and benzene dimers. They found that the decay of the S_2 to S_1 states was very rapid for both species (about 50 fs), whereas the $S_1 \rightarrow S_0$ IC decay was significantly faster in the monomer than in the dimer, 7.6 vs 100 ps. The same authors applied the PEPICO method to dynamics in ammonia clusters, investigating the dynamics of hydrogen transfer in electronically excited $(\text{NH}_3)_2$.⁸¹ By monitoring the PE signal associated with the $(\text{NH}_3)_2^+$ and NH_4^+ ions, they were able to sort out the rather complicated dynamics associated with this system, finding time constants of 170 fs for the decay of $(\text{NH}_3)_2^*$ to $\text{NH}_4^+\cdots\text{NH}_2$, and 4 ps for dissociation of the latter complex to $\text{NH}_4 + \text{NH}_2$.

3.2. Time-Resolved Photoelectron Angular Distributions

In 1989, Y. Fujimura and co-workers presciently considered the effects of Coriolis coupling on ps time-resolved photoelectron angular distributions (PADs) in a model system.⁸² These authors showed that *b*-axis Coriolis coupling leads to a *k*-coherence that is directly observable in the time-resolved PADs. In 1993, K. L. Reid independently proposed an approach to the study of excited-state dynamics through the use of time-resolved PADs.⁸³ Reid showed that the sensitivity of the PAD to the intermediate state alignment leads to evolution of the photoelectron angular distribution. Reid subsequently demonstrated this in a nanosecond-resolution experiment, using this time dependence to follow hyperfine depolarization in the $\text{NO}(A^2\Sigma^+)$ state.⁸⁴ These seminal studies opened up the possibility of using the other component of the electronic continuum—that of the free electron—as a probe of excited-state dynamics.

3.3. Theoretical Developments

In 1991, Seel and Domcke^{24,25} wrote pioneering theoretical papers on femtosecond TRPES and proposed how it could be applied to non-adiabatic dynamics in polyatomic molecules, using $S_2 \rightarrow S_1$ internal conversion (IC) dynamics in pyrazine as an example. These papers laid the foundation for the general application of fs TRPES to problems regarding excited-state non-adiabatic dynamics. Of particular significance, Domcke showed how the electronic structure of the molecular ionization continuum and the ionization correlations of the neutral configurations involved can be used to help understand the

non-adiabatic dynamics in the neutral excited state. In 1993, Meier and Engel⁸⁵ applied a treatment similar to Domcke's to TRPES of diatomic Na₂, predicting many of the features associated with coherent vibrational wave packet motion that were later observed experimentally. These authors expanded these studies in 1994, looking at opportunities for TRPES in the mapping of wave packet dynamics in double-welled potentials⁸⁶ and developing technically important approximation treatments of the photoionization dynamics, considerably simplifying the numerical task involved in computations.³⁰ In 1996, Meier and Engel studied the application of TRPES to non-adiabatic predissociation problems involving the coherent decay of sets of resonances,⁸⁷ complementing Stolow's 1996 experimental ion yield observation of these in the IBr molecule.⁸⁸ In 1997, Braun and Engel considered the role of initial temperature of the ground state in TRPES, using the hot cesium dimer as an example.⁸⁹ In 1998, Meier and Engel explicitly considered the important role of frequency chirp (i.e., the time ordering of frequencies in a broad bandwidth pulse) in fs TRPES experiments, relevant to the discussion of quantum coherent control in this area.⁹⁰

In 1997, T. Seideman developed a formal nonperturbative theory of time-resolved PADs.²⁶ This included exact (all orders) treatment of the matter-field interaction and included, in principle, the effects of both nuclear and electronic dynamics on PADs. This work laid the foundation for the development of a research program, beginning in 1999, by Seideman and co-workers on several aspects of time-resolved PADs.¹⁴

4. Experimental Methods

4.1. Photoelectron Spectroscopy of Neutrals and Anions

In any photoelectron spectroscopy measurement, the observables of interest are the electron kinetic energy (eKE) distribution and the photoelectron angular distribution (PAD). Spectrometers for femtosecond TRPES have modest energy resolution requirements as compared to modern standards for photoelectron spectrometers. The bandwidth (fwhm) of a Gaussian 100 fs pulse is $\sim 150 \text{ cm}^{-1}$. A pump-probe measurement involves the convolution of two such pulses, leading to an effective bandwidth of $\sim 25 \text{ meV}$. This limits the energy resolution required in measuring the energy of the photoelectrons. However, TRPES experiments are very data-intensive, as they require the collection of many photoelectron spectra. As a result, most neutral and all anion TRPES experiments performed to date make use of high-efficiency electron energy analyzers in which a large fraction of the photoelectrons are collected.

The analyzer most commonly used in TRPES experiments has been the magnetic bottle time-of-flight spectrometer.^{22,91} This technique uses a strong inhomogeneous magnetic field (1 T) to rapidly parallelize electron trajectories to a flight tube and a constant magnetic field (10 G) to guide the electrons to the detector.^{21,92} With careful design, the collection

efficiency of magnetic bottle spectrometers can exceed 50%, while maintaining an energy resolution essentially equivalent to the fs laser bandwidth. The highest resolution is obtained for electrons created within a small volume ($\phi < 100 \mu\text{m}$) at the very center of the interaction region. In contrast with ns laser experiments, however, it is not desirable to focus fs lasers to small spot sizes due to the inherent high intensity of such pulses, thus leading to multiphoton ionization. Longer focal lengths mean that the Rayleigh range (the "length" of the focus) extends well beyond the favorable region, leading in general to an overall lower resolution.

Magnetic bottle analyzers have been used in many neutral and anion TRPES experiments. They are relatively simple, have high collection efficiency and rapid data readout, and, importantly, permit straightforward photoelectron-photoion coincidence (PEPICO) measurements. Magnetic bottles suffer from the general disadvantage that they can only be used to determine eKE distributions; the complex electron trajectories in magnetic bottle analyzers make it impractical (if not impossible) to extract a PAD. There is an additional complication associated with the use of magnetic bottle analyzers in anion TRPES experiments. Mass-selected negative ion beams typically have laboratory kinetic energies of 1 keV or higher; hence, the velocity of the ion beam is no longer negligible compared to that of the photoelectrons. As a result, photoelectrons with the same speed in the center-of-mass frame of reference but scattered at different polar angles with respect to the ion beam will have different speeds in the laboratory frame.⁹³ This "Doppler broadening" significantly degrades the energy resolution of a high-efficiency analyzer with no angular resolution, such as a magnetic bottle, yielding eKE resolution as poor as several hundred millielectronvolts. This resolution is often sufficient for TRPES experiments but can be improved (with loss of signal) to several tens of millielectronvolts by pulsed deceleration of the ion beam, as has been demonstrated in several laboratories,^{37,94-96} or, as shown recently by Cheshnovsky,⁹⁷ by impulsive deceleration of the detached electrons.

These limitations of magnetic bottle analyzers may be overcome by the use of two-dimensional (2D) photoelectron imaging techniques, in which position-sensitive detection is used to measure the photoelectron kinetic energy and angular distributions simultaneously. When used, as is common, with CCD camera systems for image collection, one gives up rapid data readout, as multi-kilohertz readout of CCD chips is very challenging. This precludes the possibility of simple PEPICO measurements. The most straightforward 2D imaging technique is photoelectron velocity-map imaging (VMI),⁹⁸ a variant of the elegant photofragment imaging method developed by Chandler and Houston.⁹⁹ Photoelectron VMI was first demonstrated by Eppink and Parker for neutrals^{98,100} and by Bordas¹⁰¹ and Sanov¹⁰² for negative ions. Typically, a strong electric field projects nascent charged particles onto a microchannel plate (MCP) detector. The ensuing electron avalanche falls onto a phosphor screen, which is imaged by the CCD

camera. Analysis of the resultant image allows for the extraction of both energy- and angle-resolved information. In this case, a two-dimensional projection of the three-dimensional distribution of recoil velocity vectors is measured; various image reconstruction techniques^{103–105} are then used to recover the full three-dimensional distribution.

Photoelectron VMI thus yields close to the theoretical limit for collection efficiency, along with simultaneous determination of the photoelectron eKE and angular distributions. In addition, and of prime importance to anion studies, VMI eliminates the Doppler broadening observed with magnetic bottle analyzers, obviating the need for deceleration methods. In anion time-resolved photoelectron imaging (TRPEI) studies utilizing velocity-map imaging, the resolution limit closely approaches the laser bandwidth.

This 2D particle imaging approach may be used most straightforwardly when the image is a projection of a cylindrically symmetric distribution whose symmetry axis lies parallel to the two-dimensional detector surface. This requirement usually precludes the use of non-coincident pump and probe laser reference frames (i.e., other than parallel or perpendicular laser polarizations), a situation which may provide detailed information on intramolecular dynamics through the alignment dependence of the PAD. It may be preferable to adopt fully three-dimensional (3D) imaging techniques based upon “time-slicing”^{106,107} or full time- and position-sensitive detection,¹⁰⁸ where the full three-dimensional distribution is obtained directly without the introduction of mathematical reconstruction. In fs pump–probe experiments where the intensities must be kept below a certain limit (often leading to single-particle counting methods), “time-slicing” (which requires significant signal levels) may not be practical, leaving only full time- and position-sensitive detection as the option.

Modern MCP detectors can measure both spatial position (x, y) on the detector face and time of arrival (z) at the detector face.¹⁰⁸ In this situation, a weak electric field is used to extract nascent charged particles from the interaction region. Readout of the (x, y) position yields information about the velocity distributions parallel to the detector face, equivalent to the information obtained from 2D detectors. However, the additional timing information allows measurement of the third (z) component of the laboratory-frame velocity, via the “turn-around” time of the particle in the weak extraction field. Thus, these detectors allow for full 3D velocity vector measurements, with no restrictions on the symmetry of the distribution or any requirement for image reconstruction techniques. Very successful methods for full time- and position-sensitive detection are based upon interpolation (rather than pixellation) using either charge-division (such as “wedge-and-strip”)^{109,110} or crossed delay-line anode timing MCP detectors.^{111,112} In the former case, the avalanche charge cloud is divided among three conductors—a wedge, a strip, and a zigzag. The (x, y) positions are obtained from the ratios of the wedge and strip charges to the zigzag

(total) charge. Timing information can be obtained from a capacitive pick-off at the back of the last MCP plate. In the latter case, the anode is formed by a pair of crossed, impedance-matched delay lines (i.e., x and y delay lines). The avalanche cloud that falls on a delay line propagates in both directions toward two outputs. Measurement of the timing difference of the output pulses on a given delay line yields the x (or y) positions on the anode. Measurement of the sum of the two output pulses (relative to, say, a pickoff signal from the ionization laser or the MCP plate itself) yields the particle arrival time at the detector face. Thus, direct anode timing yields a full 3D velocity vector measurement. An advantage of delay line anodes over charge division anodes is that the latter can tolerate only a single hit per laser shot. This precludes the possibility of multiple coincidences, of interest in some experiments, and makes the experiment very sensitive to background, such as scattered UV light.

4.2. Photoelectron–Photoion Coincidence Methods

Photoionization (photodetachment) always produces two species available for analysis—the ion (neutral) and the electron. The extension of the photoelectron–photoion coincidence (PEPICO) technique to the femtosecond time-resolved domain was first demonstrated by Stert and Radloff and was shown to be very important for studies of dynamics in clusters.^{79,81} In these experiments, a simple yet efficient permanent magnet design “magnetic bottle” electron spectrometer was used for photoelectron time-of-flight measurements. A collinear time-of-flight mass spectrometer was used to determine the mass of the parent ion. Using coincidence electronics, the electron time-of-flight (yielding electron kinetic energy) is correlated with an ion time-of-flight (yielding the ion mass). In this manner, TRPES experiments may be performed on neutral clusters, yielding time-resolved spectra for each parent cluster ion (assuming cluster fragmentation plays no significant role). Signal levels must be kept low (much less than one ionization event per laser shot) in order to minimize false coincidences.

Time- and angle-resolved PEPICO measurements yielding photoion and photoelectron kinetic energy and angular correlations can shed new light on photodissociation dynamics in polyatomic molecules. As shown by Continetti and co-workers for the case of nanosecond laser photodetachment, correlated photofragment and photoelectron velocities can provide a complete probe of the dissociation process.^{113,114} The photofragment recoil measurement defines the energetics of the dissociation process and the alignment of the recoil axis in the laboratory frame, the photoelectron energy provides spectroscopic identification of the products, and the photoelectron angular distribution can be transformed to the recoil frame in order to extract vector correlations such as the photofragment angular momentum polarization. The integration of photoion–photoelectron timing imaging (energy and angular correlation) measurements with femtosecond time-resolved spectroscopy

was demonstrated, using timing imaging detectors, in 1999 by C. C. Hayden and co-workers^{115,116} at Sandia National Laboratories. This coincidence-imaging spectroscopy (CIS) method allows the time evolution of complex dissociation processes to be studied with unprecedented detail.

4.3. Femtosecond Laser Technology

The progress in femtosecond TRPES over the past 10 years derives from prior developments in femtosecond laser technology, since techniques for photoelectron spectroscopy have been highly developed for some time. There are several general requirements for such a femtosecond laser system. Most of the processes of interest are initiated by absorption of a photon in the wavelength range $\sim 200\text{--}350$ nm, produced via nonlinear optical processes such as harmonic generation, frequency mixing, and parametric generation. Thus, the output pulse energy of the laser system must be high enough for efficient use of nonlinear optical techniques and ideally should be tunable over a wide wavelength range. Another important consideration in a femtosecond laser system for time-resolved photoelectron spectroscopy is the repetition rate. To avoid domination of the signal by multiphoton processes, the laser pulse intensity must be limited, thus also limiting the available signal per laser pulse. As a result, for many experiments a high pulse repetition rate can be more beneficial than high energy per pulse. Finally, the signal level in photoelectron spectroscopy is often low in any case, and, for time-resolved experiments, spectra must be obtained at many time delays. This requires that any practical laser system must run very reliably for many hours at a time.

Modern Ti:sapphire-based femtosecond laser oscillators have been the most important technical advance for performing almost all types of femtosecond time-resolved measurements.¹¹⁷ Ti:sapphire oscillators are tunable over a 725–1000 nm wavelength range, have an average output power of several hundred milliwatts or greater, and can produce pulses as short as 8 fs, but more commonly 80–130 fs, at repetition rates of 80–100 MHz. Broadly tunable femtosecond pulses can be derived directly from amplification and frequency conversion of the fundamental laser frequency.

The development of chirped-pulse amplification and Ti:sapphire regenerative amplifier technology now provides millijoule pulse energies at repetition rates of >1 kHz with <100 fs pulse widths.¹¹⁸ Chirped-pulse amplification typically uses a grating stretcher to dispersively stretch fs pulses from a Ti:sapphire oscillator to several hundred picoseconds. This longer pulse can now be efficiently amplified in a Ti:sapphire amplifier to energies of several millijoules while avoiding nonlinear propagation effects in the solid-state gain medium. The amplified pulse is typically recompressed in a grating compressor.

The most successful approach for generating tunable output is optical parametric amplification of spontaneous parametric fluorescence or a white light continuum, using the Ti:sapphire fundamental or second harmonic as a pump source. Typically, an 800

nm pumped fs optical parametric amplifier (OPA) can provide a continuous tuning range of 1200–2600 nm.¹¹⁹ Noncollinear OPAs (NOPAs)¹²⁰ pumped at 400 nm provide microjoule-level $\sim 10\text{--}20$ fs pulses which are continuously tunable within a range of 480–750 nm, allowing for measurements with extremely high temporal resolution. A computer-controlled stepper motor is normally used to control the time delay between the pump and probe laser systems.

The development of femtosecond laser sources with photon energies in the vacuum ultraviolet (VUV, 100–200 nm), extreme ultraviolet (XUV, <100 nm), and beyond (soft X-ray) opens new possibilities for TRPES, including the preparation of high-lying molecular states, the projection of excited states onto a broad set of cation electronic states, and, in the soft X-ray regime, time-resolved inner-shell photoelectron spectroscopy. High harmonic generation in rare gases is a well-established and important method for generating fs VUV, XUV,¹²¹ and soft X-ray radiation.^{122–124} Harmonics as high as the ~ 300 th order have been reported, corresponding to photon energies in excess of 500 eV. Both pulsed rare gas jets and hollow-core optical waveguides^{123,125} have been used for high harmonic generation. Sorensen and co-workers¹²⁶ used the sixth harmonic (9.42 eV) of a Ti:sapphire laser (generated from the third harmonic of the Ti:sapphire second harmonic) as the pump pulse in TRPES experiments. Even higher harmonics (17th) have been incorporated into TRPES experiments by Leone and co-workers and used for time-resolved inner-shell photoelectron spectroscopy.^{127–129} As these techniques become more commonplace, the range of applicability of TRPES will be increased significantly.

Finally, it is worth noting that high harmonic generation provides the route to attosecond (10^{-18} s) pulse generation,^{130,131} generally producing wavelengths within the soft X-ray regime. Although in its infancy, the first TRPES experiments using attosecond pulses have been reported¹³² and were used to study inner-shell electronic dynamics in atoms¹³³ with sub-femtosecond time resolution. This provides a new and direct time domain approach to the study of electron correlation in atoms and molecules.

5. Applications

In the following sections, we review recent applications (1999–2003) of TRPES to problems in the dynamics of isolated molecules, anions, and their clusters.

5.1. Non-adiabatic Intramolecular Dynamics

As discussed in the Introduction, a natural application of TRPES is to problems in excited-state non-adiabatic coupling. Non-adiabatic dynamics involve a breakdown of the adiabatic (e.g., Born–Oppenheimer) approximation, which assumes that electrons “instantaneously” follow the nuclear dynamics. This approximation is exact, provided that the nuclear kinetic energy is negligible, and its breakdown is therefore uniquely due to the nuclear kinetic energy operator. Spin–orbit coupling, leading to intersystem crossing, is not a non-adiabatic process in this

sense: the Born–Oppenheimer states could be chosen to be the fully relativistic eigenstates and hence would be perfectly valid adiabatic states. Nevertheless, the description of intersystem crossing as a non-adiabatic process is seen in the literature, and we therefore include spin–orbit coupling problems in this section.

In 1998–1999, Stolow considered and experimentally investigated the use of Koopmans'-type correlations toward distinguishing states involved in non-adiabatic transitions and delineating the two limiting cases for Koopmans'-type correlations in TRPES experiments.^{41,42} Type I involves the neutral excited states α and β clearly correlating to different ion electronic continua, as suggested by Figure 3. As an example of Type I correlations, Stolow and co-workers considered ultrafast internal conversion in the linear polyene *all-trans*-2,4,6,8-decatetraene (DT). The first optically allowed transition in DT is S_2 (1^1B_u) \leftarrow S_0 (1^1A_g). The S_2 state is a singly excited configuration. The lowest excited state is the dipole-forbidden S_1 (2^1A_g) state, which arises from configuration interaction between singly and doubly excited A_g configurations. Non-adiabatic coupling, leading to ultrafast internal conversion from S_2 to S_1 , is promoted by b_u symmetry vibrational motions. As discussed in more detail elsewhere,^{39,41} the S_2 excited state electronically correlates with the D_0 (1^2B_g) ground electronic state of the cation. The S_1 state, by contrast, correlates predominately with the D_1 (1^2A_u) first excited state of the cation. As shown in Figure 4, a femtosecond pump pulse at 287 nm (4.32 eV) prepared the excited S_2 state at its vibrationless electronic origin. It then evolves into a vibrationally hot (~ 0.7 eV) S_1 electronic state via internal conversion. Using a 235 nm (5.27 eV) UV probe photon, the excited-state wave packet dynamics were probed. As the non-adiabatic coupling proceeds, the evolving electronic character of the wave packet alters the electronic photoionization channel, leading to large shifts in the time-resolved photoelectron spectrum.

The experimental photoelectron kinetic energy spectra in Figure 4 (bottom) reveal a rapid shift of electrons from an energetic peak ($\epsilon_1 = 2.5$ eV) to a broad, structured low-energy component (ϵ_2). The 2.5 eV band is due to ionization of S_2 into the D_0 ion state. The broad, low-energy band arises from photoionization of S_1 that correlates with the D_1 ion state. Its appearance is due to population of the S_1 state by internal conversion. Integration of the two photoelectron bands directly reveals the S_2 -to- S_1 internal conversion time scale of 386 ± 65 fs. It is important to note that these results contain more information than the overall (integrated) internal conversion time. The vibrational structure in each photoelectron band yields information about the vibrational dynamics, which promote and tune the electronic population transfer. In addition, it gives a direct view of the evolution of the ensuing intramolecular vibrational energy redistribution (IVR) in the "hot molecule" which occurs on the "dark" S_1 potential surface.⁴¹

In the other limiting case, Type II, the one-electron correlations, upon ionization, lead to the same cat-

ionic states. Stolow and co-workers went on to characterize the limiting cases of ionization correlations and to include, with important theoretical contributions from T. Seideman, the continuum electron as part of the final state description.¹³⁴ An example of Type II correlations is seen in the S_2 – S_1 internal conversion in the polyaromatic hydrocarbon phenanthrene (PH), discussed by Stolow and co-workers in more detail elsewhere.⁴² In the case of PH, both the S_2 and the S_1 states correlate similarly with the electronic ground state as well as the first excited state of the cation. In PH, the non-adiabatic coupling of the bright electronic state (S_2) with the dense manifold of zeroth-order S_1 vibronic levels leads to the nonradiative "decay" (dephasing) of the zeroth-order S_2 state. The energy gap between these two excited states is large, and the density of S_1 vibronic levels is extremely large compared to the reciprocal electronic energy spacing.

In this experiment, PH was excited from the S_0 1^1A_1 ground state to the origin of the S_2 1^1B_2 state with a 282 nm (4.37 eV) fs pump pulse and then ionized after a time delay Δt using a 250 nm (4.96 eV) probe photon. The S_2 1^1B_2 state rapidly internally converted to the lower lying S_1 1^1A_1 state at 3.63 eV, transforming electronic energy into vibrational energy. In PH, both the S_2 1^1B_2 and S_1 1^1A_1 states can correlate with the D_0 2^1B_1 ion ground state. The time-resolved photoelectron spectra for PH, shown in Figure 6, revealed a rapidly decaying but energetically narrow peak at $\epsilon_1 \approx 1.5$ eV due to photoionization of the vibrationless S_2 1^1B_2 state into the ionic ground state D_0 2^1B_1 , resulting in a decay time constant of 520 ± 8 fs. A broad photoelectron band, centered at about ~ 0.7 eV, in these photoelectron spectra was due to ionization of vibrationally hot molecules in the S_1 state, formed by the S_2 – S_1 internal conversion. At times $t > 1500$ fs or so (i.e., after internal conversion), the photoelectron spectrum is comprised exclusively of signals due to S_1 ionization. The S_1 state itself is long-lived on the time scale of the experiment. Despite the fact that Type II molecules present an unfavorable case for disentangling electronic from vibrational dynamics, in PH a dramatic shift in the photoelectron spectrum was seen as a function of time. This is due to the facts that PH is a rigid molecule and the S_2 , S_1 , and D_0 states all have similar geometries. The photoionization probabilities are therefore dominated by small Δv transitions. Hence, the 0.74 eV vibrational energy in the populated S_1 state should be roughly conserved upon ionization into the D_0 ionic state. Small geometry changes favor conservation of vibrational energy upon ionization and thereby permit the observation of the excited-state electronic population dynamics via a photoelectron kinetic energy analysis alone. In general, however, significant geometry changes will lead to overlapping photoelectron bands, hindering the disentangling of vibrational from electronic dynamics. As discussed below, time-resolved photoelectron angular distributions provide another view of electronically non-adiabatic processes, which may, in favorable situations, shed more light on this problem.

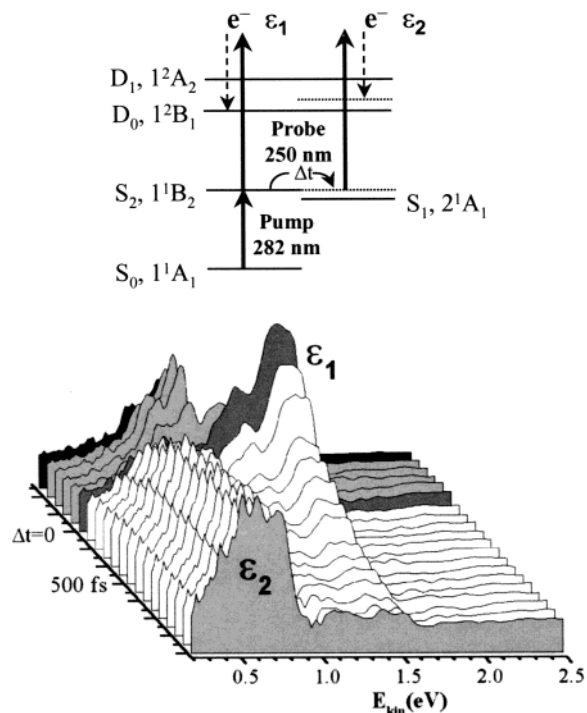


Figure 6. (Top) Energy level scheme for TRPES of phenanthrene, a molecule exhibiting Type II Koopmans' correlations. The pump laser prepares the optically bright state S_2 . Due to ultrafast internal conversion, this state converts to the lower-lying state S_1 with ~ 0.74 eV of vibrational energy. The expected corresponding Type II Koopmans' correlations are shown: $S_2 \rightarrow D_0 + e^-(\epsilon_1)$ and $S_1 \rightarrow D_0 + e^-(\epsilon_2)$. (Bottom) TRPES spectra of phenanthrene for a pump wavelength of 282 nm and a probe wavelength of 250 nm. The disappearance of the band ϵ_1 at ~ 1.5 eV and growth of the band ϵ_2 at ~ 0.5 eV represents a direct measure of the S_2 – S_1 internal conversion time (520 fs). Reprinted with permission from *Annual Reviews in Physical Chemistry* (<http://www.AnnualReviews.org>), ref 15. Copyright 2003 Annual Reviews.

The Koopmans' picture is a simplification of the ionization dynamics. Nevertheless, it provides a useful zeroth-order picture from which to consider the TRPES results. Any potential failure of this independent electron picture can always be experimentally tested directly through variation of the photoionization laser frequency—resonance structures should lead to variations in the form of the spectra with electron kinetic energy, although this effect is more likely to be prominent in PAD measurements.

In 1999, Suzuki and co-workers first applied their 2D photoelectron imaging method to the study of ps intersystem crossing (ISC) dynamics in the pyrazine S_1 1^1B_{3u} ($n\pi^*$) state and fs internal conversion in the S_2 1^1B_{2u} ($\pi\pi^*$) state.^{135,136} The importance of this method is that it allowed the determination of both energy and angular distributions. This work on ps ISC nicely complements the 1995 energy-resolved photoelectron studies of ISC dynamics in aniline and aminopyridines by Weber and co-workers.⁶⁷ The additional information provided by analysis of the PAD asymmetry parameters can be invaluable in determining the excited-state photophysical mechanisms. In their imaging experiments, Suzuki and co-workers prepared the excited state with a pump laser and used two-photon ionization as a probe. The S_1 state was

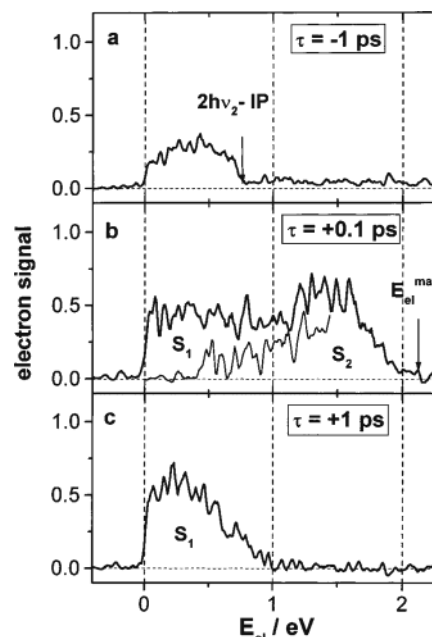


Figure 7. TRPES spectra of pyrazine pumped at 267 nm and probed at 200 nm. The S_2 and S_1 contributions can be deconvoluted. The ultrafast S_2 internal conversion occurs in about 20 fs, supporting earlier theoretical results. The S_1 state decays in 22 ps. Reprinted with permission from ref 137. Copyright 2000 American Institute of Physics.

seen to decay in ~ 100 ps. The S_2 state, lying about 7000 cm^{-1} above the S_1 origin, was also prepared with their pump pulses. As the lifetime of the pyrazine S_2 state is expected to be about 30 fs ^{24,25} and the reported time resolution in Suzuki's experiments was about 450 fs, these authors were able to observe the decay of the highly excited S_1 state formed by internal conversion. They report a lifetime of 22 ps for this and, for comparison, a lifetime of 39 ps for the perdeuterated pyrazine- d_4 molecule, also prepared at its S_2 origin. As in Weber's data, the buildup of the T_1 triplet state formed by the intersystem crossing was directly observed. The authors had initially assigned another peak in the energy-resolved spectrum to the T_2 triplet state, but this was corrected in a later publication. As Suzuki first demonstrated, the powerful combination of energy- and angle-resolved photoelectron spectra brings an important new tool into TRPES studies. The photoelectron angular distributions, which were extracted from these measurements, are discussed in a following section.

In 2000, Radloff and co-workers applied TRPES to the famous pyrazine S_2 lifetime problem,¹³⁷ connecting with Domcke's earlier calculations. Using short UV laser pulses (~ 130 fs), Radloff excited pyrazine S_2 with two different wavelengths: 200 (6.2 eV) and 196 nm (6.31 eV). To avoid the complications of intermediate resonances, dynamics were probed via single-photon ionization using pulses with wavelengths of 266.7 (4.66 eV) and 261.3 nm (4.75 eV), respectively. As shown in Figure 7, the photoelectron spectra vary significantly with time during the cross-correlation of the laser pulses. These changes are due to the ultrafast variation of the electronic character from $\pi\pi^*$ (S_2) to $n\pi^*$ (S_1), leading to a switching of the Koopmans'-type ionization correlations from the $D_1 A^2B_{1g}(\pi^{-1})$ to the $D_0 X^2A_g(n^{-1})$ cation electronic

states. By fitting the longer-lived components of the photoelectron spectra, Radloff and co-workers were able to deconvolute the S_2 photoelectron spectra and obtained a lifetime of 20 ± 10 fs for this state, confirming the theoretical estimates of Domcke. Interestingly, the S_2 photoelectron spectrum appears to show correlations with both the D_1 and D_0 cation states, although the D_1 contribution is dominant, as expected. This can be understood in terms of non-adiabatic coupling between the two cation states.¹³⁸ These experiments serve to show that, with careful dispersion management of fs UV pulses, extremely short time scale non-adiabatic processes may be directly observed.

In 2000, Stolow and co-workers investigated electronic relaxation rates in a series of simple linear α,β -enones: acrolein (i.e., propenal), methyl vinyl ketone (i.e., α -methylpropenal), and crotonaldehyde (i.e., γ -methylpropenal).¹³⁹ Excited at their S_2 ($\pi\pi^*$) origins, these molecules internally convert to the S_1 ($n\pi^*$) on ultrafast time scales (30–50 fs). As is well-known in aldehyde and ketone photophysics, the low-lying $n\pi^*$ state leads to ultrafast intersystem crossing rates and triplet photochemistry. The triplet product quantum yields depend on the competition, in the S_1 state, between intersystem crossing to triplets and internal conversion to the S_0 ground state. Very dramatic effects on the S_1 relaxation rates due to the location of the methyl group were observed: upon S_2 ($\pi\pi^*$) excitation, the S_1 – S_0 internal conversion rate in crotonaldehyde (γ -methyl) was ~ 5 times more rapid than the same in either methyl vinyl ketone (α -methyl) or acrolein (no methyl), the latter two having very similar S_1 – S_0 internal conversion rates. One might expect, in the Golden Rule sense, that the methyl substituent increases the density of vibrational states and therefore a faster decay rate obtains. The identical number of degrees of freedom in methyl vinyl ketone and crotonaldehyde suggests that vibrational density of states is not the dominant effect. The methyl effect on the torsional conical intersections at the C=C bond could be due to a change in diabatic vs adiabatic torsional dynamics at the conical intersection (an inertial effect due to the lowering of the torsional frequency upon methylation) and, possibly, to a subtle re-ordering of the conical intersections upon methylation (an electronic effect).¹⁴⁰ The methyl group effect on C=C conical intersections seen in the α,β -enones is of general interest because it illustrates how simple substitutions could be used to provide an important new type of control over the electronic branching ratios.¹³⁹

In 2001, G. Gerber, A. H. Zewail, T. Baumert, and co-workers studied the famous *cis*-stilbene photoisomerization problem using a combination of mass spectrometry and magnetic bottle TRPES.¹⁴¹ Zewail and co-workers had previously determined the S_1 lifetime to be 320 fs when the molecule was excited with a 285 nm pump pulse.¹⁴² In this study, a 267 nm pump pulse excited the molecule to the S_1 state. A 400 nm probe pulse was used for two-photon ionization of the excited-state wave packet. The results indicated that two long-lived photoproducts were formed.

In 2001, Soep, Mestdagh, Visticot, and co-workers applied fs–ns time scale spectroscopies to study excited-state dynamics in tetrakis(dimethylamino)ethylene (TDMAE) over a wide range of time scales: from femtosecond to picosecond to nanosecond.¹⁴³ Using a combination of fluorescence, ion, and photoelectron detection schemes, the authors followed the complete evolution of the excited states. Pump–probe measurements were performed at 200, 266, and 400 nm excitation wavelengths, with the Ti:sapphire fundamental (800 nm) used as the probe color. The TDMAE molecule has an unusually low ionization potential of 5.5 eV. At 200 nm excitation, strong fragmentation of the parent ion was observed. At 266 nm pump, the TRPES results showed significant variation. At zero time delay, a sharp peak near zero electron kinetic energy is observed. By 300 fs, this becomes a double-peaked structure with maxima near 0 and 0.8 eV. The decay of the sharp peak and the growth of the 0.8 eV peak were commensurate, with a time constant of ~ 300 fs. At 400 nm pump, a cross-correlation signal was observed, indicative of an extremely fast or nonresonant process, followed by a small but slowly decaying pedestal. At 266 nm, the dynamics were interpreted in terms of a transition to a low-lying Rydberg state plus the $\pi\pi^*$ valence state. By analogy with ethylene, the 300 fs time scale was assigned to the C–C twist upon approach to the N–V states' conical intersection. Subsequent formation of the zwitterionic $\pi^*\pi^*$ Z state was inferred. This example is important because it shows the connection of the fs TRPES results with the longer time scale fluorescence measurements in order to determine the dynamics over multiple time scales.

In 2001, Radloff and co-workers applied the time-resolved PEPICO technique to the internal conversion dynamics of toluene and the toluene dimer.¹⁴⁴ These were excited to a vibrationally excited state within the S_2 manifold via 150 fs pump pulses at 202 nm (6.14 eV), followed by fs single-photon ionization at 267 nm. Toluene makes an interesting comparison with the earlier time-resolved PEPICO studies of benzene monomer and dimer^{79,80} due to its lower symmetry. Both toluene monomer and dimer S_2 states were observed to decay with a time constant of ~ 50 fs. Time-resolved photoelectron spectra coincident with the toluene dimer are shown in Figure 8. The rapid decay of the S_2 state and the formation of the long-lived S_1 state can be seen. By analogy with benzene, the very high S_2 internal conversion rates were attributed to a conical intersection near the S_2 origin, leading to the formation of vibrationally excited S_1 states. This S_1 lifetime in the toluene monomer was determined to be 4.3 ps. Surprisingly, in the toluene dimer, the lifetime of the vibrationally excited S_1 state was greater than 100 ps. Furthermore, despite the large internal energy, little fragmentation of the dimer was observed. This suggests that the S_1 vibrational dynamics involve intramolecular dynamics that have very poor coupling to the intermolecular vibrations.

In 2001, Suzuki and co-workers applied the time-resolved 2D imaging technique to their continuing studies of pyrazine excited-state dynamics.¹⁴⁵ In that

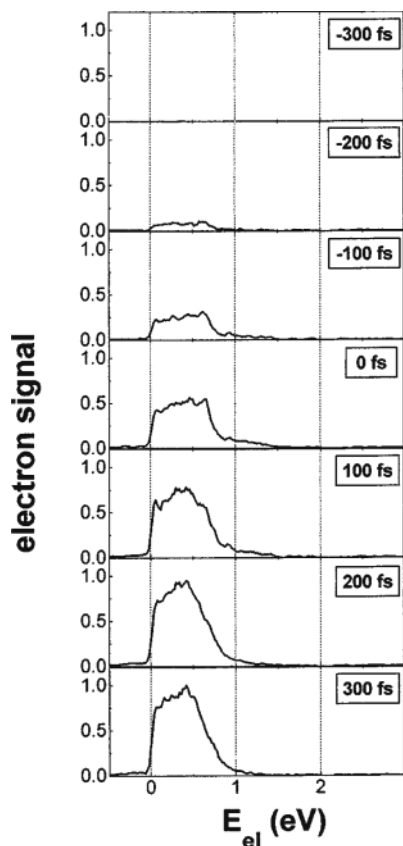


Figure 8. Time-resolved PEPICO spectra of toluene dimer with $\lambda_{\text{pump}} = 202$ nm and $\lambda_{\text{probe}} = 269$ nm, showing vibrational structure. The ultrafast S_2 internal conversion occurs in ~ 50 fs for both monomers (not shown) and dimers. By contrast, the S_1 internal conversion takes only 4.3 ps for the monomer but > 100 ps for the dimer. Again, the PEPICO technique allows complete separation of these channels. Reprinted with permission from ref 144. Copyright 2001 American Chemical Society.

paper, the authors investigated in detail the spectroscopy and dynamics of the 3s and 3p Rydberg states involved in their previous two-probe photon ionization studies of the pyrazine S_1 state.¹³⁵ Through variation of the pump laser wavelength from 401 to 330 nm, series of singlet $3s(\pi^{-1})$, triplet $3s(n^{-1})$, and triplet $3pA(n^{-1})$ Rydberg states with sub-ps lifetimes were observed. As discussed in a following section, the time-resolved photoelectron angular distributions (PADs) and their variation with pump-probe polarization geometry were cleanly observed via the 2D imaging method, and this provided essential information on the state assignments. This work also nicely illustrates the importance of understanding the variety of laboratory-frame alignment effects that can occur in TRPES experiments on excited states of polyatomic systems.

In 2001, G. Stock and co-workers developed a new computational scheme for the efficient calculation of fs TRPES spectra in polyatomic molecules.¹⁴⁶ To avoid the “costly” discretization of the ionization continuum, these authors made use of the fact that the ionization yield at a fixed photoelectron energy is formally equivalent to the transient absorption spectrum into a single excited electronic state. Use was then made of a new convolution scheme for the

rapid calculation of the transient absorption spectra.¹⁴⁷ These authors applied their scheme to the four-mode vibronic coupling problem in S_2 pyrazine, including three neutral states (S_2 , S_1 , and S_0) and two ionic states (D_0 and D_1), and treated the finite duration of the laser pulses in a numerically exact manner. Compared with the earlier work of Domcke,^{24,25} this work included new ab initio data, incorporated another vibrational mode (ν_{9a}) known to be important in the dynamics, and explicitly included D_0 – D_1 vibronic coupling in the cation states. To model the experimental results of Radloff and co-workers,¹³⁷ pulse durations of 100 fs were chosen. The simulations reproduced the ~ 20 fs time scale for the internal conversion and showed a significant red shift of the photoelectron spectrum, reflecting the vibrational energy redistribution in the S_1 state. A comparison of the calculated vs experimental photoelectron spectra showed that the simulations were missing the low-energy photoelectrons seen in the experiments. It was suggested that these could originate from the autoionization of Rydberg states. This work is important because it opens up new methods for the direct comparison of experimental with theoretical TRPES in real polyatomic systems.

In 2002, K. L. Reid and co-workers presented a ps TRPES study of intramolecular dynamics in S_1 *p*-fluorotoluene (pFT).¹⁴⁸ These researchers emphasized the importance of the vibrational energy resolution obtainable with ps pulses for the study of intramolecular vibrational energy redistribution (IVR). As compared with *p*-difluorobenzene (pDFB), pFT exhibits anomalous IVR “lifetimes”: at ~ 2000 cm^{-1} excess energy in S_1 , the IVR “lifetimes” are 150 and 3.5 ps for pDFB and pFT, respectively.¹⁴⁹ The methyl group internal rotation was thought to play an important role in this effect. In these TRPES studies, an excess S_1 vibrational energy of 1200 cm^{-1} was employed. Photoelectron spectra recorded at 5, 10, 30, and 60 ps time delays showed deterioration in the resolvable vibrational structure, particularly at higher ion internal energies. This evolution was attributed to IVR in the S_1 manifold and supported the previous chemical timing studies of Parmenter.¹⁴⁹ The well-resolved vibrational structure in the photoelectron spectra should permit further analysis in terms of vibrational energy flow models.

In 2002, A. Stolow, I. C. Chen, and co-workers studied substituent effects in electronic relaxation dynamics using a series of monosubstituted benzenes as model compounds.¹⁵⁰ They focused on the first and second $\pi\pi^*$ states of these aromatic systems and on substituents which were expected to have electronic effects. Six benzene derivatives were studied: benzaldehyde (BZA), styrene (STY), indene (IND), acetophenone (ACP), α -methylstyrene (α -MeSTY), and phenylacetylene (ϕ ACT). This choice of substituents addressed several points: (i) the effect of the substituent on the electronic states and couplings; (ii) the effect of the substituent on the rigidity or floppiness of the molecular frame; (iii) a comparison of Type I with Type II Koopmans’ systems; and (iv) the potential effects of autoionization resonances (i.e., non-Koopmans’ behavior) on the observed dynamics.

Three electronically distinct substituents were chosen: C=O, C=C, and C≡C. For the C=C, potential off-axis conjugation effects with the ring in STY were contrasted with the lack of these in the C≡C of ϕ ACT. For the heteroatomic substituent C=O, the influence of the additional $n\pi^*$ state on the $\pi\pi^*$ dynamics was investigated by comparing BZA with STY and ACP with α -MeSTY. The effects of vibrational dynamics and densities of states on the electronic relaxation rates were studied via both methyl ("floppier") and alkyl ("more rigid") ring substitution: STY was compared with both the floppier α -MeSTY and the much more rigid IND; BZA was compared with the floppier ACP. Both BZA and ACP have Type I Koopmans' ionization correlations, and the rest have Type II correlations, allowing for another comparison of these two cases. To investigate the potential effects of autoionization resonances, these authors varied the ionization probe photon energy significantly (~ 0.4 eV). In these systems, the form of the photoelectron spectra and the fits to the lifetime data were invariant with respect to probe laser frequency.

A sample TRPES spectrum, STY at $\lambda_{\text{pump}} = 254.3$ nm and $\lambda_{\text{probe}} = 218.5$ nm, is shown in Figure 9 (top). The $S_1(\pi\pi^*)$ component grows in rapidly, corresponding to the ultrafast internal conversion of the $S_2(\pi\pi^*)$ state. The $S_1(\pi\pi^*)$ component subsequently decays on a much longer ps time scale. It can be seen that, despite STY being an unfavorable Type II case, the two bands are well enough resolved to allow for unambiguous separation of the two channels and determination of the sequential electronic relaxation time scales. Energy integration over each band allows for extraction of the electronic relaxation dynamics. The time-dependent $S_2(\pi\pi^*)$ 0^0 photoelectron band integral yields for STY are also shown in Figure 9 (bottom, a). The open circles represent the pump-probe cross-correlation (i.e., the experimental time resolution) at these wavelengths. Integration over the $S_2(\pi\pi^*)$ 0^0 photoelectron band is shown as the solid circles. The solid line is the best fit to the $S_2(\pi\pi^*)$ channel, yielding a lifetime of 52 ± 5 fs. In Figure 9 (bottom, b), the time-dependent $S_1(\pi\pi^*)$ photoelectron band integral yields for STY are shown, obtained from a fit to the long delay part of the data, yielding a lifetime of 88 ± 8 ps for the state $S_1(\pi\pi^*)$. Overall, these results and the results obtained for the other five substituted benzenes demonstrate that the TRPES method is well-suited to the quantitative study of electronic relaxation processes, producing facile, direct, and accurate measurements of electronic relaxation rates that are in quantitative agreement with the currently accepted understanding of aromatic photophysics.

In 2003, Suzuki and co-workers applied the time-resolved 2D imaging method to the study of pyridazine excited-state dynamics.¹⁵¹ These authors pumped pyridazine to its $S_1(n\pi^*)$ origin and probed via resonant two-photon ionization, obtaining a lifetime of 323 ps attributed to internal conversion. Measured lifetimes were a strong function of S_1 excess vibrational energy, decreasing from 323 ps at the origin to 235, 181, and 123 ps at 300, 900, and 1900 cm^{-1} excess energy, respectively. The photo-

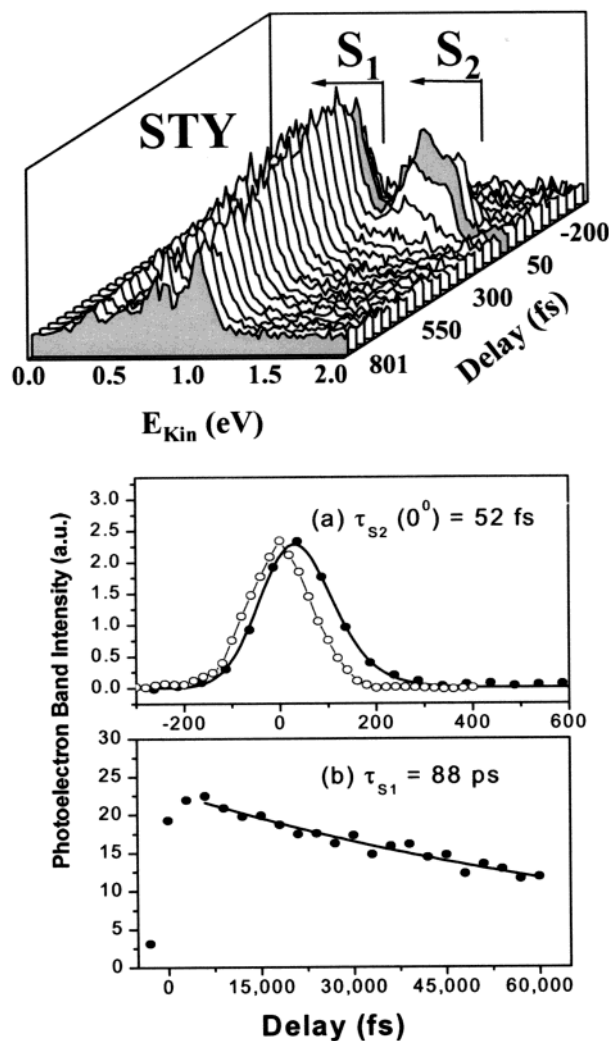


Figure 9. (Top) TRPES spectrum shown for styrene (STY) with $\lambda_{\text{pump}} = 254.3$ nm and $\lambda_{\text{probe}} = 218.5$ nm. The energetics and IP allow for assignment of the photoelectron bands to ionization of $S_2(\pi\pi^*)$ and $S_1(\pi\pi^*)$, as indicated. The S_2 state decays on ultrafast time scales. The S_1 state decays on a much longer (ps) time scale. (Bottom) (a) Time-dependent $S_2(\pi\pi^*)$ 0^0 photoelectron band integral yields for STY, yielding a decay time constant of 52 fs. Open circles represent the laser cross-correlation at these wavelengths. (b) Time-dependent $S_1(\pi\pi^*)$ photoelectron band integral yields for STY obtained from a fit to the long time delay part of the data (not shown). Reprinted with permission from ref 150. Copyright 2002 American Chemical Society.

electron imaging method allowed identification of the intermediate states resonances as $3s(n^{-1})$ and $3p(n^{-1})$ Rydberg series. In contrast with the earlier studies of excited-state dynamics in pyrazine,¹⁴⁵ pyridazine interestingly showed no evidence of intersystem crossing dynamics (i.e., no triplet-state formation). Analysis of the PADs indicated mostly p-wave emission from the $3s$ state, whereas the $3p$ photoemission was comprised of a mixture of partial waves. Careful analysis determined the term values of the $3s$ and $3p$ series to be 5.69 ± 0.03 and 6.28 ± 0.04 eV, respectively. This work demonstrates the quantitative accuracy of the photoelectron imaging method in the study of excited Rydberg states in polyatomic molecules.

5.2. Excited-State Intramolecular Proton Transfer

Excited-state intramolecular proton transfer (ESIPT) processes are important for both practical and fundamental reasons.¹⁵² *o*-Hydroxybenzaldehyde (OHBA) is the simplest aromatic molecule displaying ESIPT and serves as a model system amenable to comparison with theory. Stolow and co-workers used fs TRPES to study ESIPT in OHBA, monodeuterated ODBA, and an analogous two-ring system, hydroxy-acetonaphthone (HAN), as a function of pump laser wavelength, tuning over the entire enol $S_1(\pi\pi^*)$ absorption band of these molecules.^{153,154} The experimental scheme is depicted in Figure 10 (top), showing energetics for the case of OHBA. Excitation with a tunable pump laser $h\nu_{\text{pump}}$ forms the enol tautomer in the $S_1(\pi\pi^*)$ state. ESIPT leads to ultrafast population transfer from the S_1 enol to the S_1 keto tautomer. On a longer time scale, the S_1 keto population decays via internal conversion to the ground state. Both the enol and keto excited-state populations are probed by ionization with a probe laser $h\nu_{\text{probe}}$, producing the two photoelectron bands ϵ_1 and ϵ_2 .

In Figure 10 (bottom) are TRPES spectra of OHBA at an excitation wavelength of 326 nm. Two photoelectron bands, ϵ_1 and ϵ_2 , with distinct dynamics were observed. Band ϵ_1 is due to photoionization of the initially populated S_1 enol tautomer, and band ϵ_2 is due to the photoionization of the S_1 keto tautomer. The decay of band ϵ_1 yields an estimated upper limit of 50 fs for the lifetime of the S_1 enol tautomer. In experiments with ODBA, no isotope effect was observed, suggesting that the barrier in the OH stretch coordinate must be very small or nonexistent, consistent with ab initio calculations.^{155,156} As is common in TRPES, these spectra also give insights into the dynamics on the “dark” S_1 keto state. The picosecond decay of band ϵ_2 corresponds to S_1 keto internal conversion to the ground state. The wavelength-dependent S_1 keto internal conversion rates in OHBA and ODBA likewise revealed no significant isotope effect. The measured internal conversion rates are very fast (1.6–6 ps over the range 286–346 nm), considering the large energy gap of 3.2 eV between the ground and excited states. One possibility is that fast internal conversion in such systems is due to an efficient conical intersection involving a $\pi\sigma^*$ state and large-amplitude hydroxy H-atom motion.^{155,156} The observed absence of an isotope effect on S_1 keto internal conversion in ODBA does not support this mechanism. Rather, the comparison with internal conversion rates in HAN suggests that interactions with a nearby $n\pi^*$ state may play an important role in the keto internal conversion, as discussed in detail elsewhere.¹⁵³ This example serves to illustrate how TRPES can be used to study the dynamics of biologically relevant processes such as ESIPT and that it reveals details of both the proton-transfer step and the subsequent dynamics in the “dark” state formed after the proton transfer.

Related to ESIPT, *intermolecular* hydrogen-transfer reactions in ammonia^{157,158} and indole–ammonia¹⁵⁹ clusters have been studied in detail by Radloff and co-workers using time-resolved PEPICO methods. In a combined experimental–theoretical study

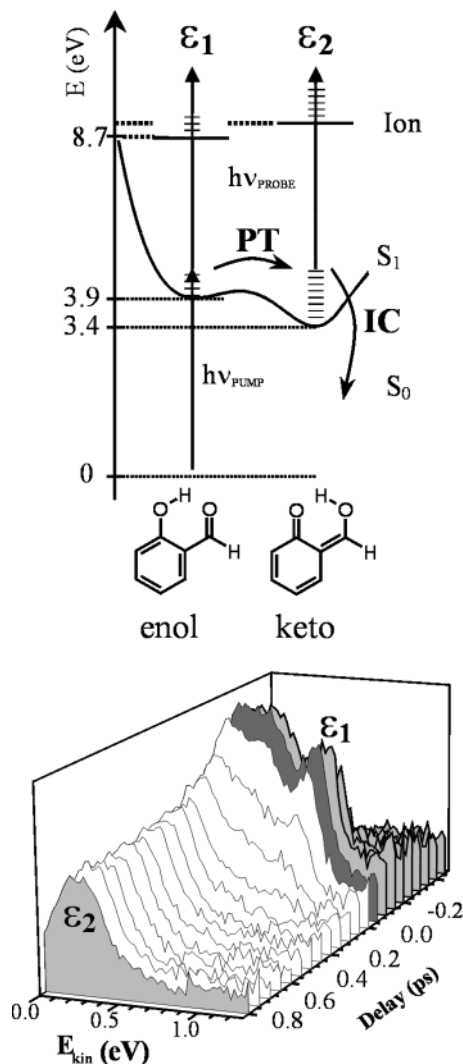


Figure 10. (Top) Energetics for excited-state proton transfer in OHBA, showing the enol and keto forms. Excitation with a pump laser $h\nu_{\text{pump}}$ forms the enol tautomer in the $S_1(\pi\pi^*)$ state. ESIPT leads to ultrafast population transfer from the S_1 enol to the S_1 keto tautomer. On a longer time scale, the keto S_1 population decays via internal conversion to the keto ground state. Both the enol and keto excited-state populations are probed via ionization with a probe laser $h\nu_{\text{probe}}$, producing the two photoelectron bands ϵ_1 and ϵ_2 . (Bottom) TRPES spectra of OHBA at an excitation wavelength of 326 nm and a probe laser wavelength of 207 nm. Two photoelectron bands were observed: ϵ_1 due to ionization of the S_1 enol, and ϵ_2 due to ionization of the S_1 keto. Band ϵ_1 was observed only when the pump and probe laser beams overlapped in time, indicating a sub-50 fs time scale for the proton transfer. Band ϵ_2 displayed a wavelength-dependent lifetime in the picosecond range, corresponding to the energy-dependent internal conversion rate of the dark S_1 keto state formed by the proton transfer. Reprinted with permission from ref 154. Copyright 2001 American Institute of Physics.

of the 200 nm excitation of the ammonia dimer, Radloff observed that the $(\text{NH}_3)_2 \tilde{A}$ state evolves into the $\text{NH}_4\text{--NH}_2$ complex via hydrogen transfer.¹⁵⁷ The time-resolved photoelectron spectra coincident with the dimer cation show a dramatic change from a broad (>1 eV) band at short times (100–500 fs) to a much narrower and lower energy band by 2–4 ps. By contrast, the time-resolved photoelectron spectra coincident with the NH_4^+ cation show broad features

that do not evolve much with time. These were attributed to fragmentation of vibrationally excited $(\text{NH}_3)_2^+$ cations and are therefore complementary to the photoelectron spectra of the bound dimer cations. The results were interpreted in terms of a model in which the initially excited $(\text{NH}_3)_2 \tilde{\text{A}}$ state proceeds via N–N stretching to a conical intersection with the charge-transfer state $\text{NH}_4^+\text{NH}_2^-$, leading to NH_4-NH_2 products. The narrowing of the photoelectron bands with time was attributed to the shorter progressions expected for the $\text{NH}_4-\text{NH}_2 \rightarrow \text{NH}_4^+\text{NH}_2 + e^-$ ionization channel, as opposed to the longer progressions expected for the $(\text{NH}_3)_2 \tilde{\text{A}} \rightarrow (\text{NH}_3)_2^+ + e^-$ channel.

Radloff and co-workers subsequently extended their PEPICO studies to larger ammonia clusters as well as deuterated clusters¹⁵⁸ using a sophisticated three-pulse arrangement. The probing of the hydrogen-transfer state, prepared by 200 nm excitation, was mediated by a near-infrared (832, 1200, or 1400 nm) control pulse which excited this state to a higher electronically excited state, which could then be ionized by a delayed fs 400 nm pulse. This helped to differentiate the initially excited $\tilde{\text{A}}$ state, which decays in 180–270 fs, from the longer-lived (ps) H-transfer state. The excited-state dynamics of the 200 nm excited $(\text{NH}_3)_3 \tilde{\text{A}}$ trimer was very different from that of the dimer. Using an 832 nm control pulse, the $(\text{NH}_3)\text{NH}_4(3\text{p})\text{NH}_2$ state was observed to have a lifetime of 2.7 ps, which upon deuteration lengthened to 32 ps. The lifetime of the H-transfer state decreased dramatically with cluster size, diminishing to ~ 150 fs for the hexamer $(\text{NH}_3)_6$. In contrast to the dimer, these results suggest a fast internal conversion mechanism in which the $(\text{NH}_3)\text{NH}_4(3\text{p})\text{NH}_2$ state decays to a lower-lying $(\text{NH}_3)\text{NH}_4(3\text{s})\text{NH}_2$ state, which then rapidly dissociates.

Indole, the chromophore of tryptophan, is a very important model system for studying biomolecule photophysics. Calculations of the isolated molecule and indole–water clusters suggest that a low-lying $\pi\sigma^*$ state, populated via internal conversion from the initially excited $\pi\pi^*$ state, plays a crucial role in the photophysics.^{160,161} Radloff and co-workers applied the time-resolved PEPICO method to study photo-induced H-transfer in indole– $(\text{NH}_3)_n$ clusters.¹⁵⁹ Complex dynamics involving internal conversion, hydrogen transfer, rearrangement, and dissociation were discerned, with different observations for small ($n = 1-3$) as opposed to larger ($n > 4$) clusters. Inspired by theory, an ultrafast $\pi\pi^* \rightarrow \pi\sigma^*$ internal conversion model was used to interpret the results. For the smaller clusters ($n = 1-3$), the internal conversion (time scale of ~ 150 fs) was followed by H-transfer, leading to a structural rearrangement on the tens to hundreds of ps time scale. A minor but competing dissociative channel operating on the 80–140 ps time scale was also observed. In the larger clusters ($n > 4$), the initial ultrafast internal conversion was not seen, likely due to unfavorable Franck–Condon factors. Nevertheless, structural rearrangements subsequent to H-transfer were observed. These results illustrate how time-resolved PEPICO can add a valuable new dimension to the study of complex

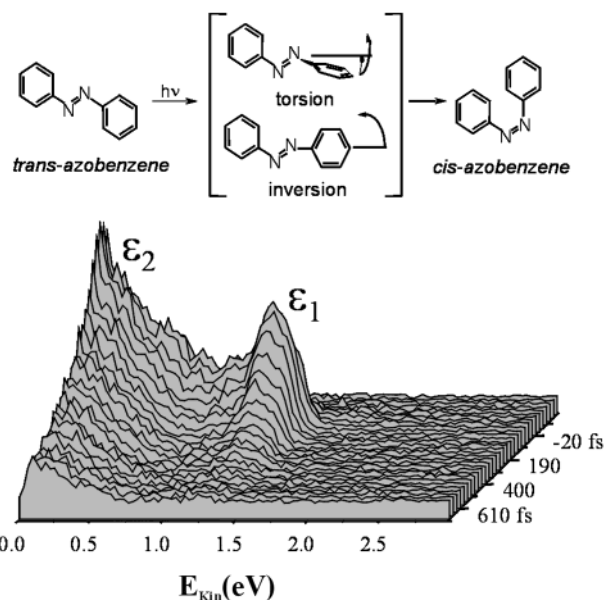


Figure 11. (Top) Photoisomerization dynamics of *trans*- to *cis*-azobenzene, indicating torsional and inversion pathways. (Bottom). TRPES spectra of *trans*-azobenzene excited at 330 nm and probed at 207 nm. Two photoelectron bands, ϵ_1 and ϵ_2 , were observed, having identical laser-limited rise times but differing decay rates ($\tau_1 = 130$ fs, $\tau_2 = 410$ fs) and differing Koopmans' ionization correlations. These results indicate that there is a previously unrecognized $\pi\pi^*$ state, S_3 , involved in the dynamics, suggesting a new model of *trans*-azobenzene photoisomerization dynamics. Reprinted with permission from ref 162. Copyright 2003 American Chemical Society.

competing reaction and electronic relaxation channels in molecular clusters.

5.3. Photophysics of Model Molecular Switches

Active molecular-scale electronics⁹ involves the use of molecules as transistors, switches, modulators, etc. and requires a dynamical process, which couples changes in optical or electrical properties to molecular rearrangements such as isomerization. As optical or electrical properties are governed by the electronic wave function and molecular rearrangements are vibrational in character, the underlying physical process in molecular electronic switches is the non-adiabatic coupling of electronic with vibrational motions. It is the competition between fast molecular electronic processes—some desired, some not—which will govern the efficiency and stability of active molecular-scale electronic devices, and therefore the rational design of such devices should include considerations of excited-state non-adiabatic processes.

Stolow and co-workers applied the TRPES method to the study of electronic relaxation in *trans*-azobenzene (AZ),¹⁶² often considered the prototypical fast molecular electronic switch as its photoisomerization¹⁶³ is the basis for numerous functional materials. Despite this great interest in azobenzene, the basic photoisomerization mechanism remained disputed:¹⁶⁴ in contrast to the expectations of Kasha's rule, the isomerization quantum yields decrease rather than increase with increasing photon energy. In Figure 11 (top), the two possible isomerization channels, pro-

ceeding via either a planar pathway (“inversion”) or a nonplanar, twisted pathway (“torsion”), are shown. Previous studies determined that isomerization in the first excited state, S_1 , proceeds along the inversion coordinate.¹⁶³ The second excited state, S_2 , is generally thought to be the $N=N$ analogue of the $C=C \pi\pi^*$ state in stilbene, and it is thought that, somehow, motion along the torsional coordinate in S_2 is responsible for the observed reduction in isomerization yield. Recent time-resolved studies suggested that photoisomerization proceeds via the inversion coordinate in S_1 . The role of the torsional isomerization pathway remains controversial. Theoretical studies have supported both torsion and inversion pathways but disagreed on the states involved in the excited-state relaxation.

In Figure 11 (bottom), a time-resolved photoelectron spectrum for excitation of AZ to the origin of its S_2 state is shown.¹⁶² Two photoelectron bands, ϵ_1 and ϵ_2 , with differing lifetimes and differing Koopmans' correlations were observed. Due to these two differences, the ϵ_1 and ϵ_2 bands must be understood as arising from the ionization of two different electronic states. Furthermore, as both bands rise within the laser cross-correlation, they are due to direct photoexcitation from S_0 and not to secondary processes. Therefore, to account for different lifetimes, different Koopmans' correlations, and simultaneous excitation from S_0 , the existence of an additional state, S_3 , which overlaps spectroscopically with S_2 must be invoked.¹⁶² According to the Koopmans' analysis (based upon assignment of the photoelectron bands) and to high-level, large active space complete active space self-consistent field (CASSCF) calculations, this new state S_3 corresponds to $\pi\pi^*$ excitation of the phenyl rings.¹⁶² The π^* excitation in the ring does not directly “break” the $N=N$ bond and therefore is expected to lead to reduced isomerization quantum yields. This mechanism differs greatly from that of all earlier models in that those always assumed that a single bright state, the S_2 ($N=N \pi\pi^*$) state, exists in this wavelength region.¹⁶² This example shows how TRPES can be used to study competing electronic relaxation pathways in a model molecular switch, revealing hidden yet highly important electronic states that can be very hard to discern via conventional means.

5.4. Superexcited States

As discussed above, for a single active electron, photoionization transitions are restricted to molecular orbitals containing an electronic configuration differing only by a single-electron vacancy. In the outer valence region (i.e., within a few electronvolts of the IP), two-electron transitions are rare but can occur, usually weakly, because of electron correlation.²³ This situation, however, can potentially change when an intermediate resonance is introduced. An intermediate state can have very different ionization correlations than the ground state. A possible outcome of this is the preparation of “superexcited” valence states: highly excited valence (as opposed to Rydberg) states lying above the IP. From the point of view of TRPES, superexcited states complicate the understanding of ionization correlations, PADs, and

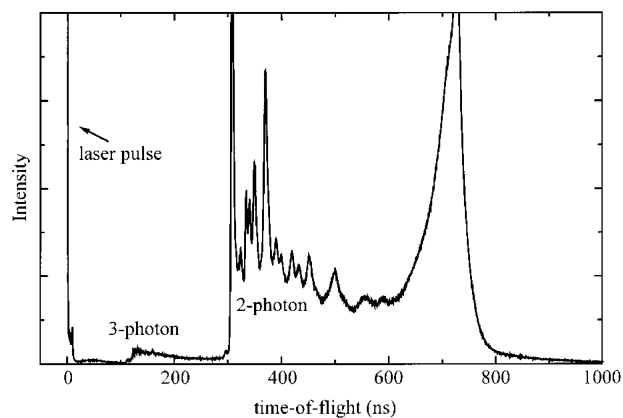


Figure 12. Photoelectron spectrum of phenol using 180 fs, 275 nm laser pulses. Processes due to both two-photon and three-photon ionization are observed, the latter arising from preparation and subsequent ionization of a superexcited valence state. This decays on ultrafast time scales to Rydberg manifolds, yielding characteristic structures. Reprinted with permission from ref 165. Copyright 2001 American Chemical Society.

Franck–Condon analysis. Therefore, the extent to which such states contribute to the ionization dynamics is worthy of consideration. In particular, in 2001, P. Weber and co-workers investigated the role of superexcited states in the fs multiphoton photoelectron spectroscopy of the S_1 and S_2 states of phenol^{165,166} and the S_2 state of 1,3-cyclohexadiene.¹⁶⁷

As an illustration of effects due to superexcited states, Weber and co-workers excited phenol to the S_1 level, whereupon a second photon excited it to a total energy of 9 eV, about 0.5 eV above the IP.¹⁶⁵ In Figure 12, a photoelectron spectrum is shown for fs laser ionization of phenol at 275 nm, via the S_1 state. While the major features can be readily explained in terms of the well-known two-photon photoelectron spectrum, a small peak is seen at higher electron kinetic energies due to three-photon ionization. Weber and co-workers have examined this small three-photon signal in considerable detail for both phenol and cyclohexadiene. This signal is characterized in terms of a superexcited valence state prepared by two pump laser photons. Superexcited states are often very short-lived and can decay via autoionization, internal conversion to Rydberg series, and neutral dissociation. In these experiments, the superexcited complex was ionized by a third time-delayed laser pulse. As long as autoionization is a minor channel, the two-photon photoelectron spectrum may be interpreted in the conventional manner. Analysis of the three-photon spectrum requires, as Weber and co-workers show, considerable care. Their two-color, three-photon photoelectron spectra are composed of multiple overlapping components with varying lifetimes. Many of these were assigned to Rydberg series, and two clear series could be assigned to quantum defects of 0.80 and 0.32, respectively, associated most likely with a ground-state core. The authors suggest that the primary superexcited state is a valence state due to the promotion of two electrons from the HOMO to the LUMO: in other words, the S_1 state must resonantly absorb the same photon as that used for the resonant $S_0 \rightarrow S_1$ transition.

Weber subsequently studied superexcited states in phenol prepared via the S_2 state.¹⁶⁶ In this case, polarization and orbital energy studies suggest a superexcited state also at 9 eV but with a configuration due to single-electron excitation of the [HOMO - 2] orbital into the [LUMO + 1] orbital. As the superexcited states formed by S_1 and S_2 excitation will be both of A_1 symmetry, it is likely that these two states will mix, thus forming a superexcited valence complex. In addition, Stolow and co-workers determined, via TRPES, the S_2 lifetime of phenol to be <50 fs,¹⁶⁸ leading Weber to suggest that the admixture of configurations in the superexcited complex will vary with time delay, further complicating the analysis.

In 2001, Weber and co-workers studied 9 eV superexcited states in 1,3-cyclohexadiene,¹⁶⁷ prepared via resonant two-color, three-photon ionization through the S_2 1B_u state. The three-photon spectra revealed two prominent Rydberg series with quantum defects of 0.58 and 0.98. In the analysis, the kinetic energy of the emitted electron was assumed independent of the vibrational excitation of the core, a reasonable assumption for high-lying Rydberg states. Weber confirmed this by tuning over the broad S_2 absorption profile in cyclohexadiene, showing that the Rydberg assignment was invariant with respect to the pump laser frequency.

In 1999, Stolow and co-workers used the photoionization of superexcited states to help confirm time scales of non-adiabatic processes in *all-trans*-decatetraene.^{39,41} In this case, 235 nm probe ionization of the 287 nm excited $S_2(^1B_u)$ state was compared with 352 nm probe ionization of this same state. In these cases, the shape of the $S_2 \rightarrow D_0$ photoelectron band was invariant, and identical decay times (400 fs) were extracted for the lifetime of the S_2 state. In the case of 352 nm ionization, however, a broad band at higher kinetic energies grew in with a time constant of 400 fs. This band is due to two-photon ionization of the vibrationally excited $S_1(2^1A_g)$ state formed via the 400 fs internal conversion. By contrast, no two-photon ionization of the $S_2(^1B_u)$ state was observed.

It is interesting to consider why, at invariant probe laser intensity, the 352 nm photoionization process switches from single-photon ionization of S_2 to two-photon ionization of S_1 : in both cases, the first 352 nm photon is already above the ionization potential, and therefore the S_1 ionization is due to absorption of a second photon in the ionization continuum. This switching can be rationalized through a consideration of the relative rates of two competing processes: second photon absorption vs direct or autoionization. For the case of S_2 , the Koopmans' correlation is with D_0 , and therefore the ionization is direct. In other words, the ionization is extremely rapid, and second photon absorption cannot compete. For the case of S_1 , the Koopmans' correlation is with D_1 . The D_1 state, however, is one-photon energetically inaccessible at 352 nm, and therefore the transition is into a superexcited complex, likely including Rydberg series converging on the D_1 threshold. For these to emit an electron into the D_0 continuum channel,

there must be an electronic rearrangement, which would have a finite autoionization rate (in fact, this process was not observed, and the superexcited state likely decays via neutral channels). In this case, it appears that the absorption of a second photon competes effectively with any autoionization. These two-photon experiments not only confirm the one-photon results but also demonstrate the symmetry selectivity of the photoionization process itself.

Perhaps the most general test available to experimentalists to prove that a TRPES spectrum is not adversely affected by the autoionization of superexcited states is to considerably vary the probe photon frequency, keeping the pump photon frequency fixed. Tuning across an autoionizing resonance is expected to lead to significant changes in the form of the photoelectron spectrum, precluding a simple Franck-Condon and Koopmans'-type analysis. In 2002, Stolow and co-workers investigated the potential role of autoionization resonances through the study of a series of six substituted benzenes, varying the probe photon wavelength from 219 to 208 nm—an over 2400 cm^{-1} change in ionization energy.¹⁵⁰ For example, the S_2 0^0 lifetime of benzaldehyde was probed using these two different probe wavelengths. Identical time constants of 440 ± 8 fs were obtained for both 208 and 219 nm probes, suggesting that the ionization dynamics are very likely direct and not significantly contaminated by the autoionization of superexcited states in these systems.

Finally, we note that resonance phenomena in the ionization continuum are likely to have a more significant effect on photoelectron angular distributions than angle-integrated kinetic energy distributions. An energy dependence of angular momentum barriers to electron escape could lead to phase shifts between partial waves, thus altering the angular distributions while having minimal effects on the kinetic energy distributions.

5.5. Time-Resolved VUV/XUV/X-ray Photoelectron Spectroscopy

The examples of TRPES discussed so far have considered only outer valence shell photoionization. However, due to the development of fs high harmonic and soft X-ray sources, there is growing interest in the development of time-resolved inner-shell photoelectron spectroscopies. These have been applied to surface physics problems for some time.¹⁶⁹

As opposed to using high harmonic radiation as a probe, it is possible to use it as a pump of highly excited states in molecules. In 2000, Sorensen, Svensson, L'Huillier, and co-workers used Ti:sapphire sixth harmonic radiation (9.42 eV) as the pump pulse in a TRPES study of the $^1\Sigma_u^+ 3d\pi 3R'''\nu_2 = 1$ Rydberg states of C_2H_2 .¹²⁶ This was the first TRPES example of using high harmonic radiation to prepare a wave packet in a very high lying electronic state of a molecule. These highly excited states are known to predissociate rapidly to $C_2H^* + H$. The TRPES measurements directly determined the lifetimes of the $3R'''$ states to be ~ 150 fs.

In 2001, Leone and co-workers applied a time-resolved soft X-ray photoelectron spectroscopy tech-

nique to the dissociation dynamics of a diatomic molecule: Br_2 .¹²⁸ Using high harmonic generation in Ar, these researchers generated fs pulses at the 17th harmonic (26.4 eV, 47 nm) of the 800 nm Ti:sapphire laser, compressed them in a grazing double-grating arrangement, and combined them with fs 400 nm pump pulses for a time-resolved study. The 400 nm pulse excited ground-state $\text{Br}_2(X^1\Sigma_g^+)$ to its dissociative $C^1\Pi_u$ state, correlating to two ground-state $\text{Br}(^2P_{3/2})$ atoms. The time-resolved formation of $\text{Br}(^2P_{3/2})$ atoms was directly observed in the X-ray photoelectron spectra, with an estimated dissociation time of ~ 40 fs. In this energy regime, the analysis is complicated by both multiple cross-correlation features, including ATI, excited-state molecular photoionization, and product-state photoionization as well as the numerous final states of the ion that are energetically accessible. The photoelectron spectrum of the recoiling Br atom did not appear to shift with time delay. It was also observed that the atomic fragments had much larger ($\sim 40\times$) photoionization cross sections than the parent molecule. In 2002, these same researchers presented a more extensive study of time-resolved X-ray photoelectron spectroscopy of Br_2 dissociation dynamics.¹²⁹ In that case, they used five different high harmonics (13th, 15th, 17th, 19th, and 21st) and were able to elucidate several of the competing photoionization channels. Transient features associated with the molecule in the process of dissociation were directly observed. Interestingly, this feature seems to have enhanced intensity as compared with the molecular ground state. As Leone and co-workers have shown, the ability to easily change the X-ray photoelectron energy (from one harmonic to the next) brings a powerful new tool into the TRPES arsenal.

In a recent 2003 study, V. Blanchet, S. Sorensen, D. Gauyacq, A. L'Huillier, and their co-workers used high harmonic radiation to pump the high-lying $F4_0^2$ and $E4-5_0^2$ Rydberg states (~ 2 eV below the ionization potential) in C_2H_2 and C_2D_2 molecules.¹⁷⁰ The $F^1\Sigma_u^+(3d\pi_g)$ Rydberg state absorbs most strongly in this region and exhibits symmetric stretching excitation of the C–C triple bond. In this experiment, these researchers doubled their high-power Ti:sapphire pulse to 396 nm and then used third harmonic generation of this in xenon to generate fs VUV pulses tunable around 132 nm (9.4 eV). The authors discussed the role of laser chirp in TRPES studies. Any chirp in the high harmonic pulses means that the total photoelectron energy shifts with time, leading to energy shifts of the photoelectron bands during the cross-correlation overlap of the laser pulses. These authors made detailed studies of the chirp of their high harmonic pulses and used this information to develop a new method for extracting time- and energy-resolved information about the dissociation dynamics. Using their time–energy scale method, the predissociation lifetimes for the C_2H_2 Rydberg states were measured to range from 20 to 200 fs, and for C_2D_2 from 150 to 600 fs. It would not be possible to extract information about the time scales of the molecular dynamics without a full analysis of the chirp. This study both serves as a warning and

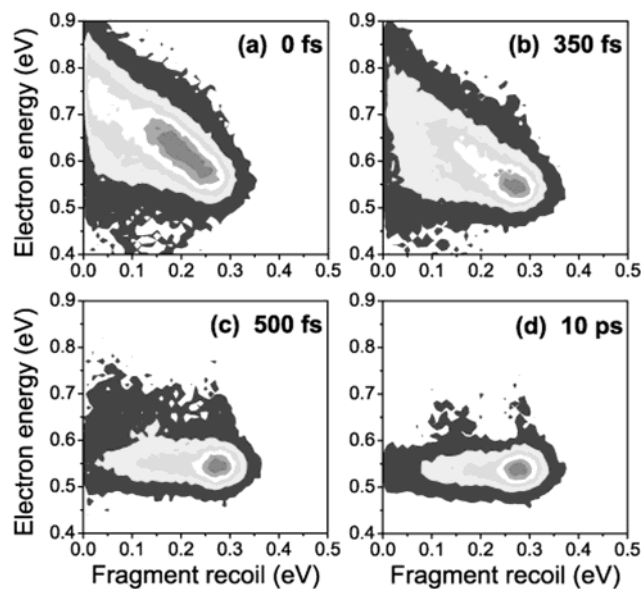


Figure 13. Coincidence-imaging spectroscopy of dissociative multiphoton ionization processes in NO_2 through energy–energy correlations using ~ 100 fs laser pulses at 375.3 nm. The two-dimensional maps show, at time delays of 0 fs, 350 fs, 500 fs, and 10 ps, the correlation between the photoelectron kinetic energy (abscissa) and NO photo-fragment recoil energy (ordinate). The intensity distributions change from a negative correlation at early times to uncorrelated at later times, yielding information about the molecule as it dissociates. Reprinted with permission from ref 115. Copyright 1999 American Institute of Physics.

indicates the potential opportunity for the use of laser chirp in TRPES.

5.6. Neutral Photodissociation Dynamics

The most interesting case for photochemistry is that of unbound excited states or excited states coupled to a dissociative continuum. The dissociative electronically excited states of polyatomic molecules can exhibit very complex dynamics, usually including non-adiabatic processes. As illustrated by Blanchet and Stolow in 1998 in a study of the NO dimer,⁷⁷ TRPES may be used to study the photodissociation dynamics of neutral polyatomic molecules.

In 1999, Hayden, Continetti, and co-workers applied the newly developed coincidence-imaging spectroscopy (CIS) technique to the photodissociation dynamics of NO_2 .¹¹⁵ The CIS method allows for energy- and angle-resolved (i.e., full 3D momentum vector imaging) detection of both electrons and ions in coincidence and represents the most differential TRPES measurements made to date. These authors studied the dissociative multiphoton ionization of NO_2 at 375.3 nm. This was identified as a three-photon transition to a repulsive surface, correlating with $\text{NO}(C^2\Pi) + \text{O}(^3P)$ fragments. The $\text{NO}(C)$ was subsequently ionizing by a single photon, yielding $\text{NO}^+(X^1\Sigma^+)$. As a first illustration of the multiply differential information obtained via CIS, Hayden and co-workers used energy–energy correlations to plot photoelectron kinetic energy vs $\text{NO}(C)$ photo-fragment kinetic energy, as a function of time, as shown in Figure 13. At early times, 0 and 350 fs, there is a negative correlation between electron and

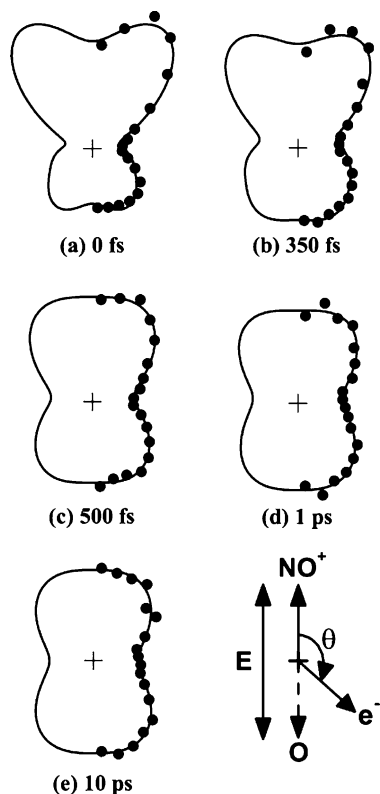


Figure 14. Coincidence-imaging spectroscopy of dissociative multiphoton ionization processes in NO_2 with ~ 100 fs laser pulses at 375.3 nm, using angle–angle correlations. The polar plots show, at time delays of 0 fs, 350 fs, 500 fs, 1 ps, and 10 ps, the angular correlation between the ejected electron and NO photofragment when the latter is ejected parallel to the laser field polarization vector. The intensity distributions change from a forward–backward asymmetric distribution at early times to a symmetric angular distribution at later times, yielding detailed information about the molecule as it dissociates. Reprinted with permission from ref 116. Copyright 2000 American Physical Society.

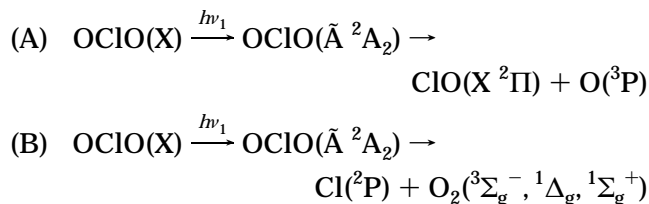
fragment recoil energy. This is the form expected for a molecule in the process of dissociating, where there is a tradeoff between ionization energy and fragment recoil energy. At longer time delays, 500 fs and 10 ps, the NO(C) fragment is no longer recoiling from the O atom—it is a free particle—and the photoelectron spectrum obtained is simply that of free NO(C); hence, the negative correlation vanishes.

In a subsequent study, Hayden, Continetti, and co-workers again applied the CIS method to the same multiphoton $\text{NO}_2^* \rightarrow \text{NO(C)} + \text{O}$ process, but this time making use of angle–angle correlations.¹¹⁶ By measuring the angle of recoil of both photoelectron and photofragment in coincidence, the photoelectron angular distribution (PAD) may be transformed into the photofragment recoil frame, for each recoil angle and time delay. As an example, in Figure 14, the time-resolved recoil-frame PAD is shown for the case of photofragments ejected parallel to the laser polarization axis. It can be seen that at early times, 0 and 350 fs, the PAD is highly asymmetric. The breaking of forward–backward symmetry in the recoil frame originates from NO(C) polarization due to the presence of the O atom from which it is recoiling. At

longer times, 1 and 10 ps, this forward–backward asymmetry vanishes as the NO(C) becomes a free particle. This once again shows the power of CIS in obtaining highly detailed information about molecules in the process of dissociating.

In 1999, Radloff and co-workers studied the 267 nm photodissociation dynamics of CF_2I_2 ,¹⁷¹ using the time-resolved PEPICO method. CF_2I_2 has a broad and featureless absorption spectrum in the 230–400 nm region due to the overlap of several dissociative continua. Analysis of the photoelectron spectra revealed that three electronic states are involved and that an ultrafast non-adiabatic process (~ 30 fs) precedes dissociation (~ 100 fs). The dissociation products were determined to be $\text{CF}_2 + \text{I} + \text{I}$, as no CF_2I fragments or photoelectron spectra were observed. Due to the intensity of the pump laser pulses, dissociative multiphoton processes involving both two and three pump photons were also observed. At the two-photon level, direct formation of molecular I_2 was observed, consistent with earlier work. At the three-photon level, highly excited $\text{I}(nd)$ atom channels were observed in the photoelectron spectra. The coincident detection of photofragments and photoelectrons was crucial to disentangling these various processes.

In 2001, Radloff and co-workers applied the time-resolved PEPICO method to the photodissociation of ClO_2 using very short (~ 50 fs) pump pulses at 398 nm.¹⁷² This reaction had previously been studied using TRPES by Chen and co-workers at 386 nm.⁵³ At 398 nm, two channels are open:



The yield of channel B is $\sim 4\%$ at 398 nm (3.11 eV). At wavelengths below 399.2 nm (3.1 eV), channel A is directly open. In addition, an ultrafast spin–orbit induced internal conversion $\tilde{\text{A}}^2\text{A}_2 \rightarrow \tilde{\text{A}}^2\text{A}_1$ process is allowed. The $\tilde{\text{A}}^2\text{A}_1$ state can either dissociate via channel A or undergo further internal conversion to the $^2\text{B}_2$ state. This latter state may then dissociate through both channels A and B. Using the time-resolved photoelectron spectra coincident with each of OCIO^+ , ClO^+ , O_2^+ , and Cl^+ ions, Radloff and co-workers were able to unravel the complex dissociation dynamics of this molecule, using various multiphoton dissociation and ionization processes. The spin–orbit-induced $\tilde{\text{A}}^2\text{A}_2 \rightarrow \tilde{\text{A}}^2\text{A}_1$ transition was determined to have a time constant of 7 ps. The nascent $\tilde{\text{A}}^2\text{A}_1$ state decayed by both dissociation and internal conversion, with an overall time constant of ~ 250 fs. The $^2\text{B}_2$ state formed by the subsequent internal conversion then decayed on a 750 fs time scale. These latter two channels were unresolved in the earlier TRPES study by Chen.⁵³ This once again illustrates the great utility of time-resolved photoelectron–photoion coincidence spectroscopy in the study of complex reaction mechanisms.

In 2002, V. Engel and co-workers proposed the use of TRPES to study the complex photodissociation dynamics of the metal carbonyl $\text{Fe}(\text{CO})_5$.^{173,174} A long-standing problem in the study of metal carbonyl UV photochemistry is the competition between neutral dissociation followed by ionization and the dissociative ionization of both parent molecule and photofragments. As both types of processes produce fragment ions with broad and featureless kinetic energy distributions, it is very difficult to discern them via ion detection alone. Engel shows via calculation that, due to the differing ionization potentials of the $\text{Fe}(\text{CO})_n$ ($n = 2-4$) fragments, shifts in the photoelectron spectra are expected as a function of time. This should likely assist the disentangling of the various ionization/fragmentation channels, allowing for direct measurements of the neutral dissociation channels.

In 2002, Meier and Engel used both classical trajectory and quantum wave packet calculations to model the direct dissociation of the H_2O ($\tilde{\text{A}}^1\text{B}_1$) state probed by fs TRPES.³¹ The authors calculated that, with a 6 fs VUV pump pulse at 155 nm, the dissociation dynamics of H_2O ($\tilde{\text{A}}^1\text{B}_1$) is revealed directly by TRPES, using a 6 fs XUV probe pulse at 86.7 nm (14.3 eV). As the H atom separated from OH, the photoelectron spectra shifted, in 10–20 fs, from a broad peak at 0.4 eV to a sharper peak at 0.1 eV. Importantly, the time-resolved photoelectron spectrum could be calculated classically via an extension of the impulse approximation. This points the way toward future applications of classical mechanics in TRPES calculations in larger systems where quantum or semiclassical calculations are prohibitively expensive.

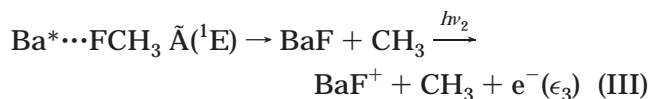
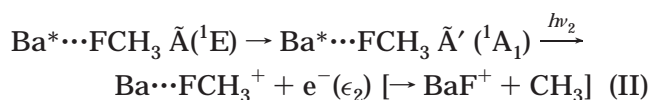
Following the earlier study of 210 nm photodissociation dynamics of the $(\text{NO})_2$ dimer,⁷⁷ Hayden, Stolow, Shaffer, and co-workers applied the CIS method to this same problem. Initial results using both energy- and angle-resolved correlation maps revealed new details of the dissociation dynamics.¹⁷⁵ The previously proposed two-step non-adiabatic photodissociation mechanism at 210 nm was independently supported by these results. Suzuki and co-workers have further studied this system via time-resolved charged particle imaging toward deconvolving non-adiabatic and photodissociation dynamics. An initial study,¹⁷⁶ performed with a 200.5 nm pump wavelength, compared the valence-state decay lifetime determined from time-dependent $(\text{NO})_2^+$ photoion intensity with $(\text{NO})_2$ 3s Rydberg state population growth monitored via time-resolved photoelectron imaging. These time scales were found to be commensurate at ~ 200 fs. The dimer Rydberg state yields a more energetic and anisotropic photoelectron angular distribution relative to the valence state and correlates to the $\text{NO}(\text{X}) + \text{NO}(\text{A})$ photodissociation channel. A series of time-resolved pump–probe experiments were performed with 200.5 nm pump and 250, 270, and 290 nm probe pulses toward characterizing non-adiabatic decay of the initially excited valence state and the dissociation of the Rydberg state through changes in measured PADs. Though the dimer Rydberg and $\text{NO}(\text{A})$ states yield nearly isoenergetic photoionization features, a subtle shift

of ionization energy, coupled to a change in anisotropy of this peak, indicated a ~ 1 ps time scale for reaching the free $\text{NO}(\text{A})$ asymptote through dissociation. In a subsequent study,¹⁷⁷ these researchers extended investigation of the dimer valence-state electronic dephasing rate compared to the dimer 3s Rydberg state growth following excitation at various wavelengths between 200 and 235 nm. These time scales were found to match for excitation wavelengths below 220 nm and indicated a lifetime contraction with decreasing pump wavelength. While an effective photodissociation lifetime additionally depends on the dimer Rydberg lifetime, these results corroborate photofragment imaging studies reported by Demyanenko et al.¹⁷⁸ that find higher fragment anisotropy for higher excitation energies in this region, suggested to result from shortened dimer lifetimes.

5.7. Neutral Reaction Dynamics

The study of bimolecular reaction dynamics via the femtosecond pump–probe technique is challenged by the broad radial distribution function, $g(r)$, found in (almost) any gas. Even if a bimolecular reaction is photoinitiated by a short-pulse laser, this distribution of nearest-neighbor distances means that the reactive collisions will occur over a broad range of times, completely blurring the short time scale of the collision dynamics itself. The solution to this paradox was presented by Zewail and co-workers in 1987 in a seminal study of the $\text{H} + \text{CO}_2$ reaction,¹⁷⁹ namely to use van der Waals clusters to hold reactants (in this case HI and CO_2) in close proximity and in a well-defined geometry, thus forcing a single “collision time”.

The applications of femtosecond TRPES to bimolecular reaction dynamics are still in their infancy, having been first demonstrated by Radloff and co-workers for the $\text{Ba} + \text{CH}_3\text{F}$ reaction using the PEPICO method.¹⁸⁰ In this experiment, the $\text{Ba}\cdots\text{FCH}_3$ van der Waals complex was the reactant state. Pumped at $h\nu_1 = 618$ nm, the $\text{Ba}\cdots\text{FCH}_3$ complex is excited to the $\tilde{\text{A}}(^1\text{E})$ state, correlating to the $\text{Ba } ^1\text{P}$ ($6s6p$) state. Reactions proceed and were probed ($h\nu_2 = 400$ nm) as follows:



The $\tilde{\text{A}}^1\text{E} \rightarrow \tilde{\text{A}}' ^1\text{A}_1$ internal conversion (II) was directly observed via TRPES (via bands ϵ_1 and ϵ_2), yielding a time constant of 270 fs. The harpooning reaction (III) occurred rapidly (~ 50 fs), following internal conversion. At longer time delays (several ps), only photoelectron spectra of the BaF product (band ϵ_3) were observed. This study lays the ground-

work for future applications of TRPES in neutral clusters to the study of bimolecular reactions dynamics, a subject which is already well-established in time-resolved studies of anionic clusters (vide infra).

5.8. Anion TRPES: I_2^- Nuclear Wave Packet Dynamics

As mentioned in the Introduction, anion TRPES allows one to track both excited- and ground-state dynamics, in contrast to most neutral experiments that are restricted to excited-state studies. The capabilities of anion TRPES are illustrated through reference to discussion of diiodide anion (I_2^-) dynamics. I_2^- has many desirable properties from the perspective of anion TRPES experiments. Its constituent atoms are sufficiently heavy that its nuclear dynamics can be followed with ~ 100 fs laser pulses. It has two strong electronic transitions, the $A' \ ^2\Pi_{g,1/2} \leftarrow X^2\Sigma_u^+$ and $B^2\Sigma_g^+ \leftarrow X^2\Sigma_u^+$ bands, that may be accessed using the fundamental (~ 790 nm) and second harmonic (~ 395 nm) of a Ti:sapphire femtosecond laser. Finally, the photodetachment cross sections of I_2^- and I^- are quite large. For these reasons, I_2^- is an excellent model system for TRPES as well as several variations of the basic experiment, which are depicted pictorially in Figure 15 and are explained in context below.

The first anion TRPES experiment probed the dissociation dynamics of I_2^- excited to its $A' \ ^2\Pi_{g,1/2}$ state, schematically depicted in Figure 15a.³⁶ I_2^- was excited to this dissociative excited state by a broadband ~ 80 fs pulse at 780 nm, launching a wave packet that propagates toward separated $I + I^-$ products, and was subsequently probed by photodetachment with a 260 nm pulse of ~ 100 fs duration. Only the "atomic" $I^- \rightarrow I(^2P_{3/2})/I^*(^2P_{1/2}) + e^-$ detachment features were observed at the latest pump-probe delays (> 425 fs), while additional transients, arising from detachment to the A'/A and B states of I_2 , were observed between 0 and 200 fs at lower binding energies than the atomic features. Quantum mechanical simulations of the experiment were undertaken using a wave packet propagation scheme²⁹ and the best available potential energy curves for I_2^- and I_2 . Experiment and simulation indicated dissociation by 100 fs.

A subsequent study,³⁷ performed at higher resolution and simulated with a more accurate experimentally derived anion ground-state potential,¹⁸¹ produced an accurate potential for the $A' \ ^2\Pi_{g,1/2}$ dissociative state. These higher-resolution TRPE spectra are displayed in Figure 2. Here, a long-time shift of ~ 10 meV in the position of the nominal $I^- \rightarrow I(^2P_{3/2}) + e^-$ feature was observed, revealing a long-range attractive well in the dissociative state arising from charge-induced dipole, charge-induced quadrupole, and dispersion interactions. The excited A' state was empirically characterized to have a 17 ± 10 meV well at 6.2 ± 0.6 Å by fitting to a simulation performed with an efficient wave packet propagation scheme.¹⁸²

While TRPES experiments nominally provide information on the dynamics of the excited state accessed by the pump pulse, variations on this experiment can probe the ground state, generally by

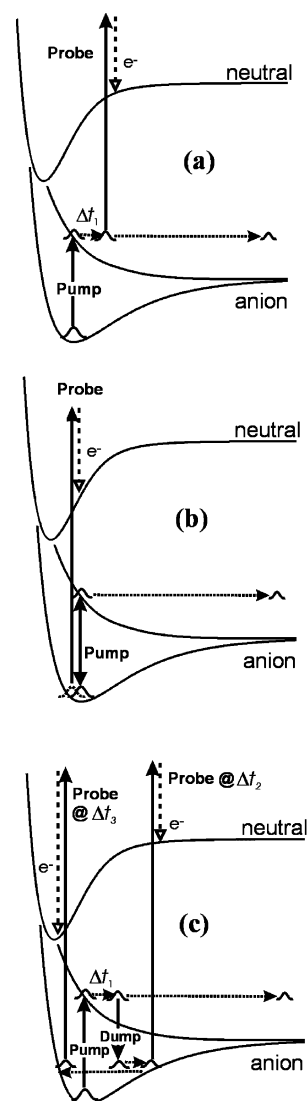


Figure 15. Experimental versatility of TRPES applied to anion systems exemplified with I_2^- . (a) Femtosecond photoelectron spectroscopy (FPES), whereby ultrafast (fs) dissociation dynamics initiated by a ~ 780 nm pump pulse ($A' \ ^2\Pi_{g,1/2} \leftarrow X^2\Sigma_u^+$) are subsequently probed via ~ 260 nm detachment at variable delays. (b) Resonant impulsive stimulated Raman scattering (RISRS) FPES, in which ground-state vibrational dynamics, initiated by scattering, are probed via FPES. (c) Femtosecond stimulated emission pumping (FSEP) FPES, in which ground-state wave packets are generated at various average vibrational quanta through a ~ 800 nm pump–near-IR dump process and are subsequently probed with FPES.

producing coherent vibrational wave packet motion on the ground state that can be followed by TRPES, as depicted schematically in Figure 15b. In the first example of this type, the pump pulse used to excite the $A' \ ^2\Pi_{g,1/2} \leftarrow X^2\Sigma_u^+$ transition in I_2^- was also shown to create a coherent superposition of the $v = 0$ and $v = 1$ vibrational levels on the ground $X^2\Sigma_u^+$ state, thereby creating a wave packet whose motion could be detected by oscillations in the TRPE spectrum at selected electron kinetic energies.¹⁸¹ This ground-state excitation process, resonant impulsive stimulated Raman scattering (RISRS), could then be used to obtain the fundamental vibrational frequency of I_2^- , 110 cm^{-1} .

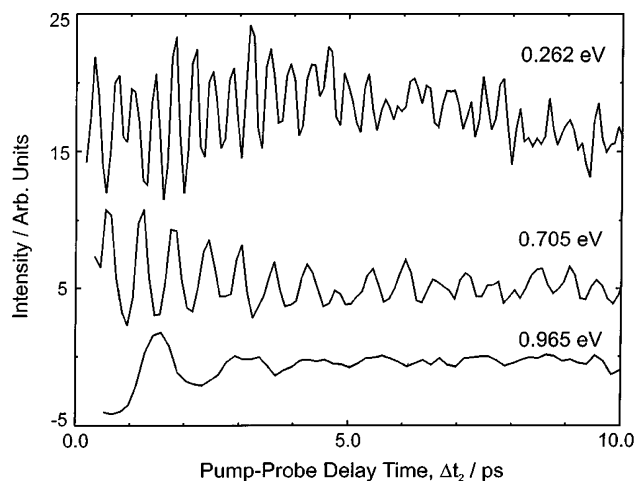


Figure 16. Vibrational wave packet dynamics measured on the I_2^- ground state ($X^2\Sigma_u^+$) through FSEP–FPES. Vibrational wave packets are generated in the anion ground state through FSEP (Figure 15c) at various average vibrational energies (0.262, 0.705, 0.965 eV) to within 2% of the dissociation limit. Wave packet dynamics, probed by FPES, are monitored by oscillation of high eKE photoelectron signal, arising from detachment at the inner turning point (ITP) of the anion potential well. Oscillation periods reveal average vibrational spacings within each excitation window, while recurrences reflect the anharmonicity of the diatomic potential. Reprinted with permission from ref 183. Copyright 2000 American Institute of Physics.

In a more sophisticated ground-state wave packet excitation scheme, femtosecond stimulated emission pumping (FSEP),¹⁸³ femtosecond pump and dump pulses create a ground-state wave packet with average vibrational energy $E_{\text{exc}} = h\nu_{\text{pump}} - h\nu_{\text{dump}}$ (Figure 15c). The pump pulse is resonant with the $A' \ ^2\Pi_{g,1/2} \leftarrow X^2\Sigma_u^+$ transition, while the dump pulse, applied 50–150 fs after the pump pulse, drives some of the dissociating excited-state wave packet back to the ground state. By tuning the dump pulse, E_{exc} was varied from 0.262 eV up to 0.993 eV; the latter value is within 2% of the I_2^- bond dissociation energy. Wave packet oscillations were monitored via detachment with a third time-delayed femtosecond pulse (UV), producing high-energy electrons from detachment to the neutral ground state as the packet reaches the inner turning point (ITP) of the anion potential. ITP detachment signal oscillations arising from I_2^- vibrational wave packet motion at low, intermediate, and high excitation energies are shown in Figure 16. Fourier transformation of these oscillations yielded the I_2^- vibrational frequency as a function of E_{exc} , while wave packet rephasing times as a function of E_{exc} probed the anharmonicity of the ground-state potential. The frequency and anharmonicity information from the RISRS and FSEP experiments was used to construct an accurate I_2^- ground-state potential that was improved relative to previously calculated curves.

TRPES, RISRS, and FSEP experiments have all been applied to clustered I_2^- as well as the bare anion. Results from these experiments are described in subsequent sections.

5.9. Dissociation Dynamics of Polyatomic Anions

Experiments with triatomics present the added complication of energy-dependent ion–neutral product branching ratios. In such a pump–probe experiment, Ganteför and co-workers⁷⁵ examined Au_3^- dissociation from 0 to 3600 ps following ~ 3.0 eV excitation. Photodetachment signal measured at early delays was attributed to an activated complex populated following nuclear relaxation from the initially excited configuration. This complex was determined to decay subsequently toward separated products with a lifetime of 1500 ± 200 ps and with preferential production of the lowest energy product channel, $Au^- + Au_2$. Pumping at 3.14 eV resulted in a significantly shorter-lived complex (< 50 ps) with a factor of 2.5 increase in the $Au_2^-:Au^-$ product ratio.

Time-resolved PES of I_3^- , photodissociated at 390 nm, revealed both I^- and I_2^- photofragments,¹⁸⁴ in contrast to results of similar experiments done in the solution phase.^{185,186} The TRPE spectra showed distinguishable contributions corresponding to depletion of I_3^- reactant and growth of I^- and I_2^- products. With aid from two-dimensional wave packet simulations, the I^- photoproduct was determined to arise from three-body dissociation along the symmetric stretch of I_3^- . The I_2^- products were formed in a coherent superposition of vibrational levels, observable through oscillations in the TRPE spectra. Similar effects were seen in the solution-phase photodissociation of I_3^- using transient absorption, but much greater vibrational excitation was seen in the gas-phase experiments. The I_3^- features in the TRPE spectra showed oscillatory structure from RISRS excitation of the symmetric stretch, yielding a vibrational frequency of 112 ± 1 cm^{-1} .

5.10. Photodissociation, Recombination, and Reaction Dynamics in Anionic Clusters

TRPES experiments on size-selected clusters in which an anion chromophore is solvated with a known number of solvent species offer a detailed probe of how clustering affects the dynamics of relatively simple systems. The pioneering work by Lineberger and co-workers^{187–191} on $I_2^-(CO_2)_n$ and $I_2^-(Ar)_n$ clusters, in which the I_2^- chromophore was photodissociated and the masses of the resulting ion daughter fragments were measured, showed profound effects of clustering on the I_2^- dissociation dynamics. The recoiling photofragments interact with the surrounding solvent species, resulting in a size-dependent yield of caged daughter ions from solvent-induced $I + I^-$ recombination. Time-resolved experiments by Lineberger, in which the absorption recovery time of the I_2^- was measured, yielded overall time constants for recombination and vibrational relaxation of the clustered I_2^- . These aspects of the dynamics have been explored by Parson and Coker in a series of theoretical simulations.^{192–197} TRPES experiments on these clusters offer a more complete picture of their dynamics subsequent to photoexcitation.

Greenblatt et al. investigated the TRPE spectra of $I_2^-(Ar)_{n \leq 20}$ and $I_2^-(CO_2)_{n \leq 16}$ clusters in a series of

papers.^{198–201} The maximum sizes in both cases represent complete solvent shells. In all the clusters, dissociation of the I_2^- chromophore subsequent to excitation of the $A' \ ^2\Pi_{g,1/2} \leftarrow X^2\Sigma_u^+$ occurs on a time scale similar to that of bare I_2^- , 200–300 fs, resulting in the production of solvated I^- within the cluster. The extent of solvation at these short times, before any solvent rearrangement or other dynamics have occurred, can be determined from the positions of the features in the PE spectra and confirms the anomalous charge-switching nature of the $A' \ ^2\Pi_{g,1/2}$ state predicted by Parson and co-workers,¹⁹⁷ in which the electron is localized on the less-solvated iodine atom. In small clusters (≤ 9 Ar atoms, or ≤ 6 CO_2 molecules), where no recombination occurs, the TRPE spectra show relatively small shifts, reflecting solvent rearrangement dynamics as the I and I^- fragments separate.

In the larger Ar clusters, recombination of I_2^- is observed on the X and $A' \ ^2\Pi_{g,3/2}$ states. The PE spectra were analyzed to yield the number of solvent atoms remaining as a function of time for both states of the recombined I_2^- , and the extent of vibrational relaxation for clusters with I_2^- in the X state. In $I_2^-(Ar)_{20}$, it was found that energy transfer to the solvent atoms via vibrational relaxation was slightly faster (~ 100 ps) than energy loss from the cluster through Ar evaporation, indicating temporary storage of energy within the Ar cluster modes. Vibrational relaxation of the recombined I_2^- in the larger $I_2^-(CO_2)_n$ clusters was found to be significantly faster (< 5 ps) than in $I_2^-(Ar)_{20}$, in agreement with the absorption recovery experiments by Lineberger.¹⁹⁰ However, solvent evaporation was clearly much slower, and comparison to the tandem mass spectrometric data obtained by Lineberger¹⁸⁹ showed that evaporation was incomplete for pump–probe delay times as long as 200 ps. The faster relaxation and slower evaporation times are consistent with the stronger solute–solvent coupling and higher solvent density of states in $I_2^-(CO_2)_n$ clusters.

The effects of clustering on dissociation and recombination dynamics have also been studied in a series of TRPES experiments by Zewail and co-workers^{202–204} on molecular oxygen cluster anions, $(O_2^-)_{n \geq 3}$, and clusters in which O_6^- is solvated by another species (N_2 , Xe, N_2O). Previous work by Hiraoka²⁰⁵ and Johnson²⁰⁶ showed that $(O_2)_n^-$ clusters with $n > 2$ have an intact O_4^- core. Johnson found that the $n > 2$ clusters undergo photodissociation in the near-infrared, a process attributed to charge transfer from the O_4^- core to the O_2 solvent(s). Zewail's experiments showed that excitation of pure or mixed clusters at 800 nm resulted in biexponential growth of the O_2^- photoproduct. The fast process ($\tau_1 = 100$ –500 fs) was assigned to back electron transfer to the O_4 core, followed by dissociation on an optically inaccessible repulsive state, while the slower process ($\tau_2 \approx 1$ –10 ps) was attributed to vibrational predissociation of a vibrationally excited O_2^- solvent molecule formed by the initial charge-transfer step. τ_2 generally increased with cluster size, consistent with a statistical evaporation process. In the study of mixed clusters, it was found that dissociation via vibrational predissociation

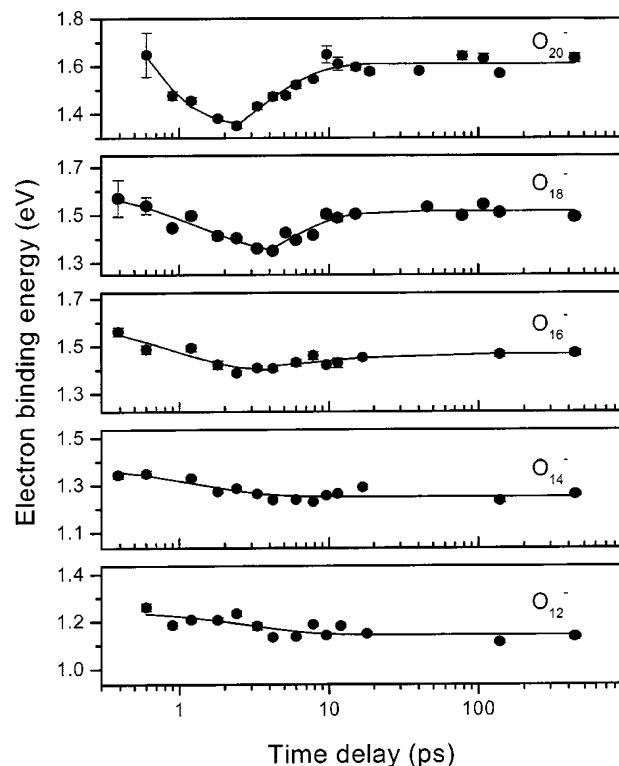


Figure 17. Time-resolved measurements of $(O_2)_n^-$, $n = 6$ –10, photofragment photoelectron spectral peak position: Circles, experiment; line, fit. Recovery at high binding energies, arising from O_4^- photodetachment, for clusters $n > 7$ indicates O_2 – O_2^- recombination with increased cluster size. Reprinted with permission from ref 204. Copyright 2003 American Institute of Physics.

was more prevalent for $O_6^-(N_2O)$ than for any other comparably sized cluster, and that the time scale for this channel was much slower, e.g., 7.7 ps vs 2.1 ps for $O_6^-(Xe)$. This result was attributed to rapid V–V energy transfer from the transient O_2^- solvent molecule to the N_2O .

The largest oxygen clusters showed evidence of a previously unseen phenomenon in clusters: cage-induced recombination of molecular photofragments.²⁰⁴ As shown in Figure 17, TRPE spectra of $(O_2)_n^-$ clusters with $n > 7$ exhibited recovery at high electron binding energy at times intermediate (2–4 ps) to electron transfer/direct dissociation and slow vibrational relaxation. This shift was assigned to cage-induced recombination of O_2 and O_2^- to form vibrationally excited O_4^- , followed by O_2 evaporation. The slow time scale of this molecule–molecule caging relative to the atom–atom recombination seen in clustered I_2^- was attributed to the need for proper orientation of the two molecular species for caging to occur.

In a recent variation on the clustered I_2^- TRPE experiments, motivated by neutral studies of bimolecular reactions utilizing cluster-constrained geometries, Wester et al.²⁰⁷ investigated the reaction dynamics of the symmetric S_N2 reaction of I^- with CH_3I by TRPES of the precursor complex $I_2^- \cdot CH_3I$. The reaction was initiated by photodissociating the I_2^- chromophore with a pump pulse at either 790 or 395 nm. Immediately after the pump pulse, the reactants formed an $I^- \cdot CH_3I$ complex, with an inter-

nal energy dependent on the energy of the pump photon. For 790 nm pump photons, only stable complexes were observed, while at 395 nm, about two-thirds of the complexes decayed back to the reactants, $\text{I}^- + \text{CH}_3\text{I}$, on the time scale of the experiment (<100 ps). These unstable complexes exhibit biexponential dissociation dynamics: 80% decayed with a fast time constant of about 0.75 ps and 20% with a slow time constant of about 10 ps. This biexponential decay and the observed shift of the $\text{I}^- \text{CH}_3\text{I}$ photoelectron peak during a time span of about 5 ps are indicative of “apparent non-RRKM behavior” of the complex, reflecting the evolution of vibrational energy flow in the complex on a time scale comparable to or slower than that of dissociation. The observed dynamics are similar to those seen in classical trajectory calculations on entrance channel complexes formed in bimolecular $\text{Cl}^- + \text{CH}_3\text{Cl}$ collisions.

5.11. Anion Vibrational Wave Packet and Relaxation Dynamics

Just as the TRPES experiments on the photodissociation of bare I_2^- provide a basis for understanding the clustered I_2^- experiments described in the previous section, RISRS and FSEP experiments on I_2^- lay the groundwork for understanding vibrational wave packet spectroscopy and dynamics in clusters of I_2^- . Experiments in which vibrational wave packets are generated in clusters probe the conditions under which coherent wave packet motion can be detected, and how the populations and phases initially encoded into the wave packet evolve with time, thereby providing new insight into spectroscopy and relaxation dynamics in clusters.

For example, Zanni et al.²⁰⁸ used RISRS to examine solvent effects on the I_2^- fundamental vibrational frequency. For $\text{I}_2^- (\text{Ar})_n$ clusters, no spectral shifts were observed for $n \leq 6$, while the $n = 12$ and 18 clusters showed blue shifts of 1.5 and 3 cm^{-1} , respectively. The clusters $\text{I}_2^- (\text{CO}_2)_n$, $n = 4, 9$, showed blue shifts of 2 and 4.5 cm^{-1} , respectively. Hence, only blue shifts were observed, and these increased with the number of solvent species and strength of the chromophore–solvent interaction.

Such explorations were subsequently expanded to further examine solvent–chromophore interactions and solvent mediation of vibrational relaxation by exciting higher in the potential well with FSEP. A series of papers by Davis et al.^{209–211} explored dynamics in $\text{I}_2^- (\text{X})_n$ clusters ($\text{X} = \text{Ar}$ and CO_2) subsequent to coherent vibrational excitation of the I_2^- chromophore at a series of excitation energies E_{exc} . The relaxation dynamics of the I_2^- were followed using two observables in the TRPE spectra. At short times, wave packet recurrences at the inner turning point of the I_2^- potential resulted in oscillations in the signal at high electron kinetic energy, just as in bare I_2^- . However, dephasing was more rapid and irreversible in the clusters (3–4 ps in $\text{I}_2^- (\text{CO}_2)_{4,5}$, 8–10 ps in $\text{I}_2^- (\text{Ar})_{n \leq 12}$). More significantly, the oscillation frequency increased with time. The oscillation frequency reflects the spacing between adjacent vibrational energy levels, so the increase with time

is a measure of vibrational relaxation of the I_2^- in an anharmonic potential, where the level spacing increases as the vibrational quantum number drops. The increase in frequency is as large as 20 cm^{-1} for $\text{I}_2^- (\text{CO}_2)_4$ at $E_{\text{exc}} = 0.57$ eV; this implies that the wave packet loses at least 0.35 eV of vibrational energy in ~3.5 ps while maintaining its coherence.

Once dephasing of the oscillations has occurred, the above method can no longer be used. However, over a much longer time scale, the maximum eKE at which signal was observed shifted to lower energy, and this effect was used to follow vibrational relaxation dynamics for times as long as 200 ps. Exponential fits yielded relaxation time constants $\tau = 4$ –5 ps for $\text{I}_2^- (\text{CO}_2)_{4,5}$. Relaxation times for $\text{I}_2^- (\text{Ar})_n$ clusters were generally larger (e.g., $\tau = 27$ ps for $\text{I}_2^- (\text{Ar})_9$ at $E_{\text{exc}} = 0.57$ eV), but showed much more variation on cluster size and excitation energy. This variation reflects the similar time scales for vibrational energy flow and solvent evaporation in $\text{I}_2^- (\text{Ar})_n$ clusters, as opposed to $\text{I}_2^- (\text{CO}_2)_n$ clusters, where vibrational energy flow is much faster than solvent evaporation.

5.12. Charge-Transfer-to-Solvent and Solvated Electron Dynamics

Solvated halide anions have been known to exhibit broad ultraviolet absorption bands arising from ejection of excess electrons into the surrounding solvent, the charge-transfer-to-solvent (CTTS) bands.^{212–214} The dynamics of electron solvation subsequent to CTTS excitation is an active area in condensed-phase dynamics.^{215–218} Remarkably, features analogous to the bulk CTTS bands have been observed in the photodetachment spectroscopy of relatively small clusters; Serxner et al.²¹⁹ observed them in $\text{I}^- (\text{H}_2\text{O})_{n=2-4}$, while Cheshnovsky^{220,221} observed much narrower but analogous features in $\text{I}^- (\text{Xe})_{4-54}$ clusters. These results motivated a series of TRPES studies of the CTTS excited states in solvated halide clusters,^{222–226} with the goal of understanding how an inherently bulk phenomenon, electron solvation, manifests itself in finite clusters.

The first such studies, by Lehr et al.,^{222,227} examined CTTS precursors of $\text{I}^- (\text{H}_2\text{O})_n$ and $\text{I}^- (\text{D}_2\text{O})_n$ clusters, $n = 4$ –6. In these experiments, CTTS precursor states were prepared by ~100 fs UV laser pulses and subsequently probed by detachment at various delays at 790 nm. Significantly different dynamics were observed within this size range. The TRPE spectra for the $n = 4$ clusters were indicative of simple population decay of the CTTS state via autodetachment. However, significant spectral shifts toward lower eKE (or toward higher vertical binding energy, VBE) were seen in the TRPE spectra of the larger clusters on a time scale of several hundred fs, as depicted in Figure 18, and these shifts were attributed to stabilization of the diffuse electron in the CTTS excited state by reorganization of the water molecules.

An alternative interpretation of these experiments was proposed by Chen and Sheu,²²⁸ based on electronic structure calculations²²⁹ that indicated a repulsive interaction between the CTTS electron and the I atom. They proposed that the spectral shifts

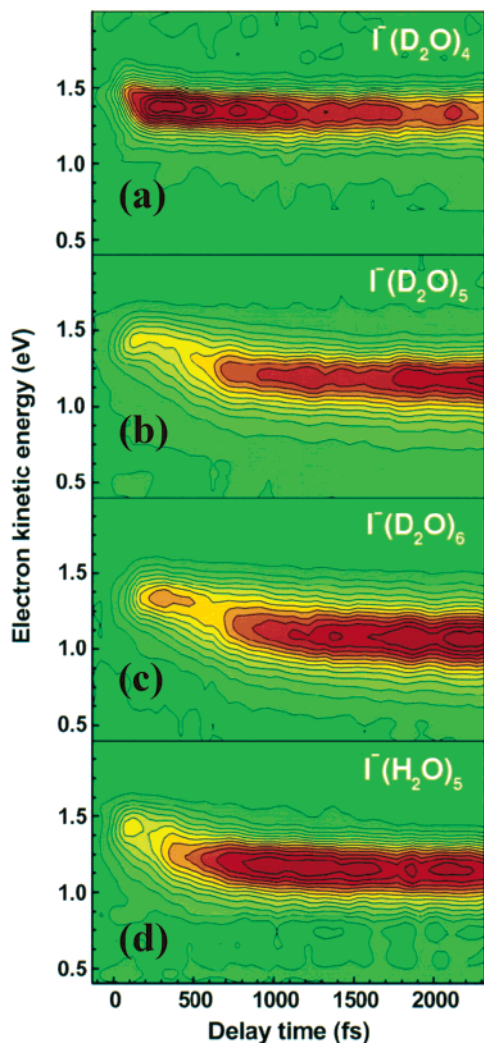


Figure 18. Femtosecond photoelectron spectra of $\text{I}^-(\text{D}_2\text{O})_n$, $n = 4-6$ (a–c), and $\text{I}^-(\text{H}_2\text{O})_5$ (d) plotted as 2D contour plots of electron kinetic energy (eKE) with respect to pump–probe delay. Dramatic spectral shifts for clusters with $n > 4$ suggest solvent reorganization dynamics following CTTS excitation. Reprinted with permission from *Science* (<http://www.aas.org>), ref 222. Copyright 1999 American Association for the Advancement of Science.

resulted from the I atom leaving the cluster rather than solvent reorganization. Davis et al.²²⁶ pointed out that this interpretation was difficult to reconcile with the difference between the $n = 4$ and larger clusters, and with the slightly faster dynamics in clusters of H_2O vs D_2O . Calculations by Vila and Jordan²³⁰ provided further support for solvent reorganization immediately after CTTS excitation, while calculations by Timerghazin and Peslherbe²³¹ on $\text{I}^-(\text{H}_2\text{O})_3$ indicate both solvent network dynamics and elongation of the iodine-to-solvent distance in subsequent relaxation. At this point, the detailed dynamics of these clusters remain somewhat of an open question, but probably involve a combination of solvent dynamics and iodine motion.

CTTS clusters composed of other solvents with varying polarities were investigated by Frischkorn et al.²²⁵ and Davis et al.,²²⁴ revealing different dynamics for various solvent types. Similar to hydrated clusters, CTTS-excited $\text{I}^-(\text{NH}_3)_n$ and $\text{I}^-(\text{CH}_3\text{OH})_n$ exhibit a time-dependent shift in electron binding

energy, concomitant with an increase in electron detachment cross section, associated with partial solvation and a subsequent localization of the diffuse excess electron. In contrast to $\text{I}^-(\text{H}_2\text{O})_n$, these clusters exhibit monotonically increasing VBE shifts with increasing solvation rather than a size-critical VBE shift. $\text{I}^-(\text{CH}_3\text{OH})_n$ clusters exhibited spectral evolution similar to that of $\text{I}^-(\text{NH}_3)_n$, indicating partial solvation of the extra electron within a few picoseconds, though this is followed by a long-time shift to lower binding energies, suggesting the possibility of solvent evaporation or the contribution of two solvent configurations to the observed dynamics.

TRPES experiments on the CTTS states of $\text{I}^-(\text{Xe})_n$ clusters were performed by Zanni et al.²²³ for clusters with as many as 38 Xe atoms. Two sets of transitions were studied, corresponding to excitation of $[\text{I}^*(^2\text{P}_{1/2})\text{Xe}_n]^-$ and $[\text{I}^*(^2\text{P}_{3/2})\text{Xe}_n]^-$ CTTS states. The $[\text{I}^*(^2\text{P}_{3/2})\text{Xe}_n]^-$ states decayed on a time scale of 500–1500 fs and showed no VBE shifts, indicating no solvent rearrangement. The decay was attributed to spin–orbit-induced autodetachment ($[\text{I}^*(^2\text{P}_{1/2})\text{Xe}_n]^- \rightarrow \text{I}^*(^2\text{P}_{3/2})\text{Xe}_n + e^-$); longer lifetimes for the larger clusters implied solvent screening of the delocalized excited electron from the spin–orbit-excited iodine core. The lower $[\text{I}^*(^2\text{P}_{3/2})\text{Xe}_n]^-$ CTTS state ($n = 6-13$), previously suggested to be bound with respect to detachment,^{220,221,232,233} exhibited no appreciable decay out to hundreds of picoseconds.

Another key aspect of the solvated electron problem is the dynamics of electronically excited hydrated electrons. In aqueous solution, hydrated electrons exhibit a broad absorption band around 700 nm,²³⁴ and the development of a complete and coherent model describing the dynamics associated with this band has been the subject of a vast experimental and theoretical literature over the years.^{235,236} These considerations have motivated many investigations of water cluster anions, $(\text{H}_2\text{O})_n^-$, focusing on their energetics and spectroscopy.²³⁷⁻²³⁹ Weber et al.²⁴⁰ have performed one-color, two-photon photoelectron spectroscopy at 800 nm on $(\text{H}_2\text{O})_n^-$ anions with as many as 100 water molecules. They observed a band in the PE spectrum that was clearly attributable to resonant excitation of the excited electronic state in these clusters, which is the cluster analogue to the hydrated electron excited state. As seen in Figure 19, this band “tunes” to the excitation wavelength with increasing cluster size. Preliminary one-color pump–probe experiments at 800 nm showed the lifetime of this state to be less than 150 fs, the cross-correlation of the laser pulses. These experiments nicely complement the solvated halide experiments described above, with the overall body of work providing considerable insight into the dynamics of diffuse electrons in clusters.

5.13. Anion Intramolecular Electronic Relaxation Dynamics

As discussed previously in this article, one of the most general applications of TRPES is to probe the dynamics of radiationless transitions, because of its unique ability to track the lifetimes and relaxation pathways of excited electronic states in molecules.

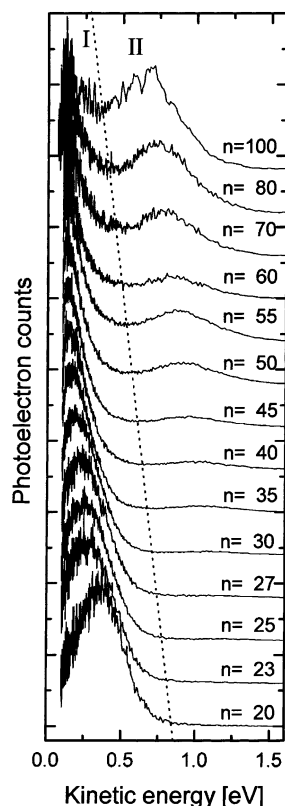


Figure 19. Resonant two-photon detachment photoelectron spectroscopy (R2PD-PES) of $(\text{H}_2\text{O})_n^-$ clusters ($n = 20$ – 100) with ~ 100 fs laser pulses. Absorption tunes to the ~ 1.5 eV (800 nm) excitation energy with increasing cluster size. Electron kinetic energy ranges associated with one- and two-photon absorption are labeled I and II, respectively. Direct two-photon detachment represents the cluster analogue of excitation to the bulk conduction band of water and competes with excited-state cluster relaxation. Reprinted with permission from ref 240. Copyright 2001 Elsevier.

Most TRPES experiments on neutrals have been of this type, as are increasing numbers in anion TRPES experiments. The major constraint in anions is the requirement of an excited electronic state below the detachment continuum, or a sufficiently long-lived state above the continuum with dynamics that are distinguishable from direct detachment (such as an autodetaching state). Both classes of excited states are generally less prevalent in anions than in neutrals, owing to the relatively low detachment energies and absence of Rydberg states in anions. On the other hand, the low detachment energies enable one to track radiationless transition pathways all the way to the ground electronic state of the anion, whereas in neutral TRPES experiments one is generally confined to excited-state processes because the ionization potential of the ground state is too high.

C_n^- clusters have been known to support multiple bound, electronically excited states. Frequency-resolved absorption experiments of these anions in rare-gas matrices and through gas-phase resonant multiphoton detachment (RMPD) have mapped excited states of these anions, as needed for this class of TRPES experiment. Minemoto et al.²⁴¹ studied the decay of the carbon trimer anion electronically excited to an above-threshold Feshbach resonance first observed in photodetachment cross-section measure-

ments.²⁴² The $^2\Delta_u$ state of C_3^- at 3.07 eV was pumped and probed at variable delay with the second harmonic of a fs Ti:sapphire amplifier such that the nature of the participating electronic states could be gleaned from the evolving spectrum. A dominant feature was assigned to a combination of direct one-photon $\text{C}_3\ ^1\Sigma_g^+ \leftarrow \text{C}_3^- \ ^2\Pi_u$ detachment and competing autodetachment from the resonantly excited state. Time-dependent peaks were assigned to direct detachment of the excited resonance to its $^3\Pi_u$ parent neutral state and a “shake-down” detachment resulting in a nominally one-electron disallowed $\text{C}_3\ ^1\Sigma_g^+ \leftarrow \text{C}_3^- \ ^2\Delta_u$ detachment. Signal from direct detachment of the excited state was determined to decay in 2.6 ± 0.7 ps.

A similar study by Frischkorn et al.²⁴³ examined irreversible electronic relaxation in C_6^- from a bound excited electronic state to the manifold of lower-lying states. Here, the $\text{C}^2\Pi_g \leftarrow \text{X}^2\Pi_u$ origin at 2.04 eV was pumped and UV-probed at various delays to investigate decay to lower-lying electronic states. Decay of the fastest electron signal occurred on a time scale of 730 ± 50 fs, while intermediate features were observed to grow in on a comparable time scale and subsequently decay on a 3.0 ± 0.1 ps time scale to a final static signal. This temporal progression was interpreted, guided by the best available neutral and anion energetics, as arising from sequential internal conversion from the initially excited *C* state through the *A* and/or *B* states. The energy and shape of the static long-time feature, accompanied by depletion recovery in the UV one-photon spectrum, suggest that relaxation ends with a highly vibrationally excited anion in its ground electronic state.

The two studies above involve energy flow between a sparse manifold of discrete electronic states. In contrast, transition metal clusters have a much higher density of electronic states, leading to the possibility that TRPES studies of such clusters will reveal the types of fast electronic relaxation processes observed in bulk metals, described better by inelastic electron–electron scattering^{244,245} than by transitions between discrete electronic states. These ideas have motivated a series of TRPES experiments on transition metal cluster anions by Pontius and co-workers.^{246–250}

For example, Pt_3^- was studied with TRPES using pump and probe pulses with photon energies of 1.5 eV.²⁴⁸ Near time zero, two-photon photoemission (2PPE) closely matches the contours of a one-photon photoelectron spectrum taken at 3.0 eV, reflecting a relatively constant density of states among unoccupied levels within the excitation window. Spectra measured at various delays from 0 fs to 500 ps exhibit a decay of structured features at low binding energy, concomitant with a buildup of structureless signal at higher binding energies. This decay (< 70 fs) was assigned to inelastic electron–electron scattering processes in which the initially excited state(s) transfer population/energy to a many-electron excited state of higher binding energy in a fast cascade.

In a similar study,²⁵⁰ Ni_3^- was pumped and probed with 3.0 eV photons; fast decay of the lowest binding energies, arising from de-excitation of the initially

populated levels, was modeled by the optical Bloch equations for a two-level system convoluted with the probing response of the experiment. A mean inelastic $e-e$ scattering rate of 215 ± 50 fs was determined, while long-time evolution of the total 2PPE was fit with an exponential decay with a constant of 450 ± 150 fs in order to estimate a mean electronic-vibrational coupling time scale.

The effect of size variation²⁴⁹ on inelastic electronic-electronic and electronic-vibrational scattering was examined with Pd_n^- . The results of this study are summarized in Figure 20, which depicts both the (normalized) time-evolving photoelectron spectra obtained for each cluster and the fit high-energy and total signal intensities that reflect electronic-electronic and electronic-nuclear relaxation pathways. Electronic relaxation time scales for Pd_3^- , Pd_4^- , and Pd_7^- are 42 ± 19 , 91 ± 17 , and 25 ± 14 fs; the faster electronic relaxation of Pd_7^- with respect to the smaller clusters is in agreement with Fermi liquid theory²⁵¹ in view of the determined extended density of unoccupied levels, whereas the faster relaxation of Pd_3^- with respect to Pd_4^- is attributed to intricacies of electronic structure for these species. Electronic-vibrational relaxation decay constants of 0.7 ± 0.3 and 1.0 ± 0.3 ps were determined for Pd_7^- and Pd_4^- , with the faster time scale for the larger cluster owing to an increased vibrational density of states.

The similarity of these time scales with those measured for the relaxation of mesoscopic and bulk transition metals^{244, 245} suggests that the high electronic level density makes the largest contribution to these decay processes. In contrast, alkali and noble metal clusters, with much lower level densities, are postulated to have much longer decay lifetimes, owing to a lowered probability for electron-electron scattering. Recent experiments by Ganteför and co-workers^{252, 253} on the electronic relaxation of excited sp metal clusters Au_3^- , Au_6^- , and Al_n^- ($n = 6-15$) reveal varied behavior relative to the above-mentioned transition metal clusters. Al_n^- clusters, with p^{n+1} configurations, were observed to decay on time scales 2–3 times longer (200–500 fs) than those of Pt_3^- and Pd_{3-7}^- , though on time scales comparable to that of Ni_3^- , consistent with the lower density of electronic states in sp metals. However, rapid relaxation of the “magic” cluster Al_{13}^- , which has a 1.5 eV HOMO–LUMO gap, suggests the participation of an effective relaxation pathway independent of electronic structure. In contrast, Au_3^- and Au_6^- (s^{n+1}) exhibit relaxation time scales between hundreds of ps to 1 ns, indicative of drastically reduced electronic densities of states. This has been explained in terms of increased interatomic interaction between Au atoms relative to other metals due to relativistic effects that increase molecular orbital splittings and bond enthalpies.

5.14. Photoelectron Angular Distributions

Progress in the study of time-resolved photoelectron angular distributions (PADs) has been reviewed recently.^{13, 14, 17} In the following, we briefly discuss developments since 1999.

Beginning in 1999, Seideman and Althorpe implemented a general nonperturbative theory²⁶ for the

calculation of time-resolved PADs in a study of molecular axis alignment in nitric oxide.⁵⁸ As discussed above, short laser pulses are inherently intense, leading to nonperturbative effects such as molecular axis alignment due to rotational Rabi cycling. These authors show that PADs in particular are quite sensitive to these, and therefore a nonperturbative theory could be required in the detailed comparison of experiment with theory. The use of even stronger pump laser fields to significantly enhance the laboratory-frame axis alignment can be included in a natural way. These authors also show that the PADs are much less sensitive to the probe laser intensity, as Rabi cycling against the ionization continuum is very difficult.

In 1999–2000, V. McKoy, K. Takatsuka, and co-workers carried out sophisticated calculations on the TRPES and time-resolved PADs of Na_2 in which the exact photoionization transition amplitudes were explicitly calculated, within the Golden Rule perturbative limit, as a function of internuclear distance.^{254–256} The molecules were assumed to be rotationless and “fixed in space” (i.e., molecular frame). In their calculation, the intermediate excited state was the $2\ ^1\Sigma_u^+$ state of Na_2 , a double-minimum state in which the character of the electronic wave function changes significantly on either side of the barrier. These authors show that this affects both the photoelectron energy and angular distributions and that the assumption of a constant transition dipole for photoionization or photodetachment is problematic when the state created by the pump pulse undergoes large-amplitude nuclear motion or, for that matter, dissociation. Baumert and co-workers²⁵⁷ experimentally verified this idea with the $2\ ^1\Sigma_u^+$ state of Na_2 , demonstrating a 4-fold increase in the photoionization probability from 3 to 9 Å within the double-minimum potential by comparing and varying an R -independent wave packet simulation to time-dependent angle-averaged photoelectron intensities arising from ionization to the bound $1\ ^2\Sigma_g^+$ and repulsive $1\ ^2\Sigma_u^+$ states of Na_2^+ . In 2000, McKoy and co-workers expanded their theoretical studies by applying their formalism to the exact (but rotationless, fixed-in-space) calculation of TRPES and time-resolved PADs in the ionic-covalent curve-crossing problem in NaI .²⁵⁸

In 1999, K. L. Reid and co-workers²⁵⁹ presented a ps time-resolved PAD study of the S_1 state of p -difluorobenzene (p -DFB). In cases of favorable ionization dynamics and in the absence of electronically non-adiabatic processes, PADs can be a direct monitor of the evolution of molecular axis distributions in the laboratory frame. These authors demonstrate that the PADs can be sensitive to rotationally mediated IVR, which leads to “irregular” rotation, as compared to a rigid rotor. Rotations about the a axis are expected to have recurrences about every 280 ps, in comparison to those about the b and c axes, about every 44 ps. Significant deviations from rigid rotor behavior were observed, indicative of IVR in the S_1 state.

Theoretical work by Reid and Underwood⁶⁰ on the extraction of molecular axis alignment from the

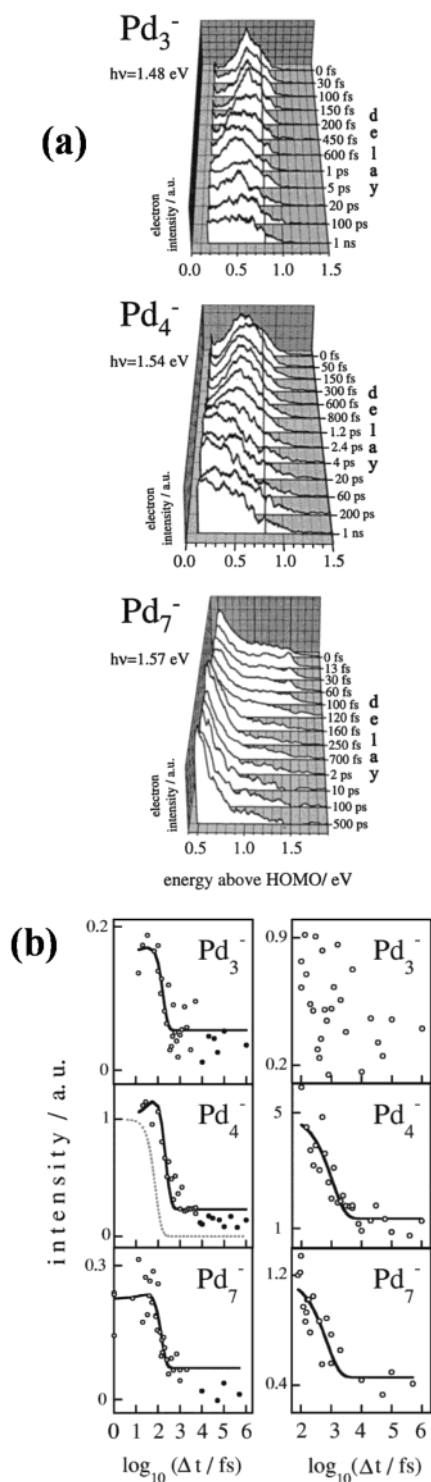


Figure 20. (a) Pump-probe photoelectron difference spectroscopy of Pd_n^- clusters ($n = 3, 4, 7$) taken with ~ 80 fs, 1.5 eV laser pulses. Spectra have been normalized to total intensity to display relative intensity evolution and have been referenced to excitation energy in excess of the cluster HOMO (1.5, 1.45, and 1.9 for 3, 4, and 7, respectively). (b) (Left) Integrated two-photon photodetachment intensity from 0.8 to 1.5 eV ($n = 3, 4$) or from 1.1 to 1.6 eV ($n = 7$) above the HOMO vs pump-probe delay. Electronic relaxation within these clusters is seen to occur on a time scale comparable to the laser pulse duration, with the dashed curve in the $n = 4$ plot indicating the autocorrelation calculated for 80 fs pulses. (Right) Integrated signal between 0.0 and 1.5 eV above the HOMO (all clusters) plotted versus pump-probe delay; exponential fits for $n = 4, 7$ at delays > 100 fs give the electronic-nuclear relaxation rates reported in the text. Reprinted with permission from ref 249. Copyright 2000 American Institute of Physics.

evolution of time-resolved PADs was presented in 2000. If the ionization dynamics remain invariant over the course of this evolution (i.e., the radial dipole matrix elements are constant), then it is possible to extract the rotational wave packet evolution from the PADs. Of particular interest to experimentalists, measurement of the PADs in two polarization geometries allows extraction of a quantity directly related to the laboratory-frame alignment. As an illustration, these authors calculate the time-resolved PADs expected for pure rotational dynamics in an ideal symmetric top (as a model of p -DFB).

The relationship between the molecular and laboratory frames in PAD studies requires consideration. In the laboratory frame (for isotropic samples), the angular anisotropy is limited by the angular momentum of the photons. Specifically, the laboratory-frame PAD of an unoriented molecule produced via absorption of n photons, followed by ionization/detachment with m photons with arbitrary polarizations, may be expressed with the angular expansion

$$I(\theta, \phi) \propto \sum_{L=0}^{2n+2m} \sum_{M=-L}^L B_{LM} Y_{LM}(\theta, \phi) \quad (5)$$

in which L must be even, $Y_{LM}(\theta, \phi)$ are spherical harmonics, and B_{LM} are the angular moments taking nonzero values with $M \leq 2n$ and $2n + 2m \leq 2J_{\text{max}}$, where J_{max} is the maximum angular momentum component of the molecular frame PAD.¹⁷ Consequently, only $B_{20} (\propto \beta_2)$ and $B_{40} (\propto \beta_4)$ are relevant to $1 + 1'$ time-resolved laboratory-frame PAD studies performed with parallel linearly polarized light. This restriction does not occur in the molecular frame, which can exhibit rich angular structures due to the highly multipolar nature of the ion core. Generally, the molecular-frame PAD is most sensitive to any intramolecular dynamics. Underwood and Reid considered the ability of laboratory-frame PAD measurements to extract information about intramolecular dynamics.²⁶⁰ In their study, these authors considered the case of C_{3v} molecules and showed how the PAD depends on the nature of the laboratory-frame alignment created by the pump laser pulse. Specifically, different excited-state electronic symmetries yield different laboratory-frame PADs, reaffirming the utility of this method for studying electronically non-adiabatic processes.

Beginning in 2000, Seideman and co-workers applied their general formalism of time-resolved PADs to polyatomic molecules.^{134,261} Using a model of the $S_2 \ ^1\text{B}_u \rightarrow S_1 \ ^2 \ ^1\text{A}_g$ internal conversion in octatetraene (OT, C_{2h}), they show that the photoelectron angular distributions are very sensitive to changes in the shape and symmetry of the excited-state electronic wave function associated with the non-adiabatic dynamics and could therefore provide complementary information to energy-resolved, angle-integrated measurements, especially in the case of Type II ionization correlations.^{42,134} In the case of OT, the PADs required the inclusion of partial waves up to $l = 6$ or 7 in order to be converged to within 10%. The asymmetry parameters for single-photon ionization of the excited S_2 and S_1 states into the ground electronic

state of the cation were found to differ significantly, suggesting that PADs should be able to directly monitor the non-adiabatic transition. Seideman and Althorpe subsequently investigated in more detail the effects of coherent rotational motion²⁶² and centrifugal rotation–vibration coupling⁵⁹ on the form of the time-resolved PADs. Importantly, the nuclear coordinate dependence of the electronic bound-free transition amplitudes did not obscure the effects of rotation–vibration coupling on the PADs. A complete discussion of the formal nonperturbative theory for calculating time-resolved PADs in polyatomic systems, including some numerical simulations, was presented by Seideman in 2001.²⁶³

In 2002–2003, Seideman and co-workers extended their theoretical methods for calculating time-resolved PADs to multivibrational-mode, polyatomic systems. Their method takes rotations into exact account, treats the fields nonperturbatively, and computes the electronic dynamics from first principles using density functional theory combined with a spline function basis set.^{27,28} Importantly, this approximate method for the electronic structure calculation should be scalable to larger systems. As a first application, they studied the ultrafast $S_2 \rightarrow S_1$ internal conversion dynamics of pyrazine, to compare with the original 1991 calculations of Domcke.^{24,25} These authors observed that the energy-resolved asymmetry parameters do indeed map out the electronic population dynamics, filtering out the fast vibrational motions that complicate the energy-resolved angle-integrated photoelectron spectra. They also note, however, that the photoelectron energy dependence of the ionization matrix elements leads to significant and nontrivial effects on the observed asymmetry parameters. This indicates that energy-integrated angle-resolved probes will likely not transparently map out the electronic population dynamics. The use of filtering of wave packet signals in order to extract information about intramolecular coupling time scales was previously considered by Seideman, Stolow, and co-workers,²⁶⁴ and PADs provide an example of this.

The development of photoelectron imaging techniques (section 4) has greatly facilitated the study of time-dependent PADs. As discussed in section 5.1, in 1999 T. Suzuki and co-workers applied 2D time-resolved photoelectron imaging (TRPEI) to the study of intersystem crossing (ISC) in the pyrazine S_1 $^1B_{3u}$ ($n\pi^*$) and S_2 $^1B_{2u}$ ($\pi\pi^*$) states.^{135,136} The β_2 anisotropy parameters at 60 ps delay were measured to be 1.1 and 1.7 for the S_1 and T_1 states, respectively. The full analysis of the PADs could be complicated by the expected energy dependence of the ionization amplitudes for π electron ejection²⁶⁵ and by intermediate resonances in the two-photon ionization scheme. The authors report that no dramatic evolution in the form of the PADs was observed in these experiments.

In 2001, Suzuki and co-workers applied their TRPEI technique to the study of excited-state rotational wave packet dynamics in the pyrazine S_1 $^1B_{3u}$ ($n\pi^*$) state.²⁶⁶ Using a two-photon ionization scheme, the authors were able to probe the evolving laboratory-frame S_1 molecular axis distribution

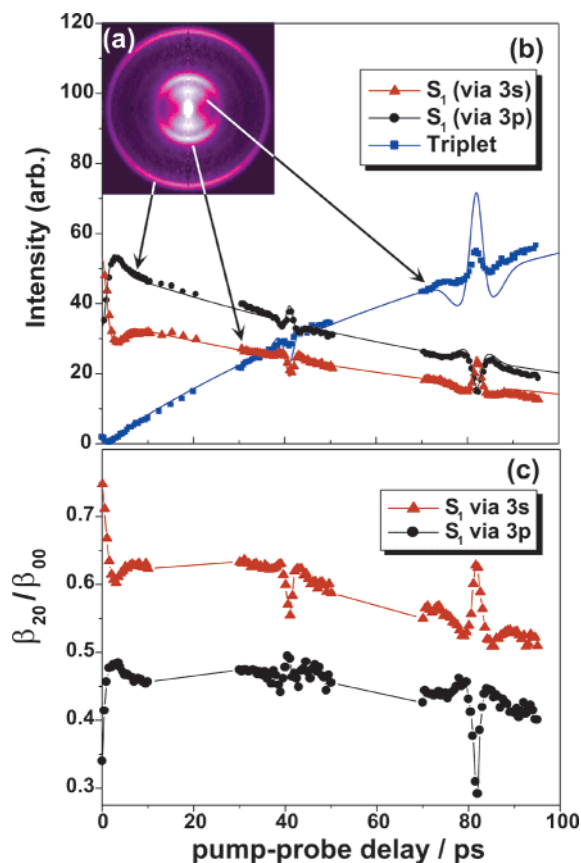


Figure 21. Time-resolved photoelectron imaging of rotational wave packet dynamics in pyrazine excited states, pumped at 323 nm and probed via two-photon ionization at 401 nm. (a) Inverse Abel-transformed image of photoelectrons from pyrazine $[1 + 2']$ ionization at a time delay of 30 ps. (b) Time evolution of the intensity of the photoelectron spectra corresponding to the S_1 state via a 3s resonance, the S_1 state via a 3p resonance, and the triplet state. (c) Time evolution of the normalized β_{20} asymmetry parameter for photoelectron spectra corresponding to the S_1 state via a 3s resonance, the S_1 state via a 3p resonance, and the triplet state. Rotational revivals are seen in both the intensities and asymmetry parameters. The solid lines are fits to the rotational coherence. Reprinted from ref 266. Copyright 2001 American Physical Society.

through both a 3s (parallel transition) and a 3p (perpendicular transition) Rydberg state. As shown in Figure 21, beautiful rotational revivals are seen in both the signal intensity and asymmetry parameters. The atomic-like 3s orbital produces predominantly $p\pi$ -type electrons. The 3p ionization channel, by contrast, requires outgoing partial waves of a_g symmetry. Interestingly, rotational revivals were also seen in the triplet manifold ionization channel. The reduced intensity in the triplet revival structure was attributed to the much larger number of energy levels (~ 20) in the superposition after the intersystem crossing. Using single-probe photon ionization (200 nm), a characteristic 4-fold symmetry was seen in the PADs near $t = 0$, which vanished by ~ 3 ps, from which time a rather featureless PAD without revival structures was observed. A more complete discussion of the ionization dynamics of the pyrazine 3s and 3p Rydberg states followed in 2001.¹⁴⁵

As discussed in section 5.6, in 2000 Hayden and co-workers used the 3D coincidence-imaging spec-

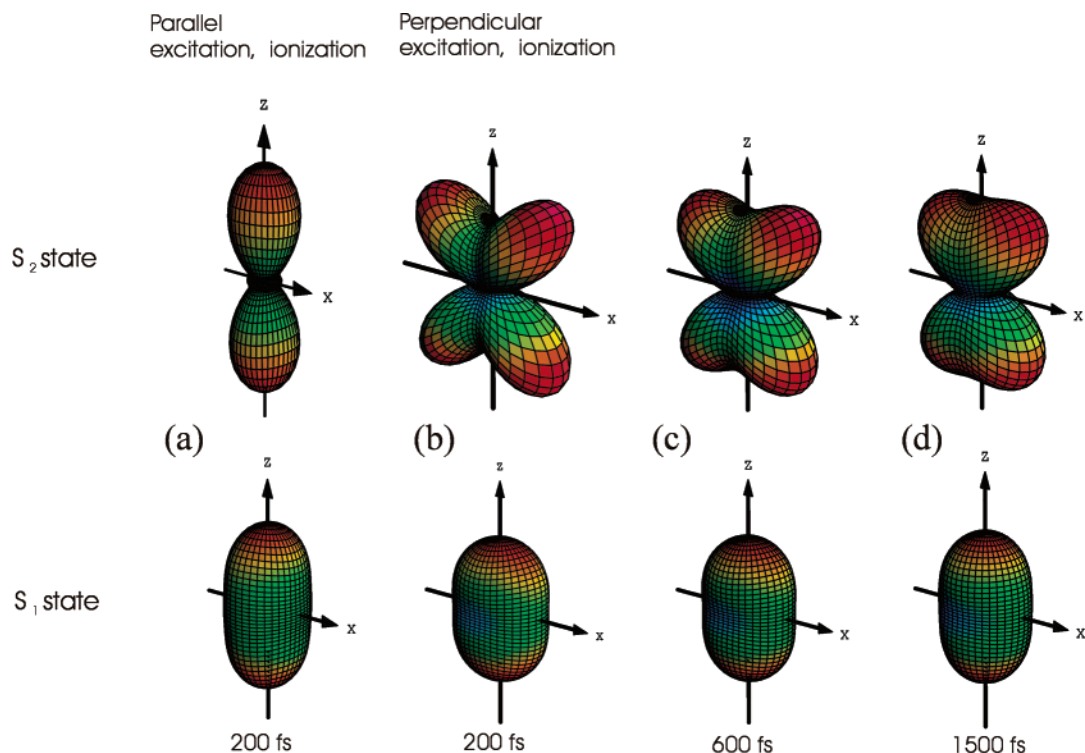


Figure 22. Time-resolved photoelectron angular distributions (PADs) from fs ionization of DABCO. Here, the optically bright S_2 $^1E'$ state internally converts to the dark S_1 $^1A_1'$ state on ps time scales. (a) PADs at 200 fs time delay for pump and probe polarization vectors, both parallel to the spectrometer axis. The difference in electronic symmetry between S_2 and S_1 leads to significant changes in the form of the PAD. (b) PADs at 200 fs time delay for pump polarization parallel and probe polarization perpendicular to the spectrometer axis, showing the effects of laboratory-frame molecular alignment. (c,d) The PADs evolve as a function of time due to molecular axis rotational wave packet dynamics. Used with permission from C. C. Hayden, unpublished.

troscopy (CIS) method to observe the evolution of molecular-frame PADs during the photodissociation of NO_2 .¹¹⁶ In 2002, Hayden and co-workers studied the S_2 $^1E' \rightarrow S_1$ $^1A_1'$ internal conversion in triethylenediamine (DABCO) using the CIS method. This work represents the current state of the art in studying intramolecular dynamics via time-resolved PADs. As shown in Figure 22, dramatic evolution of the PADs is seen for both the decaying S_2 state (top) and the forming S_1 state (bottom). When the probe laser is parallel to the pump laser (a), the initial S_2 state PAD is dumb-bell-shaped. For perpendicular ionization (b), it is a quadrupolar structure. Both of these types of PADs evolve in time, reflecting the intramolecular dynamics. It is interesting to note that the quadrupolar structure seen in the S_2 PADs using perpendicular polarizations would not be observable using the 2D photoelectron imaging technique. Together with the non-cylindrically symmetric PADs observed in NO_2 photodissociation, this work illustrates the technical advantages of 3D over 2D particle imaging methods.

The first anion TRPEI experiments were reported by Davis et al.²⁶⁷ in 2003, in which I_2^- dissociation along the A' $^2\Pi_{g,1/2}$ state following absorption at 793 nm was examined. With a dissociation lifetime well-established from previous FPES studies, I_2^- presented a useful standard for this new application. Time-resolved radially-integrated PES reflect the same dynamics as observed in the previous studies, and as the anion dissociation occurs on a time scale much shorter than molecular rotation, changes in the

PAD anisotropy as a function of pump–probe delay reflect evolution of the electronic structure through dissociation. The leading anisotropy β_2 drops significantly from 0 to 250 fs, corresponding to the time interval in the electron kinetic energy spectrum in which the Γ^- photoproduct becomes evident. However, β_2 continues to evolve at delay times as large as 700–800 fs, at which point the photofragments are separated by more than 10 Å, while at longer times (>1 ps) the anisotropy matches that of Γ^- (-0.520 ± 0.035), arising from s- and d-wave interference. The changes in β_2 around 700–800 fs were attributed to an electric field-induced mixing between the A' and X electronic states, with g and u symmetry, respectively, at large internuclear separations where the two states are nearly degenerate. This mixing leads to a change in the character of the orbital in which the electron resides, from an orbital which has equal amplitude on two weakly interacting I atoms to one which is localized on a single I atom, so that photodetachment occurs from truly separated $\text{I} + \text{I}^-$ products.

In another time-resolved anion photoelectron imaging experiment, similar in vein to Suzuki's pyrazine experiments,¹³⁵ subtle temporal evolution in the photoelectron anisotropy following detachment from the long-lived B $^2\Sigma_g^+$ state of C_2^- was examined by [1 + 1'] pump–probe photodetachment.²⁶⁸ C_2^- PADs and anisotropy modulations are depicted in Figure 23. The PADs show a full revival at ~ 8900 fs, consistent with the well-known rotational constant

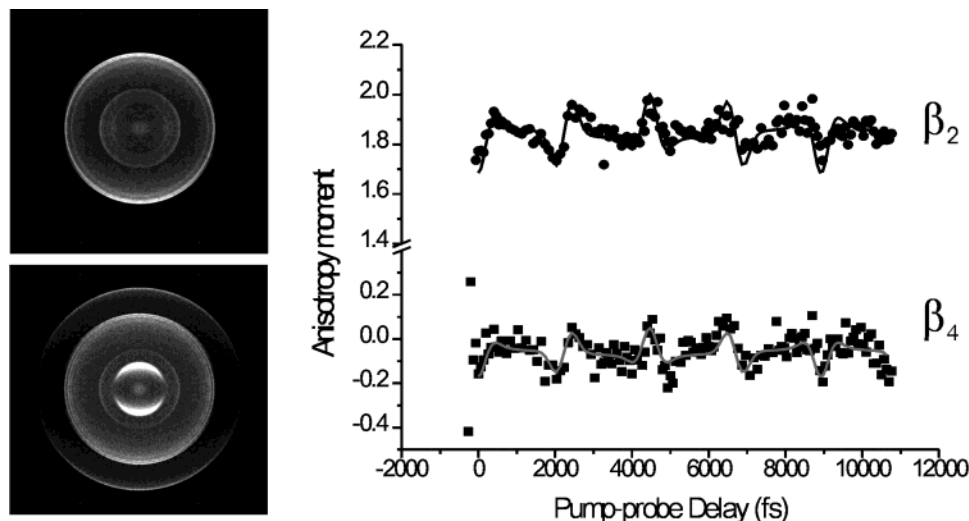


Figure 23. (Top left) One-photon C_2^- photodetachment PAD at 264 nm. (Bottom left) Two-color $[1 + 1]C_2^-$ photodetachment PAD (541 + 264 nm) measured with a ~ 100 ps pump-probe delay. (Right) Second- and fourth-order anisotropy moments measured as a function of pump-probe delay. Solid curves are quantitative fits to a calculated molecular alignment function. Reprinted with permission from ref 268. Copyright 2003 Elsevier.

for the B state of C_2^- (1.87 cm^{-1}). This experiment is the first application of rotational coherence spectroscopy to an anion. Furthermore, qualitative analysis of the anisotropy oscillation in reference to molecular alignment following a parallel transition in a simple diatomic, guided by ideas put forth by Sanov,¹⁰² Reed,²⁶⁹ and Reid and Underwood,⁶⁰ provides some insight into the molecular-frame detachment process, indicating a detachment wave with larger amplitude perpendicular rather than parallel to the molecular axis.

6. Conclusions and Future Directions

We have presented a comprehensive review of time-resolved photoelectron spectroscopy as applied to the dynamics of gas-phase neutral and anionic molecules and clusters. TRPES and its variants are powerful, relatively new techniques that lend themselves to highly detailed time-resolved studies of inter- and intramolecular dynamics. We have attempted to describe the utility of this technique for studying a variety of fundamental photochemical and photophysical processes. TRPES directly probes the evolution of nonstationary states (wave packets) via projection onto the “universal” final state of the electronic continuum. With appropriate choice of photoionization/photodetachment wavelength, TRPES is capable of revealing electronic and nuclear dynamics and their couplings, including dynamics in “dark” states, thus permitting identification of all involved states and time scales. The signature of rotational wave packet dynamics associated with time-evolving molecular axis alignment distributions and the elucidation of vector correlations have been observed through angularly resolved variants of TRPES. To date, TRPES has been applied to an impressive range of photophysical and photochemical problems.

Future applications of this technique will benefit from ongoing developments in detector technologies, femtosecond and attosecond laser sources, and non-

linear optical frequency conversion schemes as well as synchrotron and free electron laser accelerator physics. These developments will push the scope of TRPES research to include molecular-frame measurements, photofragment-photofragment scalar and vector correlations, extreme time scales, and inner-shell dynamics. For example, the use of shaped, intense nonresonant laser fields to create field-free alignment in polyatomic systems^{270,271} will combine with 2D and 3D imaging variants of TRPES to probe molecular-frame dynamics. Further development of the multiply differential photoelectron-photofragment coincidence and coincidence-imaging methods will permit highly detailed investigation of statistical and nonstatistical photoinduced charge and energy flow, an area of fundamental dynamical interest and of interest in applications to the gas-phase photophysics of biomolecules.²⁷² The development of high average power femtosecond VUV/XUV sources and the dawn of attosecond science present the possibility of probing highly excited states, core dynamics, and electron correlation in real time. Parallel theoretical developments in *ab initio* molecular dynamics methods for studying non-adiabatic processes in polyatomic molecules/anions and in new methods for calculating photoionization/photodetachment differential cross sections will play an increasingly important role in the future of TRPES. All of these areas of research present significant new experimental and theoretical challenges, and we anticipate exciting developments and contributions from many in the coming years.

7. Acknowledgments

A.S. thanks co-workers Prof. I. Fischer (Würzburg), Dr. M. J. J. Vrakking (FOM, Amsterdam), Dr. V. Blanchet (Toulouse), Dr. S. Lochbrunner (München), Dr. M. Schmitt (Würzburg), Prof. J. P. Shaffer (Oklahoma), Dr. J. J. Larsen (Aarhus), Dr. D. M. Villeneuve (NRC), Dr. T. Schultz (Max-Born-Institute, Berlin), Dr. J. G. Underwood (Open University

UK), Prof. I.-C. Chen (Tsing-Hua), Dr. S.-H. Lee (Tsing-Hua), Dr. S. Ullrich (NRC), and especially Dr. M. Z. Zgierski (NRC). A.S. also thanks Prof. K. Müller-Dethlefs (York) for discussions on ZEKE photoelectron spectroscopy, Prof. C. A. de Lange (Amsterdam) for discussions on magnetic bottle photoelectron spectroscopy, Dr. C. C. Hayden (Sandia National Laboratories) for ongoing collaborations on fs time-resolved 3D coincidence-imaging spectroscopy, Prof. T. Seideman (Northwestern) and Prof. K. L. Reid (Nottingham) for many enlightening discussions on photoelectron angular distribution measurements, and Prof. W. Domcke (München), Prof. M. Olivucci (Siena), and Prof. T. Martinez (Illinois) for numerous helpful discussions on non-adiabatic dynamics in polyatomic molecules. A.E.B. and D.M.N. gratefully acknowledge support from the National Science Foundation under Grant No. CHE-0092574 and thank their many co-workers on the anion femtosecond photoelectron spectroscopy project in their laboratory: B. Jefferys Greenblatt, Martin Zanni, Alison Davis, Christian Frischkorn, Rainer Weinkauff, Leo Lehr, Benoit Soep, Mohammed Elhanine, Arthur Bragg, Roland Wester, Aster Kammrath, and Jan Verlet.

8. References

- Zewail, A. H. *J. Phys. Chem. A* **2000**, *104*, 5660.
- Bixon, M.; Jortner, J. *J. Chem. Phys.* **1968**, *48*, 715.
- Jortner, J.; Rice, S. A.; Hochstrasser, R. M. *Adv. Photochem.* **1969**, *7*, 149.
- Henry, S. R.; Siebrand, W. In *Organic Molecular Photophysics*; Birks, J. B., Ed.; Wiley: London, 1973; Vol. 1, p 152.
- Freed, K. F. In *Radiationless Processes in Molecules and Condensed Phases*; Fong, F. K., Ed.; Springer-Verlag: Berlin, 1976; p 23.
- Stock, G.; Domcke, W. *Adv. Phys. Chem.* **1997**, *100*, 1.
- Michl, J.; Bonacic-Koutecky, V. *Electronic Aspects of Organic Photochemistry*; Wiley: New York, 1990.
- Schoenlein, R. W.; Peteanu, L. A.; Mathies, R. A.; Shank, C. V. *Science* **1991**, *254*, 412.
- Jortner, J.; Ratner, M. A. *Molecular Electronics*; IUPAC, Blackwell: Oxford, 1997.
- Haight, R.; Bokor, J.; Stark, J.; Storz, R. H.; Freeman, R. R.; Bucksbaum, P. H. *Phys. Rev. Lett.* **1985**, *54*, 1302.
- Hayden, C. C.; Stolow, A. In *Advanced Physical Chemistry*; Ng, C.-Y., Ed.; World Scientific: Singapore, 2000; p 10.
- Neumark, D. M. *Annu. Rev. Phys. Chem.* **2001**, *52*, 255.
- Suzuki, T.; Whitaker, B. J. *Int. Rev. Phys. Chem.* **2001**, *20*, 313.
- Seideman, T. *Annu. Rev. Phys. Chem.* **2002**, *53*, 41.
- Stolow, A. *Annu. Rev. Phys. Chem.* **2003**, *54*, 89.
- Stolow, A. *Int. Rev. Phys. Chem.* **2003**, *22*, 377.
- Reid, K. L. *Annu. Rev. Phys. Chem.* **2003**, *54*, 397.
- Pedersen, S.; Herek, J. L.; Zewail, A. H. *Science* **1994**, *266*, 1359.
- Steadman, J.; Syage, J. A. *Rev. Sci. Instrum.* **1993**, *64*, 3094.
- Kruit, P.; Read, F. H. *J. Phys. E: Sci. Instrum.* **1983**, *16*, 313.
- Cheshnovsky, O.; Yang, S. H.; Pettiette, C. L.; Craycraft, M. J.; Smalley, R. E. *Rev. Sci. Instrum.* **1987**, *58*, 2131.
- de Lange, C. A. In *High-Resolution Laser Photoionization and Photoelectron Studies*; Powis, I., Baer, T., Ng, C. Y., Eds.; Wiley: New York, 1995; p 195.
- Eland, J. H. D. *Photoelectron Spectroscopy*; Butterworth: London, 1984.
- Seel, M.; Domcke, W. *J. Chem. Phys.* **1991**, *95*, 7806.
- Seel, M.; Domcke, W. *Chem. Phys.* **1991**, *151*, 59.
- Seideman, T. *J. Chem. Phys.* **1997**, *107*, 7859.
- Suzuki, Y.; Stener, M.; Seideman, T. *Phys. Rev. Lett.* **2002**, *89*, 233002.
- Suzuki, Y.; Stener, M.; Seideman, T. *J. Chem. Phys.* **2003**, *118*, 4432.
- Kosloff, R. *Annu. Rev. Phys. Chem.* **1994**, *45*, 145.
- Braun, M.; Meier, C.; Engel, V. *J. Chem. Phys.* **1995**, *103*, 7907.
- Meier, C.; Engel, V. *Phys. Chem. Chem. Phys.* **2002**, *4*, 5014.
- Rubner, O.; Meier, C.; Engel, V. *J. Chem. Phys.* **1997**, *107*, 1066.
- Fischer, I.; Villeneuve, D. M.; Vrakking, M. J. J.; Stolow, A. *J. Chem. Phys.* **1995**, *102*, 5566.
- Fischer, I.; Vrakking, M. J. J.; Villeneuve, D. M.; Stolow, A. *Chem. Phys.* **1996**, *207*, 331.
- Assion, A.; Geisler, M.; Helbing, J.; Seyfried, V.; Baumert, T. *Phys. Rev. A* **1996**, *54*, R4605.
- Greenblatt, B. J.; Zanni, M. T.; Neumark, D. M. *Chem. Phys. Lett.* **1996**, *258*, 523.
- Zanni, M. T.; Batista, V. S.; Greenblatt, B. J.; Miller, W. H.; Neumark, D. M. *J. Chem. Phys.* **1999**, *110*, 3748.
- Cyr, D. R.; Hayden, C. C. *J. Chem. Phys.* **1996**, *104*, 771.
- Blanchet, V.; Stolow, A. In *Ultrafast Phenomena XI*; Elsaesser, T., Fujimoto, J. G., Wiersma, D. A., Zinth, W., Eds.; Springer Series in Chemical Physics 63; Springer-Verlag: Berlin, 1998; p 456.
- Blanchet, V.; Zgierski, M. Z.; Seideman, T.; Stolow, A. *Nature* **1999**, *401*, 52.
- Blanchet, V.; Zgierski, M. Z.; Stolow, A. *J. Chem. Phys.* **2001**, *114*, 1194.
- Schmitt, M.; Lochbrunner, S.; Shaffer, J. P.; Larsen, J. J.; Zgierski, M. Z.; Stolow, A. *J. Chem. Phys.* **2001**, *114*, 1206.
- Bandrauk, A. D. *Molecules in Laser Fields*; Marcel Dekker: New York, 1994.
- Gavrila, M. *Atoms in Intense Laser Fields*; Academic Press: San Diego, 1992.
- Zavriyev, A.; Fischer, I.; Villeneuve, D. M.; Stolow, A. *Chem. Phys. Lett.* **1995**, *234*, 281.
- Freeman, R. R.; Bucksbaum, P. H. *J. Phys. B: At. Mol. Opt. Phys.* **1991**, *24*, 325.
- Assion, A.; Baumert, T.; Helbing, J.; Gerber, G. In *Ultrafast Phenomena X*; Fujimoto, J. G., Zinth, W., Barbara, P. F., Knox, W. H., Eds.; Springer Series in Chemical Physics 62; Springer-Verlag: Berlin Heidelberg, 1996; p 270.
- Assion, A.; Baumert, T.; Helbing, J.; Seyfried, V.; Gerber, G. *Phys. Rev. A* **1997**, *55*, 1899.
- Baumert, T.; Gerber, G. *Phys. Scr.* **1997**, *T72*, 53.
- Frohmeyer, T.; Baumert, T. *Appl. Phys. B* **2000**, *71*, 259.
- Wollenhaupt, M.; Assion, A.; Bazhan, O.; Liese, D.; Sarpe-Tudoran, C.; Baumert, T. *Appl. Phys. B* **2002**, *74*, S121.
- Frohmeyer, T.; Hofmann, H.; Strehle, M.; Baumert, T. *Chem. Phys. Lett.* **1999**, *312*, 447.
- Ludowise, P.; Blackwell, M.; Chen, Y. *Chem. Phys. Lett.* **1996**, *258*, 530.
- Sun, Z. G.; Liu, H. P.; Lou, N. Q.; Cong, S. L. *Chem. Phys. Lett.* **2003**, *369*, 374.
- Seideman, T. *J. Chem. Phys.* **1995**, *103*, 7887.
- Seideman, T. *Phys. Rev. Lett.* **1999**, *83*, 4971.
- Ortigozo, J.; Rodriguez, M.; Gupta, M.; Friedrich, B. *J. Chem. Phys.* **1999**, *110*, 3870.
- Althorpe, S. C.; Seideman, T. *J. Chem. Phys.* **1999**, *110*, 147.
- Althorpe, S. C.; Seideman, T. *J. Chem. Phys.* **2000**, *113*, 7901.
- Reid, K. L.; Underwood, J. G. *J. Chem. Phys.* **2000**, *112*, 3643.
- Pallix, J. B.; Colson, S. D. *Chem. Phys. Lett.* **1985**, *119*, 38.
- Sekretka, E.; Reilly, J. P. *Chem. Phys. Lett.* **1988**, *149*, 482.
- Song, X. B.; Wilkerson, C. W.; Lucia, J.; Pauls, S.; Reilly, J. P. *Chem. Phys. Lett.* **1990**, *174*, 377.
- Smith, J. M.; Lakshminarayan, C.; Knee, J. L. *J. Chem. Phys.* **1990**, *93*, 4475.
- Syage, J. A. *Chem. Phys. Lett.* **1993**, *202*, 227.
- Syage, J. A. *J. Phys. Chem.* **1995**, *99*, 5772.
- Kim, B.; Schick, C. P.; Weber, P. M. *J. Chem. Phys.* **1995**, *103*, 6903.
- Dobber, M. R.; Buma, W. J.; Delange, C. A. *J. Chem. Phys.* **1993**, *99*, 836.
- Dobber, M. R.; Buma, W. J.; Delange, C. A. *J. Phys. Chem.* **1995**, *99*, 1671.
- Schultz, T.; Fischer, I. *J. Chem. Phys.* **1997**, *107*, 8197.
- Schultz, T.; Fischer, I. *J. Chem. Phys.* **1998**, *109*, 5812.
- Schultz, T.; Clarke, J. S.; Gilbert, T.; Deyerl, H. J.; Fischer, I. *Faraday Discuss.* **2000**, *17*.
- Baumert, T.; Thalweiser, R.; Gerber, G. *Chem. Phys. Lett.* **1993**, *209*, 29.
- Assion, A.; Baumert, T.; Helbing, J.; Seyfried, V.; Gerber, G. *Chem. Phys. Lett.* **1996**, *259*, 488.
- Ganteför, G.; Kraus, S.; Eberhardt, W. *J. Electron Spectrosc. Relat. Phenom.* **1998**, *88*, 35.
- Lopez-Martens, R.; Long, P.; Solgadi, D.; Soep, B.; Syage, J.; Millie, P. *Chem. Phys. Lett.* **1997**, *273*, 219.
- Blanchet, V.; Stolow, A. *J. Chem. Phys.* **1998**, *108*, 4371.
- Kajimoto, O.; Honma, K.; Kobayashi, T. *J. Phys. Chem.* **1985**, *89*, 2725.
- Stert, V.; Radloff, W.; Freudenberg, T.; Noack, F.; Hertel, I. V.; Jouvet, C.; Dedonderlardeux, C.; Solgadi, D. *Europhys. Lett.* **1997**, *40*, 515.
- Radloff, W.; Stert, V.; Freudenberg, T.; Hertel, I. V.; Jouvet, C.; Dedonderlardeux, C.; Solgadi, D. *Chem. Phys. Lett.* **1997**, *281*, 20.
- Stert, V.; Radloff, W.; Schulz, C. P.; Hertel, I. V. *Eur. Phys. J. D* **1999**, *5*, 97.
- Noguchi, T.; Sato, S.; Fujimura, Y. *Chem. Phys. Lett.* **1989**, *155*, 177.

- (83) Reid, K. L. *Chem. Phys. Lett.* **1993**, *215*, 25.
- (84) Reid, K. L.; Duxon, S. P.; Towrie, M. *Chem. Phys. Lett.* **1994**, *228*, 351.
- (85) Meier, C.; Engel, V. *Chem. Phys. Lett.* **1993**, *212*, 691.
- (86) Meier, C.; Engel, V. *J. Chem. Phys.* **1994**, *101*, 2673.
- (87) Braun, M.; Meier, C.; Engel, V. *J. Chem. Phys.* **1996**, *105*, 530.
- (88) Vrakking, M. J. J.; Villeneuve, D. M.; Stolow, A. *J. Chem. Phys.* **1996**, *105*, 5647.
- (89) Braun, M.; Engel, V. *Z. Phys. D* **1997**, *39*, 301.
- (90) Meyer, S.; Meier, C.; Engel, V. *J. Chem. Phys.* **1998**, *108*, 7631.
- (91) Lochbrunner, S.; Larsen, J. J.; Shaffer, J. P.; Schmitt, M.; Schultz, T.; Underwood, J. G.; Stolow, A. *J. Electron Spectrosc. Relat. Phenom.* **2000**, *112*, 183.
- (92) Wang, L. S.; Cheng, H. S.; Fan, J. W. *J. Chem. Phys.* **1995**, *102*, 9480.
- (93) Hotop, H.; Lineberger, W. C. *J. Phys. Chem. Ref. Data* **1985**, *14*, 731.
- (94) Markovich, G.; Perera, L.; Berkowitz, M. L.; Cheshnovsky, O. *J. Chem. Phys.* **1996**, *105*, 2675.
- (95) Handschuh, H.; Gantefor, G.; Eberhardt, W. *Rev. Sci. Instrum.* **1995**, *66*, 3838.
- (96) Wang, L. S.; Ding, C. F.; Wang, X. B.; Barlow, S. E. *Rev. Sci. Instrum.* **1999**, *70*, 1957.
- (97) Giniger, R.; Hippler, T.; Ronen, S.; Cheshnovsky, O. *Rev. Sci. Instrum.* **2001**, *72*, 2543.
- (98) Eppink, A. T. J. B.; Parker, D. H. *Rev. Sci. Instrum.* **1997**, *68*, 3477.
- (99) Heck, A. J. R.; Chandler, D. W. *Annu. Rev. Phys. Chem.* **1995**, *46*, 335.
- (100) Parker, D. H.; Eppink, A. T. J. B. *J. Chem. Phys.* **1997**, *107*, 2357.
- (101) Bordas, C.; Paulig, F.; Helm, H.; Huestis, D. L. *Rev. Sci. Instrum.* **1996**, *67*, 2257.
- (102) Surber, E.; Sanov, A. *J. Chem. Phys.* **2002**, *116*, 5921.
- (103) Whitaker, B. J. In *Imaging in Chemical Dynamics*; Suits, A. G., Continetti, R. E., Eds.; American Chemical Society: Washington, DC, 2000; p 68.
- (104) Vrakking, M. J. J. *Rev. Sci. Instrum.* **2001**, *72*, 4084.
- (105) Dribinski, V.; Ossaditchi, A.; Mandelshtam, V. A.; Reisler, H. *Rev. Sci. Instrum.* **2002**, *73*, 2634.
- (106) Gebhardt, C. R.; Rakitzis, T. P.; Samartzis, P. C.; Ladopoulos, V.; Kitsopoulos, T. N. *Rev. Sci. Instrum.* **2001**, *72*, 3848.
- (107) Townsend, D.; Miniti, M. P.; Suits, A. G. *Rev. Sci. Instrum.* **2003**, *74*, 2530.
- (108) Continetti, R. E.; Hayden, C. C. In *Advanced Series in Physical Chemistry: Modern Trends in Chemical Reaction Dynamics*; Liu, K., Yang, X., Eds.; World Scientific: Singapore, 2003.
- (109) Martin, C.; Jelinsky, P.; Lampton, M.; Malina, R. F.; Anger, H. O. *Rev. Sci. Instrum.* **1981**, *52*, 1067.
- (110) Continetti, R. E.; Cyr, D. R.; Osborn, D. L.; Leahy, D. J.; Neumark, D. M. *J. Chem. Phys.* **1993**, *99*, 2616.
- (111) Ali, I.; Dorner, R.; Jagutzki, O.; Nuttgens, S.; Mergel, V.; Spielberger, L.; Khayyat, K.; Vogt, T.; Brauning, H.; Ullmann, K.; Moshhammer, R.; Ullrich, J.; Hagmann, S.; Groeneveld, K. O.; Cocke, C. L.; Schmidt-Bocking, H. *Nucl. Instrum. Methods B* **1999**, *149*, 490.
- (112) Hanold, K. A.; Luong, A. K.; Clements, T. G.; Continetti, R. E. *Rev. Sci. Instrum.* **1999**, *70*, 2268.
- (113) Hanold, K. A.; Garner, M. C.; Continetti, R. E. *Phys. Rev. Lett.* **1996**, *77*, 3335.
- (114) Garner, M. C.; Hanold, K. A.; Resat, M. S.; Continetti, R. E. *J. Phys. Chem. A* **1997**, *101*, 6577.
- (115) Davies, J. A.; LeClaire, J. E.; Continetti, R. E.; Hayden, C. C. *J. Chem. Phys.* **1999**, *111*, 1.
- (116) Davies, J. A.; Continetti, R. E.; Chandler, D. W.; Hayden, C. C. *Phys. Rev. Lett.* **2000**, *84*, 5983.
- (117) Krausz, F.; Fermann, M. E.; Brabec, T.; Curley, P. F.; Hofer, M.; Ober, M. H.; Spielmann, C.; Wintner, E.; Schmidt, A. J. *IEEE J. Quantum Elect.* **1992**, *28*, 2097.
- (118) Squier, J.; Salin, F.; Mourou, G.; Harter, D. *Opt. Lett.* **1991**, *16*, 324.
- (119) Nisoli, M.; Desilvestri, S.; Magni, V.; Svelto, O.; Danielius, R.; Piskarskas, A.; Valiulis, G.; Varanavicius, A. *Opt. Lett.* **1994**, *19*, 1973.
- (120) Wilhelm, T.; Piel, J.; Riedle, E. *Opt. Lett.* **1997**, *22*, 1494.
- (121) L'Huillier, A. *J. Nonlinear Opt. Phys. Mater.* **1995**, *4*, 647.
- (122) Spielmann, C.; Burnett, N. H.; Sartania, S.; Koppitsch, R.; Schnurer, M.; Kan, C.; Lenzner, M.; Wobrauschek, P.; Krausz, F. *Science* **1997**, *278*, 661.
- (123) Rundquist, A.; Durfee, C. G.; Chang, Z. H.; Herne, C.; Backus, S.; Murnane, M. M.; Kapteyn, H. C. *Science* **1998**, *280*, 1412.
- (124) Bartels, R.; Backus, S.; Zeek, E.; Misoguti, L.; Vdovin, G.; Christov, I. P.; Murnane, M. M.; Kapteyn, H. C. *Nature* **2000**, *406*, 164.
- (125) Durfee, C. G.; Rundquist, A. R.; Backus, S.; Herne, C.; Murnane, M. M.; Kapteyn, H. C. *Phys. Rev. Lett.* **1999**, *83*, 2187.
- (126) Sorensen, S. L.; Bjorneholm, O.; Hjelte, I.; Kihlgren, T.; Ohrwall, G.; Sundin, S.; Svensson, S.; Buil, S.; Descamps, D.; L'Huillier, A.; Norin, J.; Wahlstrom, C. G. *J. Chem. Phys.* **2000**, *112*, 8038.
- (127) Nugent-Glandorf, L.; Scheer, M.; Samuels, D. A.; Bierbaum, V.; Leone, S. R. *Rev. Sci. Instrum.* **2002**, *73*, 1875.
- (128) Nugent-Glandorf, L.; Scheer, M.; Samuels, D. A.; Mulhisen, A. M.; Grant, E. R.; Yang, X. M.; Bierbaum, V. M.; Leone, S. R. *Phys. Rev. Lett.* **2001**, *87*, 193002.
- (129) Nugent-Glandorf, L.; Scheer, M.; Samuels, D. A.; Bierbaum, V. M.; Leone, S. R. *J. Chem. Phys.* **2002**, *117*, 6108.
- (130) Corkum, P. B.; Burnett, N. H.; Ivanov, M. Y. *Opt. Lett.* **1994**, *19*, 1870.
- (131) Ivanov, M.; Corkum, P. B.; Zuo, T.; Bandrauk, A. *Phys. Rev. Lett.* **1995**, *74*, 2933.
- (132) Hentschel, M.; Kienberger, R.; Spielmann, C.; Reider, G. A.; Milosevic, N.; Brabec, T.; Corkum, P.; Heinzmann, U.; Drescher, M.; Krausz, F. *Nature* **2001**, *414*, 509.
- (133) Drescher, M.; Hentschel, M.; Kienberger, R.; Uiberacker, M.; Yakovlev, V.; Scrinzi, A.; Westerwalbesloh, T.; Kleineberg, U.; Heinzmann, U.; Krausz, F. *Nature* **2002**, *419*, 803.
- (134) Blanchet, V.; Lochbrunner, S.; Schmitt, M.; Shaffer, J. P.; Larsen, J. J.; Zgierski, M. Z.; Seideman, T.; Stolow, A. *Faraday Discuss.* **2000**, *33*.
- (135) Suzuki, T.; Wang, L.; Kohguchi, H. *J. Chem. Phys.* **1999**, *111*, 4859.
- (136) Wang, L.; Kohguchi, H.; Suzuki, T. *Faraday Discuss.* **1999**, *37*.
- (137) Stert, V.; Farmanara, P.; Radloff, W. *J. Chem. Phys.* **2000**, *112*, 4460.
- (138) Seidner, L.; Domcke, W.; Vonniessen, W. *Chem. Phys. Lett.* **1993**, *205*, 117.
- (139) Shaffer, J. P.; Schultz, T.; Schmitt, M.; Underwood, J. G.; Stolow, A. In *Ultrafast Phenomena XII*; Elsaesser, T., Mukamel, S., Murnane, M., Scherer, N., Eds.; Springer Series in Chemical Physics 66; Springer-Verlag: Berlin, 2000; p 338.
- (140) Olivucci, M. Private communication.
- (141) Baumert, T.; Frohnmeyer, T.; Kiefer, B.; Niklaus, P.; Strehle, M.; Gerber, G.; Zewail, A. H. *Appl. Phys. B* **2001**, *72*, 105.
- (142) Pedersen, S.; Banares, L.; Zewail, A. H. *J. Chem. Phys.* **1992**, *97*, 8801.
- (143) Soep, B.; Mestdag, J. M.; Sorgues, S.; Visticot, J. P. *Eur. Phys. J. D* **2001**, *14*, 191.
- (144) Farmanara, P.; Stert, V.; Radloff, W.; Hertel, I. V. *J. Phys. Chem. A* **2001**, *105*, 5613.
- (145) Song, J. K.; Tsubouchi, M.; Suzuki, T. *J. Chem. Phys.* **2001**, *115*, 8810.
- (146) Hahn, S.; Stock, G. *Phys. Chem. Chem. Phys.* **2001**, *3*, 2331.
- (147) Hahn, S.; Stock, G. *Chem. Phys. Lett.* **1998**, *296*, 137.
- (148) Davies, J. A.; Reid, K. L.; Towrie, M.; Matousek, P. *J. Chem. Phys.* **2002**, *117*, 9099.
- (149) Moss, D. B.; Parmenter, C. S. *J. Chem. Phys.* **1993**, *98*, 6897.
- (150) Lee, S. H.; Tang, K. C.; Chen, I. C.; Schmitt, M.; Shaffer, J. P.; Schultz, T.; Underwood, J. G.; Zgierski, M. Z.; Stolow, A. *J. Phys. Chem. A* **2002**, *106*, 8979.
- (151) Matsumoto, Y.; Kim, S. K. K.; Suzuki, T. *J. Chem. Phys.* **2003**, *119*, 300.
- (152) Scheiner, S. *J. Phys. Chem. A* **2000**, *104*, 5898.
- (153) Lochbrunner, S.; Schmitt, M.; Shaffer, J. P.; Schultz, T.; Stolow, A. In *Ultrafast Phenomena XII*; Elsaesser, T., Mukamel, S., Murnane, M., Scherer, N., Eds.; Springer Series in Chemical Physics 66; Springer-Verlag: Berlin, 2000; p 642.
- (154) Lochbrunner, S.; Schultz, T.; Schmitt, M.; Shaffer, J. P.; Zgierski, M. Z.; Stolow, A. *J. Chem. Phys.* **2001**, *114*, 2519.
- (155) Sobolewski, A. L.; Domcke, W. *Chem. Phys.* **1994**, *184*, 115.
- (156) Sobolewski, A. L.; Domcke, W. *Phys. Chem. Chem. Phys.* **1999**, *1*, 3065.
- (157) Farmanara, P.; Radloff, W.; Stert, V.; Ritze, H. H.; Hertel, I. V. *J. Chem. Phys.* **1999**, *111*, 633.
- (158) Farmanara, P.; Ritze, H. H.; Stert, V.; Radloff, W.; Hertel, I. V. *Eur. Phys. J. D* **2002**, *19*, 193.
- (159) Lippert, H.; Stert, V.; Hesse, L.; Schultz, C. P.; Hertel, I. V.; Radloff, W. *J. Phys. Chem. A* **2003**, *107*, 8239.
- (160) Sobolewski, A. L.; Domcke, W. *Chem. Phys. Lett.* **1999**, *315*, 293.
- (161) Sobolewski, A. L.; Domcke, W. *Chem. Phys. Lett.* **2000**, *329*, 130.
- (162) Schultz, T.; Quenneville, J.; Levine, B.; Toniolo, A.; Lochbrunner, S.; Schmitt, M.; Shaffer, J. P.; Zgierski, M. Z.; Stolow, A. *J. Am. Chem. Soc.* **2003**, *125*, 8098.
- (163) Rau, H. In *Photochromism, Molecules and Systems*; Durr, H., Buas-Laurent, H., Eds.; Elsevier: Amsterdam, 1990; p 165.
- (164) Tamai, N.; Miyasaka, H. *Chem. Rev.* **2000**, *100*, 1875.
- (165) Schick, C. P.; Weber, P. M. *J. Phys. Chem. A* **2001**, *105*, 3725.
- (166) Schick, C. P.; Weber, P. M. *J. Phys. Chem. A* **2001**, *105*, 3735.
- (167) Cheng, W.; Evans, C. L.; Kuthirummal, N.; Weber, P. M. *Chem. Phys. Lett.* **2001**, *349*, 405.
- (168) Schmitt, M.; Stolow, A. Private communication.
- (169) Probst, M.; Haight, R. *Appl. Phys. Lett.* **1997**, *71*, 202.
- (170) Zamith, S.; Blanchet, V.; Girard, B.; Andersson, J.; Sorensen, S.; Hjelte, I.; Bjorneholm, O.; Gauyacq, D.; Norin, J.; Mauritson, J.; L'Huillier, A. *J. Chem. Phys.* **2003**, *119*, 3763.
- (171) Farmanara, P.; Stert, V.; Ritze, H. H.; Radloff, W. *J. Chem. Phys.* **2000**, *113*, 1705.
- (172) Stert, V.; Ritze, H. H.; Nibbering, E. T. J.; Radloff, W. *Chem. Phys.* **2001**, *272*, 99.

- (173) Erdmann, M.; Rubner, O.; Shen, Z.; Engel, V. *Chem. Phys. Lett.* **2001**, *341*, 338.
- (174) Erdmann, M.; Rubner, O.; Shen, Z.; Engel, V. *J. Organomet. Chem.* **2002**, *661*, 191.
- (175) Shaffer, J. P.; Schultz, T.; Underwood, J. G.; Hayden, C. C.; Stolow, A. In *Ultrafast Phenomena XIII*; Miller, R. D., Murnane, M. M., Scherer, N. F., Weiner, A. M., Eds.; Springer Series in Chemical Physics 71; Springer-Verlag: Berlin, 2002; p 73.
- (176) Tsubouchi, M.; de Lange, C. A.; Suzuki, T. *J. Chem. Phys.* **2003**, *119*, 11728.
- (177) Tsubouchi, M.; Suzuki, T. *Chem. Phys. Lett.* **2003**, *382*, 418.
- (178) Demyanenko, A. V.; Potter, A. B.; Dribinski, V.; Reisler, H. *J. Chem. Phys.* **2002**, *117*, 2568.
- (179) Scherer, N. F.; Khundkar, L. R.; Bernstein, R. B.; Zewail, A. H. *J. Chem. Phys.* **1987**, *87*, 1451.
- (180) Stert, V.; Farmanara, P.; Ritze, H. H.; Radloff, W.; Gasmí, K.; Gonzalez-Urena, A. *Chem. Phys. Lett.* **2001**, *337*, 299.
- (181) Zanni, M. T.; Greenblatt, B. J.; Neumark, D. M. *J. Chem. Phys.* **1997**, *107*, 7613.
- (182) Batista, V. S.; Zanni, M. T.; Greenblatt, B. J.; Neumark, D. M.; Miller, W. H. *J. Chem. Phys.* **1999**, *110*, 3736.
- (183) Zanni, M. T.; Davis, A. V.; Frischkorn, C.; Elhanine, M.; Neumark, D. M. *J. Chem. Phys.* **2000**, *112*, 8847.
- (184) Zanni, M. T.; Greenblatt, B. J.; Davis, A. V.; Neumark, D. M. *J. Chem. Phys.* **1999**, *111*, 2991.
- (185) Kuhne, T.; Vohringer, P. *J. Chem. Phys.* **1996**, *105*, 10788.
- (186) Banin, U.; Ruhman, S. *J. Chem. Phys.* **1993**, *98*, 4391.
- (187) Papanikolas, J. M.; Gord, J. R.; Levinger, N. E.; Ray, D.; Vorsa, V.; Lineberger, W. C. *J. Phys. Chem.* **1991**, *95*, 8028.
- (188) Papanikolas, J. M.; Vorsa, V.; Nadal, M. E.; Campagnola, P. J.; Buchenau, H. K.; Lineberger, W. C. *J. Chem. Phys.* **1993**, *99*, 8733.
- (189) Vorsa, V.; Campagnola, P. J.; Nandi, S.; Larsson, M.; Lineberger, W. C. *J. Chem. Phys.* **1996**, *105*, 2298.
- (190) Vorsa, V.; Nandi, S.; Campagnola, P. J.; Larsson, M.; Lineberger, W. C. *J. Chem. Phys.* **1997**, *106*, 1402.
- (191) Sanov, A.; Lineberger, W. C. *PhysChemComm* **2002**, 165.
- (192) Papanikolas, J. M.; Maslen, P. E.; Parson, R. *J. Chem. Phys.* **1995**, *102*, 2452.
- (193) Batista, V. S.; Coker, D. F. *J. Chem. Phys.* **1997**, *106*, 7102.
- (194) Delaney, N.; Faeder, J.; Maslen, P. E.; Parson, R. *J. Phys. Chem. A* **1997**, *101*, 8147.
- (195) Faeder, J.; Delaney, N.; Maslen, P. E.; Parson, R. *Chem. Phys. Lett.* **1997**, *270*, 196.
- (196) Margulis, C. J.; Coker, D. F. *J. Chem. Phys.* **1999**, *110*, 5677.
- (197) Parson, R.; Faeder, J.; Delaney, N. *J. Phys. Chem. A* **2000**, *104*, 9653.
- (198) Greenblatt, B. J.; Zanni, M. T.; Neumark, D. M. *Faraday Discuss.* **1997**, *108*, 101.
- (199) Greenblatt, B. J.; Zanni, M. T.; Neumark, D. M. *Science* **1997**, *276*, 1675.
- (200) Greenblatt, B. J.; Zanni, M. T.; Neumark, D. M. *J. Chem. Phys.* **2000**, *112*, 601.
- (201) Greenblatt, B. J.; Zanni, M. T.; Neumark, D. M. *J. Chem. Phys.* **1999**, *111*, 10566.
- (202) Paik, D. H.; Bernhardt, T. M.; Kim, N. J.; Zewail, A. H. *J. Chem. Phys.* **2001**, *115*, 612.
- (203) Paik, D. H.; Kim, N. J.; Zewail, A. H. *J. Chem. Phys.* **2003**, *118*, 6923.
- (204) Kim, N. J.; Paik, D. H.; Zewail, A. H. *J. Chem. Phys.* **2003**, *118*, 6930.
- (205) Hiraoka, K. *Chem. Phys.* **1988**, *125*, 439.
- (206) Deluca, M. J.; Han, C. C.; Johnson, M. A. *J. Chem. Phys.* **1990**, *93*, 268.
- (207) Wester, R.; Bragg, A. E.; Davis, A. V.; Neumark, D. M. *J. Chem. Phys.* **2003**, *119*, 10032.
- (208) Zanni, M. T.; Greenblatt, B. J.; Neumark, D. M. *J. Chem. Phys.* **1998**, *109*, 9648.
- (209) Davis, A. V.; Wester, R.; Bragg, A. E.; Neumark, D. M. *J. Chem. Phys.* **2002**, *117*, 4282.
- (210) Davis, A. V.; Zanni, M. T.; Frischkorn, C.; Elhanine, M.; Neumark, D. M. *J. Electron Spectrosc. Relat. Phenom.* **2000**, *112*, 221.
- (211) Davis, A. V.; Wester, R.; Bragg, A. E.; Neumark, D. M. *J. Chem. Phys.* **2003**, *119*, 2020.
- (212) Franck, J.; Sheibe, G. *Z. Phys. Chem. A* **1928**, *139*, 22.
- (213) Blandamer, M.; Fox, M. *Chem. Rev.* **1970**, *70*, 59.
- (214) Jortner, J.; Ottolenghi, M.; Stein, G. *J. Phys. Chem.* **1964**, *68*, 247.
- (215) Long, F. H.; Shi, X. L.; Lu, H.; Eisenthal, K. B. *J. Phys. Chem.* **1994**, *98*, 7252.
- (216) Kloepfer, J. A.; Vilchiz, V. H.; Lenchenkov, V. A.; Bradford, S. E. *Chem. Phys. Lett.* **1998**, *298*, 120.
- (217) Martini, I. B.; Barthel, E. R.; Schwartz, B. J. *Science* **2001**, *293*, 462.
- (218) Sheu, W. S.; Rossky, P. J. *Chem. Phys. Lett.* **1993**, *202*, 186.
- (219) Serxner, D.; Dessent, C. E. H.; Johnson, M. A. *J. Chem. Phys.* **1996**, *105*, 7231.
- (220) Becker, I.; Cheshnovsky, O. *J. Chem. Phys.* **1999**, *110*, 6288.
- (221) Becker, I.; Markovich, G.; Cheshnovsky, O. *Phys. Rev. Lett.* **1997**, *79*, 3391.
- (222) Lehr, L.; Zanni, M. T.; Frischkorn, C.; Weinkauff, R.; Neumark, D. M. *Science* **1999**, *284*, 635.
- (223) Zanni, M. T.; Frischkorn, C.; Davis, A. V.; Neumark, D. M. *J. Phys. Chem. A* **2000**, *104*, 2527.
- (224) Davis, A. V.; Zanni, M. T.; Frischkorn, C.; Neumark, D. M. *J. Electron Spectrosc. Relat. Phenom.* **2000**, *108*, 203.
- (225) Frischkorn, C.; Zanni, M. T.; Davis, A. V.; Neumark, D. M. *Faraday Discuss.* **2000**, *115*, 49.
- (226) Davis, A. V.; Zanni, M. T.; Weinkauff, R.; Neumark, D. M. *Chem. Phys. Lett.* **2002**, *353*, 455.
- (227) Zanni, M. T.; Lehr, L.; Greenblatt, B. J.; Weinkauff, R.; Neumark, D. M. In *Ultrafast Phenomena XI*; Elsaesser, T., Fujimoto, J. G., Wiersma, D., Zinth, W., Eds.; Springer Series in Chemical Physics 63; Springer-Verlag: Berlin, 1998; p 474.
- (228) Chen, H.-Y.; Sheu, W.-S. *Chem. Phys. Lett.* **2001**, *335*, 475.
- (229) Chen, H.-Y.; Sheu, W.-S. *J. Am. Chem. Soc.* **2000**, *122*, 7534.
- (230) Vila, F. D.; Jordan, K. D. *J. Phys. Chem. A* **2002**, *106*, 1391.
- (231) Timerghazin, Q. K.; Peslherbe, G. H. *J. Am. Chem. Soc.* **2003**, *125*, 9904.
- (232) Lenzer, T.; Furlanetto, M. R.; Asmis, K. R.; Neumark, D. M. *J. Chem. Phys.* **1998**, *109*, 10754.
- (233) Lenzer, T.; Furlanetto, M. R.; Pivonka, N. L.; Neumark, D. M. *J. Chem. Phys.* **1999**, *110*, 6714.
- (234) Hart, E. J.; Boag, J. W. *J. Am. Chem. Soc.* **1962**, *84*, 4090.
- (235) Migus, A.; Gauduel, Y.; Martin, J. L.; Antonetti, A. *Phys. Rev. Lett.* **1987**, *58*, 1559.
- (236) Rossky, P. J.; Schmitker, J. *J. Phys. Chem.* **1988**, *92*, 4277.
- (237) Coe, J. V.; Lee, G. H.; Eaton, J. G.; Arnold, S. T.; Sarkas, H. W.; Bowen, K. H.; Ludewig, C.; Haberland, H.; Worsnop, D. R. *J. Chem. Phys.* **1990**, *92*, 3980.
- (238) Ayotte, P.; Johnson, M. A. *J. Chem. Phys.* **1997**, *106*, 811.
- (239) Ayotte, P.; Weddle, G. H.; Bailey, C. G.; Johnson, M. A.; Vila, F.; Jordan, K. D. *J. Chem. Phys.* **1999**, *110*, 6268.
- (240) Weber, J. M.; Kim, J.; Woronowicz, E. A.; Weddle, G. H.; Becker, I.; Cheshnovsky, O.; Johnson, M. A. *Chem. Phys. Lett.* **2001**, *339*, 337.
- (241) Minemoto, S.; Muller, J.; Gantefor, G.; Munzer, H. J.; Boneberg, J.; Leiderer, P. *Phys. Rev. Lett.* **2000**, *84*, 3554.
- (242) Tulej, M.; Fulara, J.; Sobolewski, A.; Jungen, M.; Maier, J. P. *J. Chem. Phys.* **2000**, *112*, 3747.
- (243) Frischkorn, C.; Bragg, A. E.; Davis, A. V.; Wester, R.; Neumark, D. M. *J. Chem. Phys.* **2001**, *115*, 11185.
- (244) Knoesel, E.; Hotzel, A.; Hertel, T.; Wolf, M.; Ertl, G. *Surf. Sci.* **1996**, *368*, 76.
- (245) Hertel, T.; Knoesel, E.; Wolf, M.; Ertl, G. *Phys. Rev. Lett.* **1996**, *76*, 535.
- (246) Pontius, N.; Bechthold, P. S.; Neeb, M.; Eberhardt, W. *Appl. Phys. B* **2000**, *71*, 351.
- (247) Pontius, N.; Bechthold, P. S.; Neeb, M.; Eberhardt, W. *Phys. Rev. Lett.* **2000**, *84*, 1132.
- (248) Pontius, N.; Bechthold, P. S.; Neeb, M.; Eberhardt, W. *J. Electron Spectrosc. Relat. Phenom.* **2000**, *106*, 107.
- (249) Pontius, N.; Luttgens, G.; Bechthold, P. S.; Neeb, M.; Eberhardt, W. *J. Chem. Phys.* **2001**, *115*, 10479.
- (250) Pontius, N.; Neeb, M.; Eberhardt, W. *Phys. Rev. B* **2003**, *67*, 1.
- (251) Pine, D.; Nozieres, P. *The Theory of Quantum Liquids*; Benjamin: New York, 1966.
- (252) Gerhardt, P.; Niemietz, M.; Kim, Y. D.; Gantefor, G. *Chem. Phys. Lett.* **2003**, *382*, 454.
- (253) Niemietz, M.; Gerhardt, P.; Gantefor, G.; Kim, Y. D. *Chem. Phys. Lett.* **2003**, *380*, 99.
- (254) Arasaki, Y.; Takatsuka, K.; Wang, K.; McKoy, V. *Chem. Phys. Lett.* **1999**, *302*, 363.
- (255) Arasaki, Y.; Takatsuka, K.; Wang, K. H.; McKoy, V. *J. Electron Spectrosc. Relat. Phenom.* **2000**, *108*, 89.
- (256) Arasaki, Y.; Takatsuka, K.; Wang, K.; McKoy, V. *J. Chem. Phys.* **2000**, *112*, 8871.
- (257) Wollenhaupt, M.; Assion, A.; Graefe, O.; Liese, D.; Sarpe-Tudoran, C.; Wintner, E.; Baumert, T. *Chem. Phys. Lett.* **2003**, *376*, 457.
- (258) Takatsuka, K.; Arasaki, Y.; Wang, K.; McKoy, V. *Faraday Discuss.* **2000**, 1.
- (259) Reid, K. L.; Field, T. A.; Towrie, M.; Matousek, P. *J. Chem. Phys.* **1999**, *111*, 1438.
- (260) Underwood, J. G.; Reid, K. L. *J. Chem. Phys.* **2000**, *113*, 1067.
- (261) Seideman, T. *J. Chem. Phys.* **2000**, *113*, 1677.
- (262) Seideman, T.; Althorpe, S. C. *J. Electron Spectrosc. Relat. Phenom.* **2000**, *108*, 99.
- (263) Seideman, T. *Phys. Rev. A* **2001**, *6404*, 042504.
- (264) Resch, K.; Blanchet, V.; Stolow, A.; Seideman, T. *J. Phys. Chem. A* **2001**, *105*, 2756.
- (265) Piancastelli, M. N.; Keller, P. R.; Taylor, J. W.; Grimm, F. A.; Carlson, T. A. *J. Am. Chem. Soc.* **1983**, *105*, 4235.
- (266) Tsubouchi, M.; Whitaker, B. J.; Wang, L.; Kohguchi, H.; Suzuki, T. *Phys. Rev. Lett.* **2001**, *86*, 4500.
- (267) Davis, A. V.; Wester, R.; Bragg, A. E.; Neumark, D. M. *J. Chem. Phys.* **2003**, *118*, 999.

- (268) Bragg, A. E.; Wester, R.; Davis, A. V.; Kammrath, A.; Neumark, D. M. *Chem. Phys. Lett.* **2003**, *376*, 767.
- (269) Reed, K. J.; Zimmerman, A. H.; Andersen, H. C.; Brauman, J. I. *J. Chem. Phys.* **1976**, *64*, 1368.
- (270) Peronne, E.; Poulson, M. D.; Bisgaard, C. Z.; Stapelfeldt, H.; Seideman, T. *Phys. Rev. Lett.* **2003**, *91*, 043003.
- (271) Underwood, J. G.; Spanner, M.; Ivanov, M. Y.; Mottershead, J.; Sussman, B. J.; Stolow, A. *Phys. Rev. Lett.* **2003**, *90*, 223001.
- (272) Weinkauff, R.; Schermann, J. P.; de Vries, M. S.; Kleinermanns, K. *Eur. Phys. J. D* **2002**, *20*, 309.

CR020683W

